Fast Timing Detectors

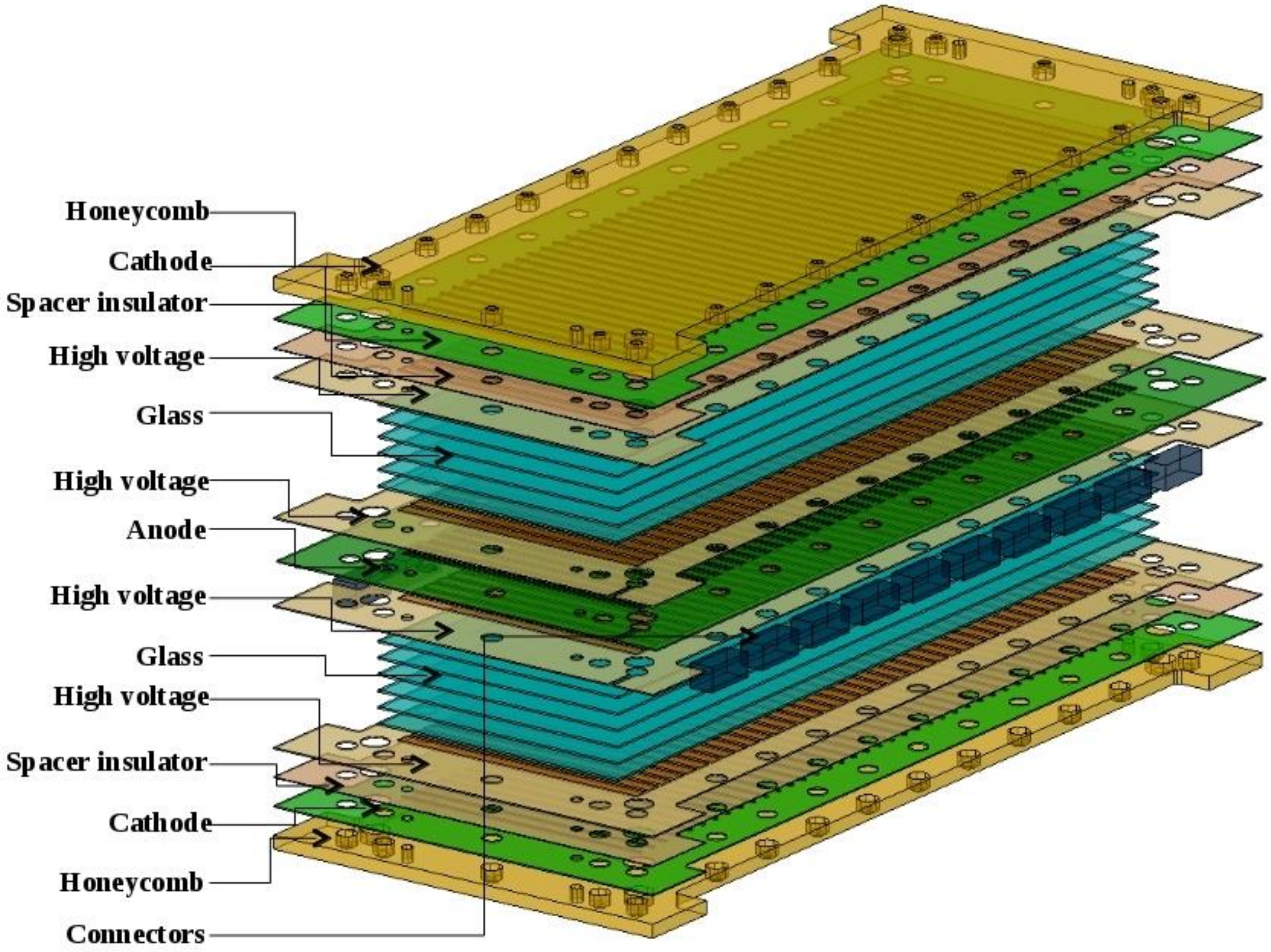

Personal background

https://www.cbm.gsi.de/

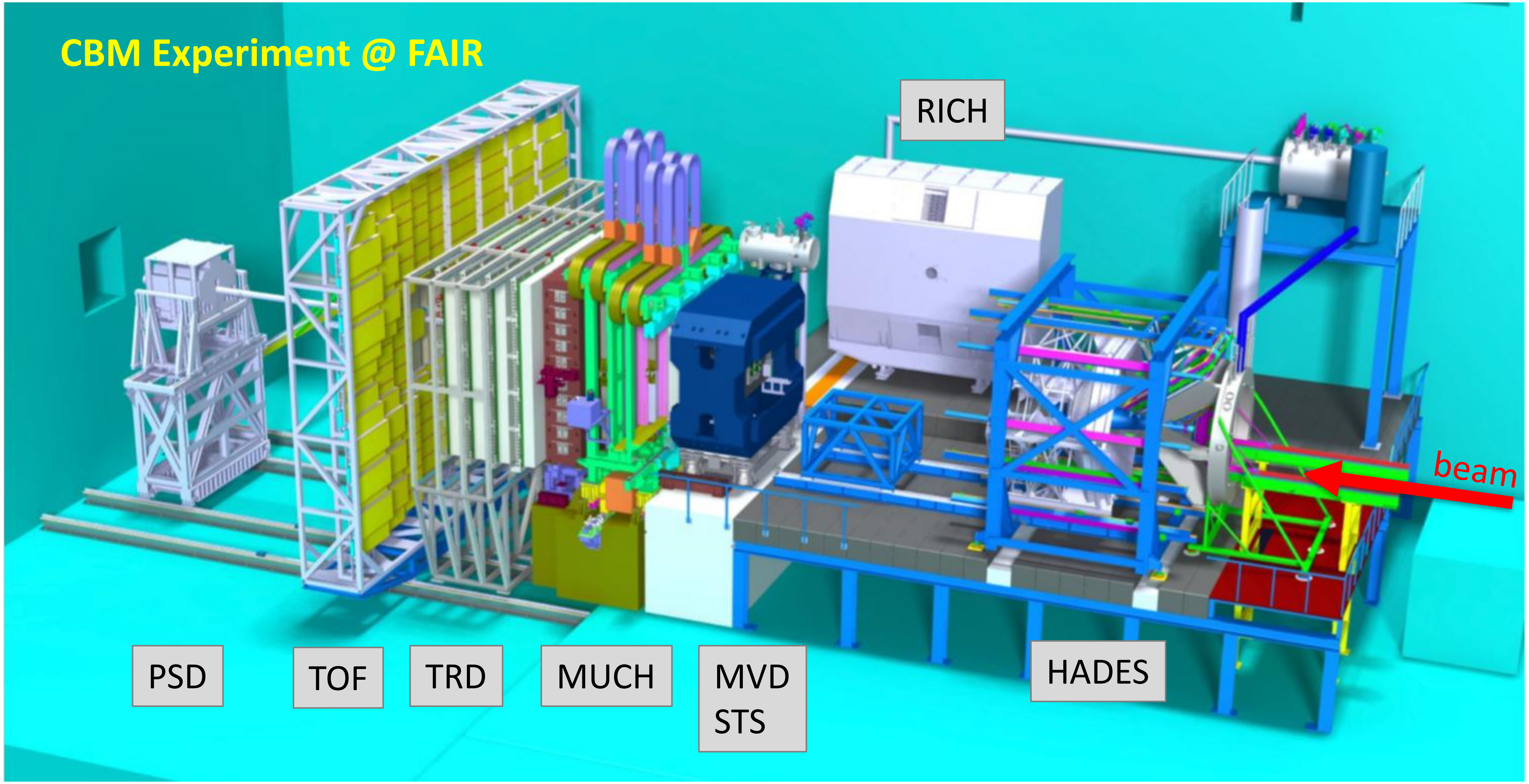

Goal: 10 MHz Au + Au interactions fully online – selected, triggerless operation (cf. Alice Run3: 50 kHz)
Start of operation: 2028 (?)

CBM requirements

Particle flux in fixed target experiments
(CBM 10 m downstream of target)

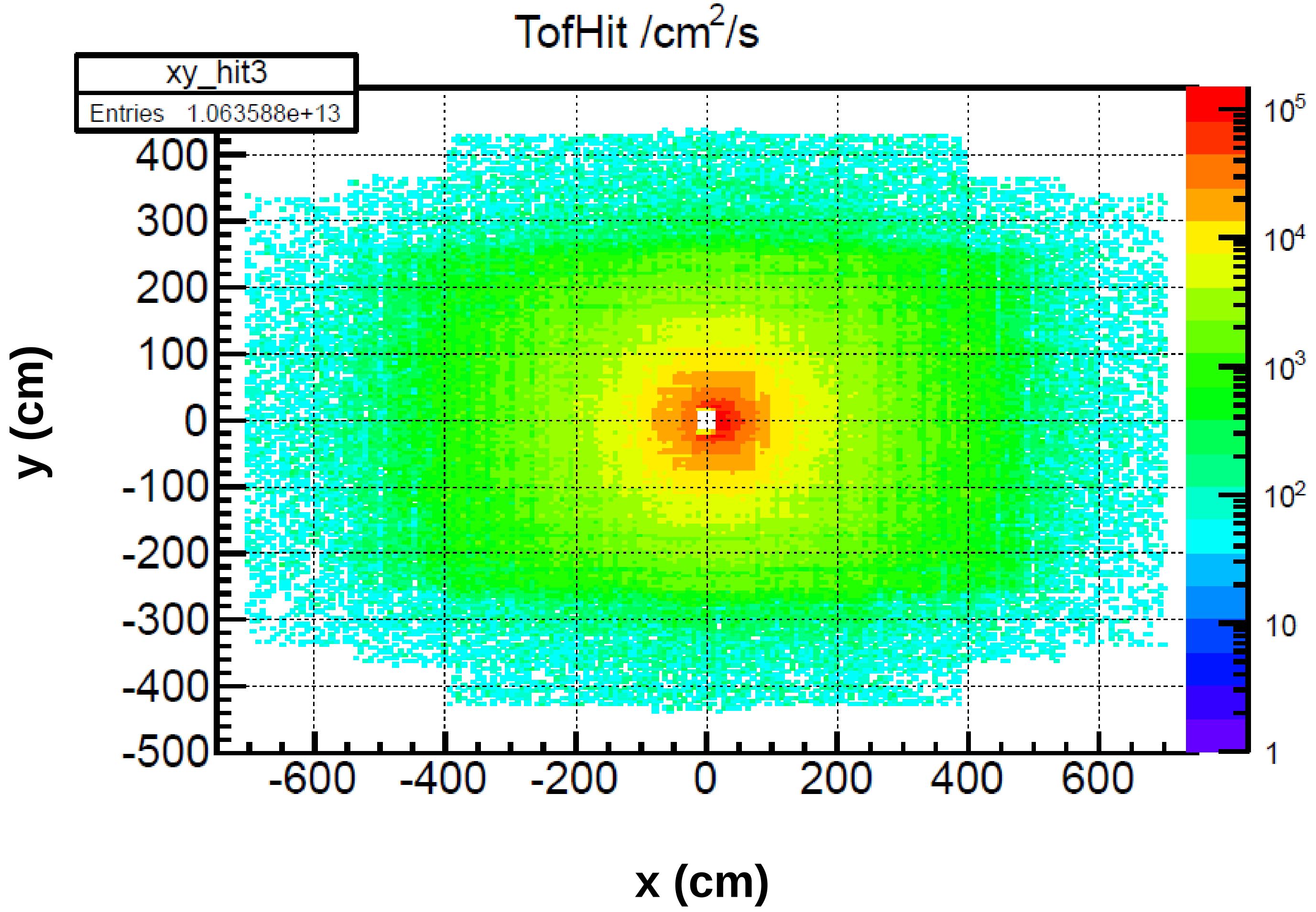

Timing resolution: < 100 ps

Efficiency: > 95%

Granularity: cm^2 – dm^2

Rate capability: 20 - 50 kHz/cm^2

Number of cells: ~ 10^5

Cost: affordable

CBM physics case: QCD phase diagram

Theory: Location of chiral cross over

F. Gao, J.M. Pawlowski, Phys.Rev.D 102 (2020) 3, 034027

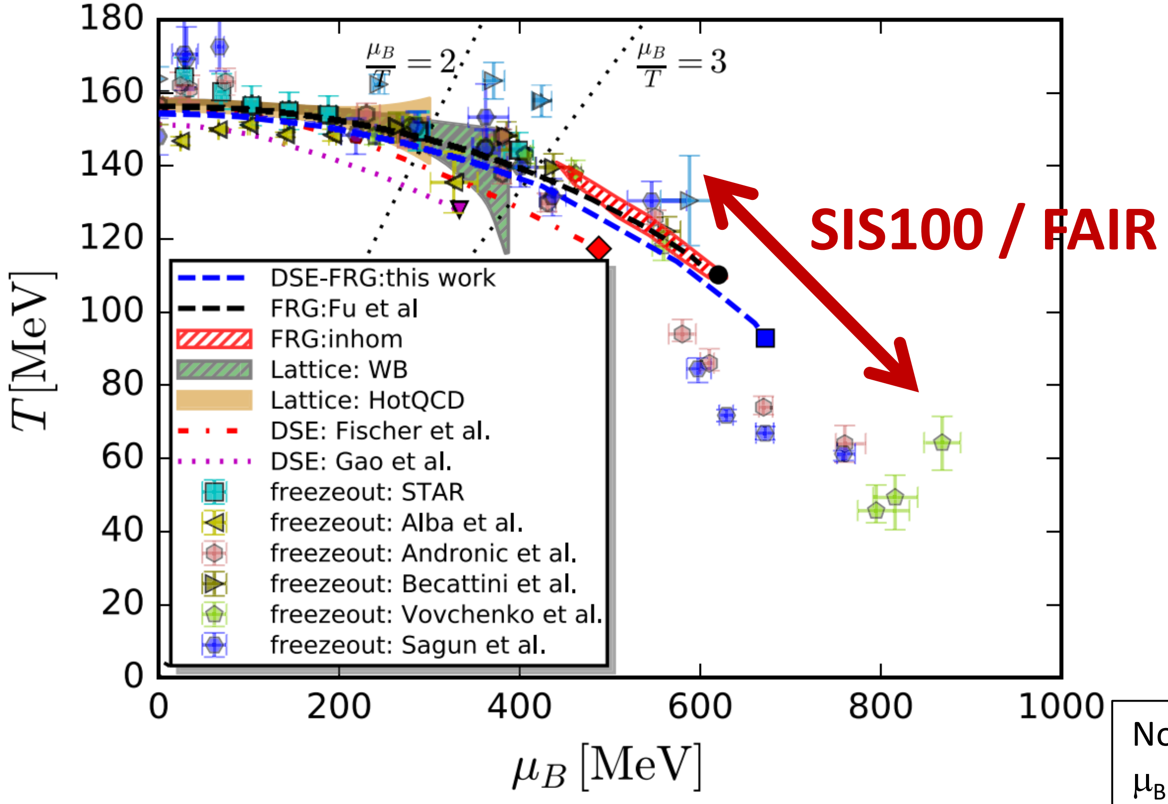

Note:
μ_B = 635 MeV
$\sqrt{s_{NN}}$ = 3.7 GeV
T = 5 AGeV

CBM Collaboration, EPJA 53 3 (2017) 60
T.Galatyuk, NPA982 (2019), update (2021)

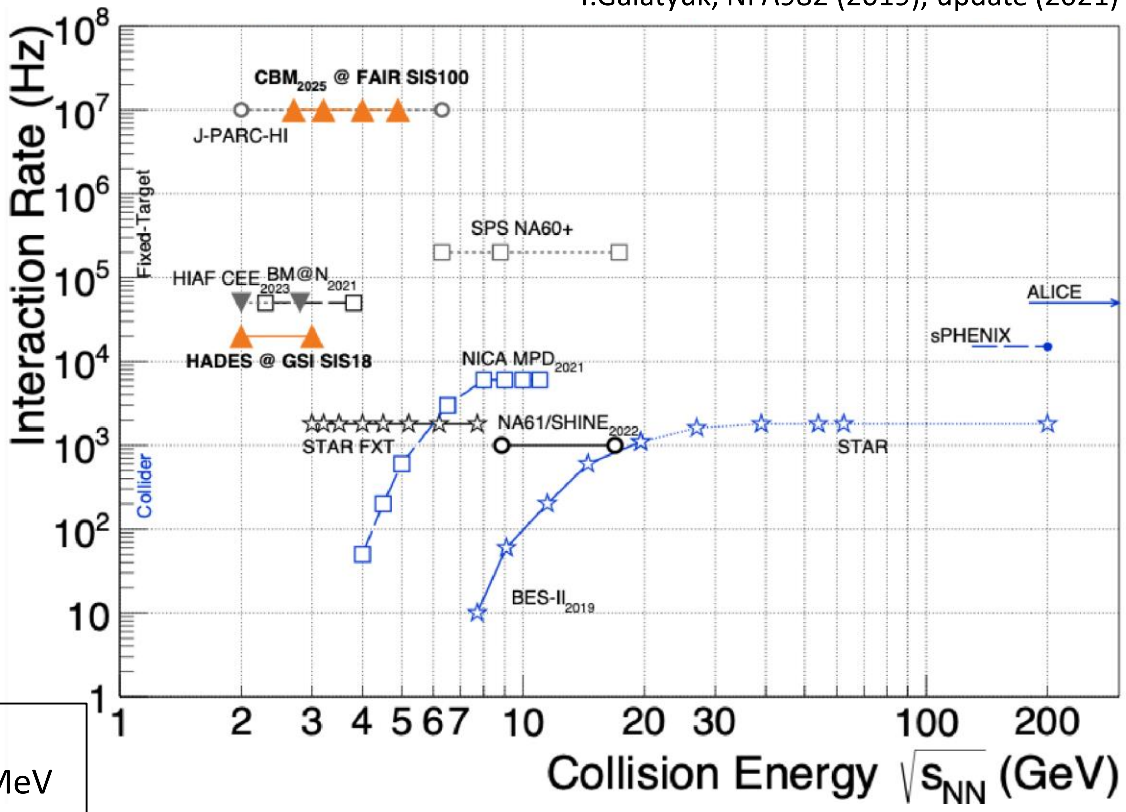

Measurement of of excitation functions of rare probes:

- Critical End Point,
- 1. order phase transition,
- Equation-of-state,
- Strange matter

Worldwide unique opportunity for CBM@SIS100
Competitors:

STAR FXT (RHIC)
BM@N (NICA)

Fast Timing Detectors: Outline

- Introduction

- Timing applications
  - Particle Identification (PID)

- Timing counter types
  - Plastic scintillator
    - with PMT readout
    - with SiPM readout
  - Multigap Resitive Plate Chambers (MRPC)
  - Diamond
  - Low Gain Avalanche Diode (LGAD=UFSD)

History: Nobelprize in Physics 1954

Walter Bothe

born 1891
died 1957

"for the coincidence method and his discoveries made therewith"

1908 – 12	Study of Physics at the University of Berlin
1913 – 29	Physikalisch – Technische Reichsanstalt, Berlin
1929	Extraordinary Professor, Berlin
1930 – 32	Professor of Physics, Giessen
1933 – 57	Director of the Institute of Physics and Max Planck Institute for Medical Research, Heidelberg

First coincidence circuit

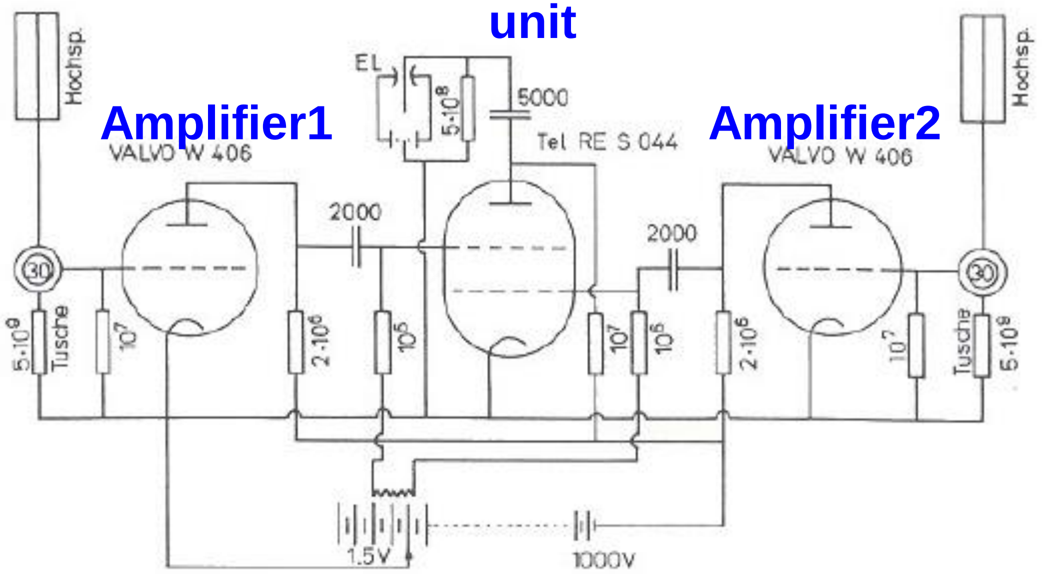

Abb.2. Erste Koinzidenzschaltung Bothes (1928). Von einer Freihandskizze in Bothes Protokollbuch abgezeichnet. EL: Einfadenelektrometer
RES 044 (S = Schutzgitter; 004 = 4 Volt Heizspannung)
W 406 (W = Niederfrequenzradioröhre für Widerstandskopplung)
406 = 4 Volt Heizspannung, 0,06 Amp Heizstrom)

Timing resolution: $\Delta t \approx 0.1$ ms

Timing applications in Nuclear and Particle Physics

Event definition

Particle Identification (PID)

Direction measurement

Cosmic air showers,

Cerenkov cone of charged particle in neutrino detectors

TOF – PET

T0 – measurements of particle beams

Particle Flow calorimetry

Spectroscopy in Neutron scattering

…

Particle identification (PID)

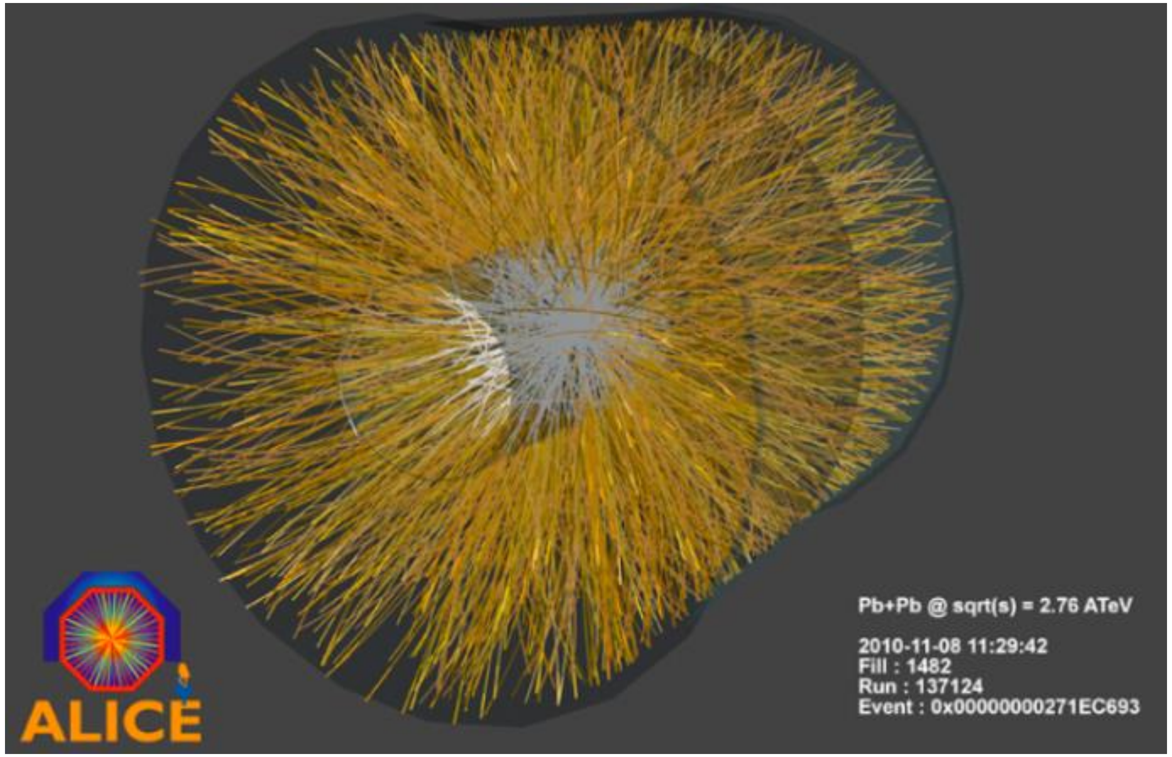

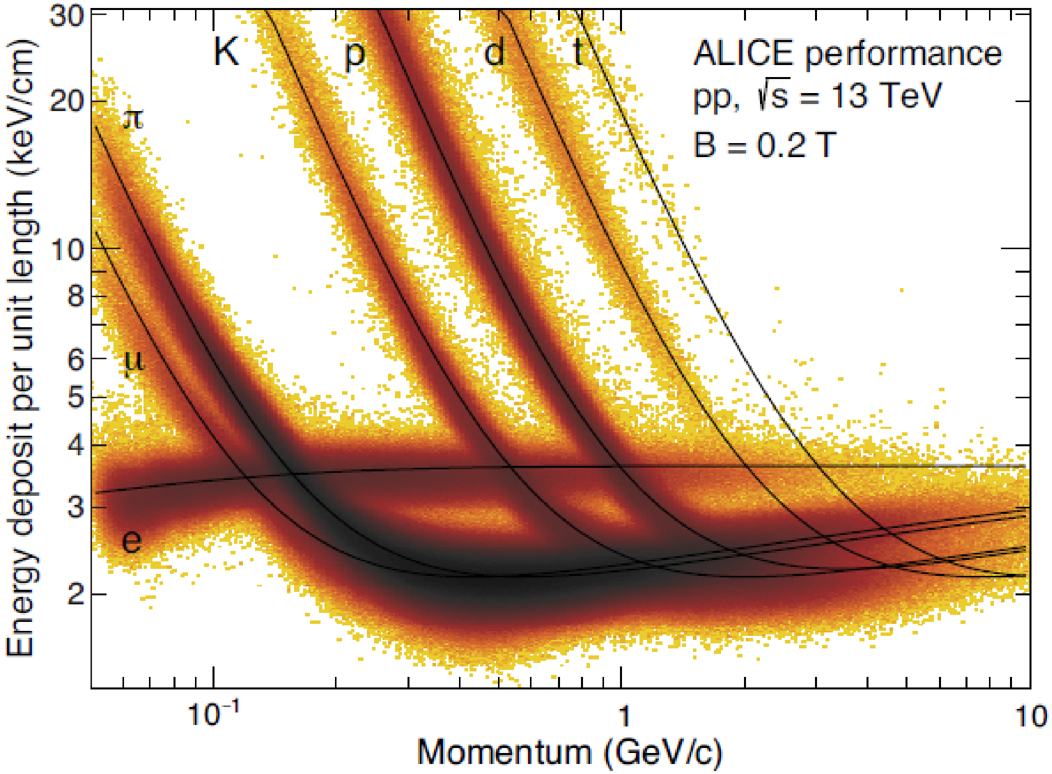

Resolve ambiguities by time of flight

Time – of – Flight (TOF) Method

Typical Setup

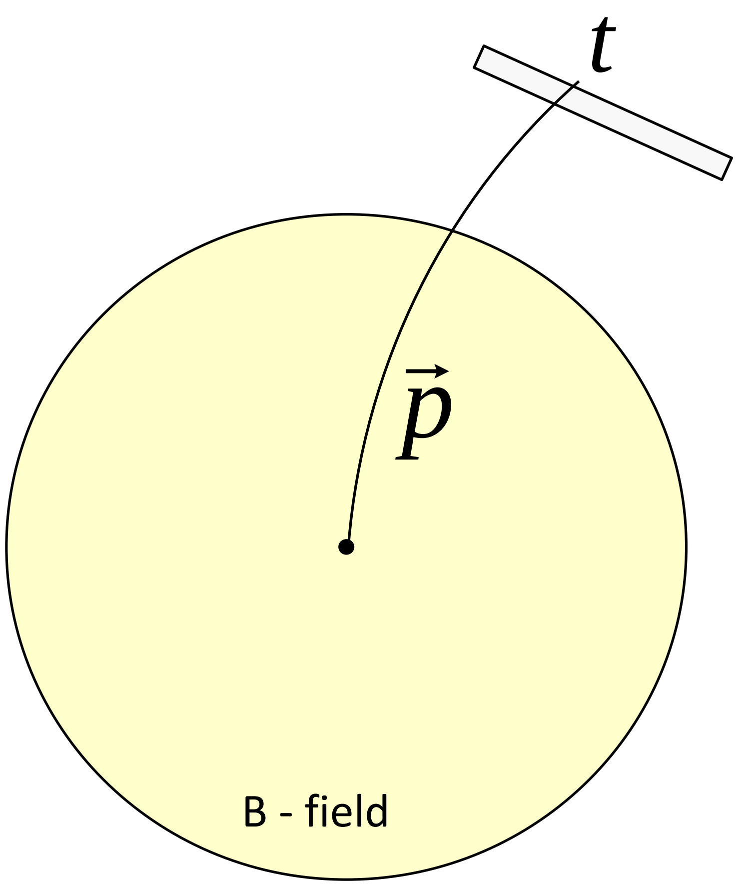

Tracking in magnetic field measures momentum.

Additional measurement of velocity allows determination of particle mass.

$$\beta = \frac{L}{ct}$$

$$p = mc\gamma\beta = \frac{mc\beta}{\sqrt{1-\beta^2}}$$

$$m^2 = \left(\frac{p}{c}\right)^2 \left(\frac{1}{\beta^2} - 1\right) = \left(\frac{p}{c}\right)^2 \left(\frac{c^2 t^2}{L^2} - 1\right)$$

L – pathlength from t=0 to measuring device

PID reach with TOF

Flight Time differences after a pathlength of 1 m

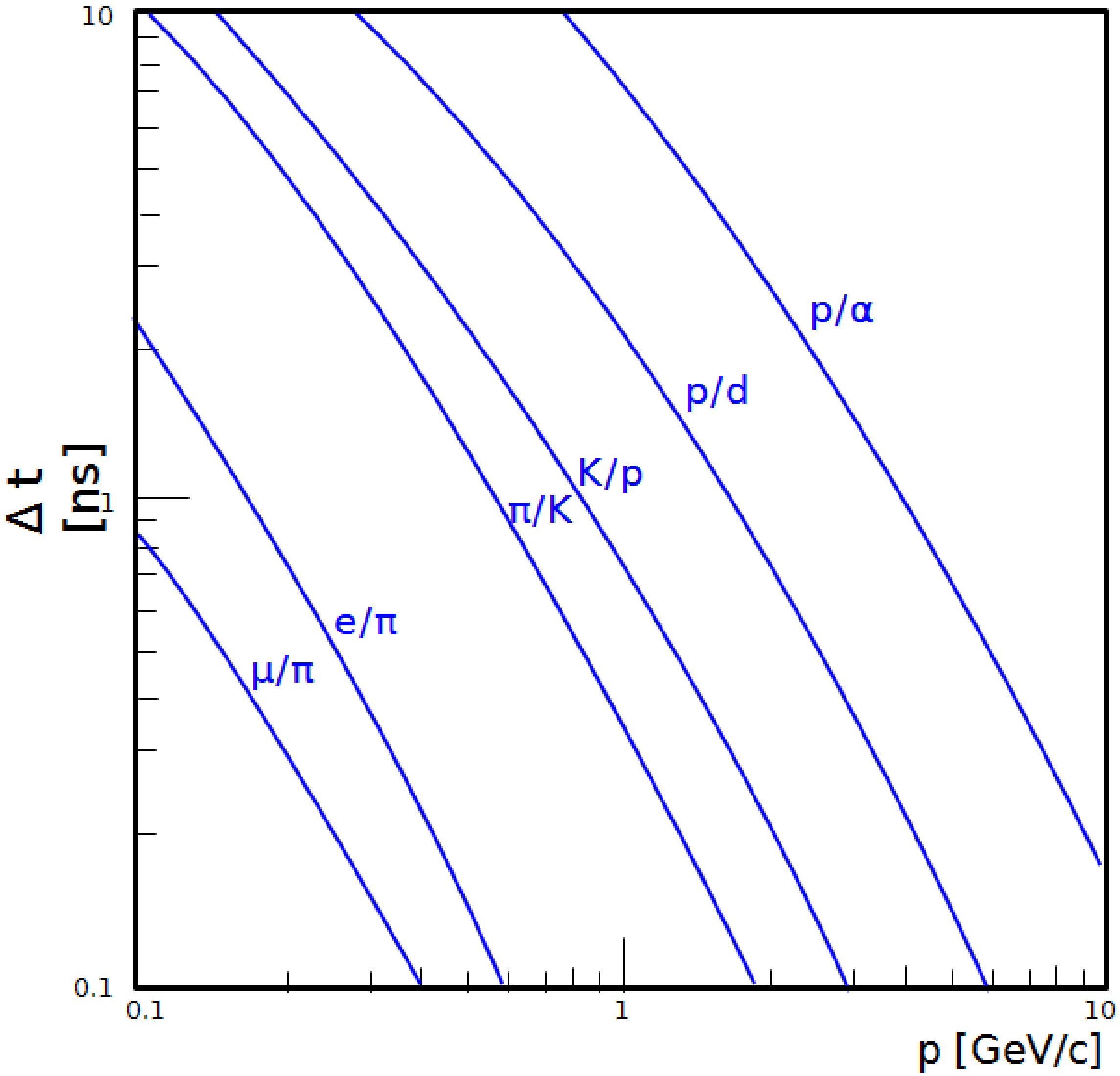

$$\Delta t = \frac{L}{c}\left(\sqrt{\frac{m_1^2c^2}{p^2}+1} - \sqrt{\frac{m_2^2c^2}{p^2}+1}\right)$$

$$\downarrow pc >> mc^2$$

$$\approx \frac{Lc}{2p^2}\left(m_1^2 - m_2^2\right)$$

TOF system time resolution requirement:

$$\Delta t > k\sigma_t$$

$$k > 3-4$$

(depends on relative abundance)

PID with TOF

A. Akindinov et al. (ALICE), EPJ Plus 128 (2013) 44

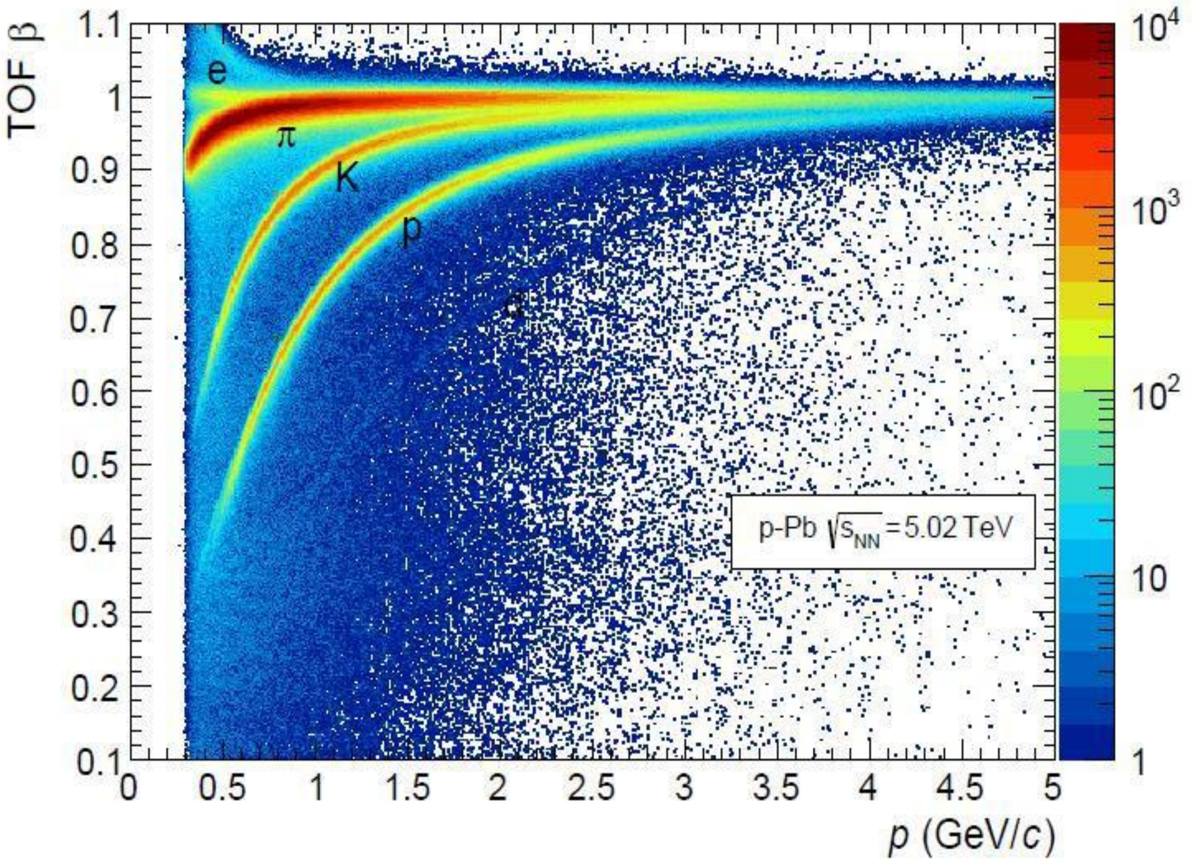

L ~ 4 m

M. Kis et al. (FOPI), NIM A 646, 27 (2011)

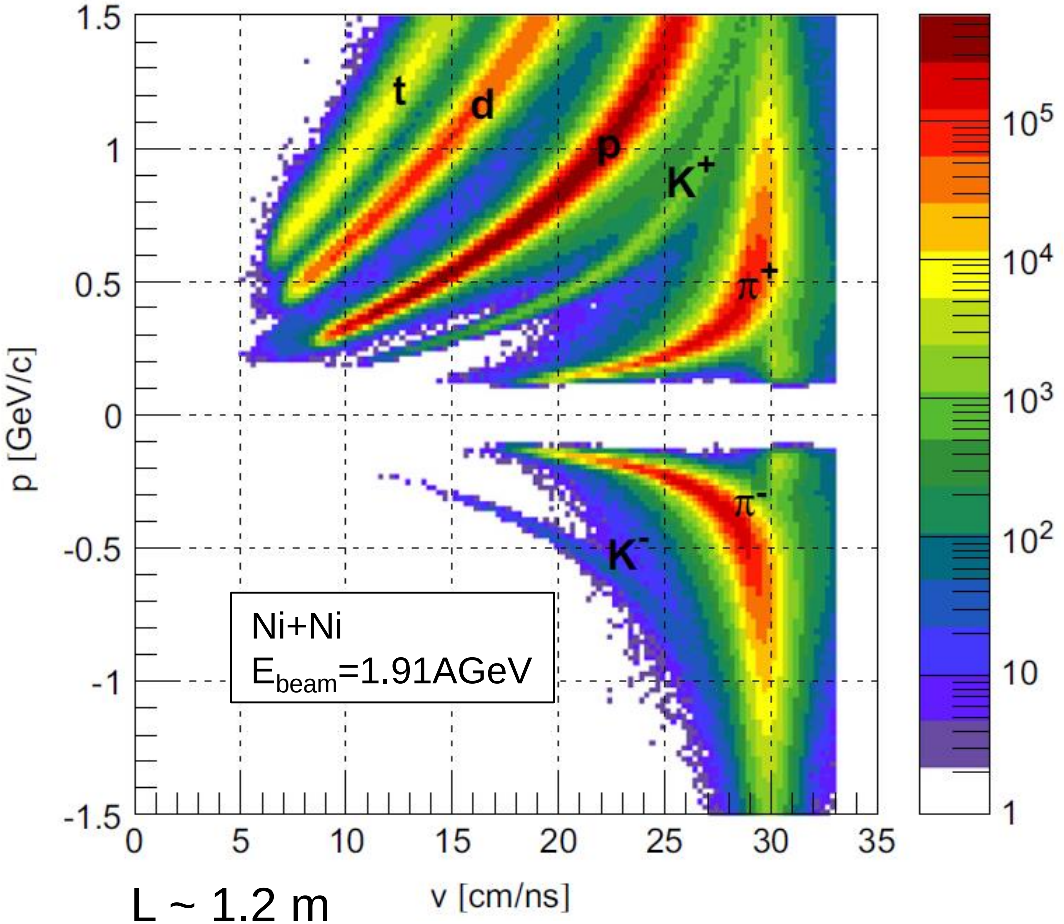

L ~ 1.2 m

TOF mass resolution

Here: c=1

$$m^2 = p^2\left(\frac{t^2}{L^2}-1\right)$$

$$\delta\left(m^2\right) = 2p\delta p\underbrace{\left(\frac{t^2}{L^2}-1\right)}_{\frac{m^2}{p^2}} + \underbrace{2t\delta t\frac{p^2}{L^2} - 2\frac{\delta L}{L^3}p^2t^2}_{\text{use } \frac{p^2t^2}{L^2}=\frac{p^2}{\beta^2}=m^2\gamma^2}$$

$$= 2m^2\frac{\delta p}{p} + 2m^2\gamma^2\frac{\delta t}{t} - 2m^2\gamma^2\frac{\delta L}{L}$$

$$\Downarrow$$

$$\left(\frac{\sigma_m}{m}\right)^2 = 4m^2\left(\left(\frac{\sigma_p}{p}\right)^2 + \gamma^4\left(\left(\frac{\sigma_t}{t}\right)^2 + \left(\frac{\sigma_L}{L}\right)^2\right)\right)$$

Typical values:

$$\frac{\sigma_p}{p} \approx 10^{-2}, \quad \frac{\sigma_t}{t} \approx 10^{-1}, \quad \frac{\sigma_L}{L} \approx 10^{-3}$$

Timing error dominates !

Typical m2 plot (simulation CBM)

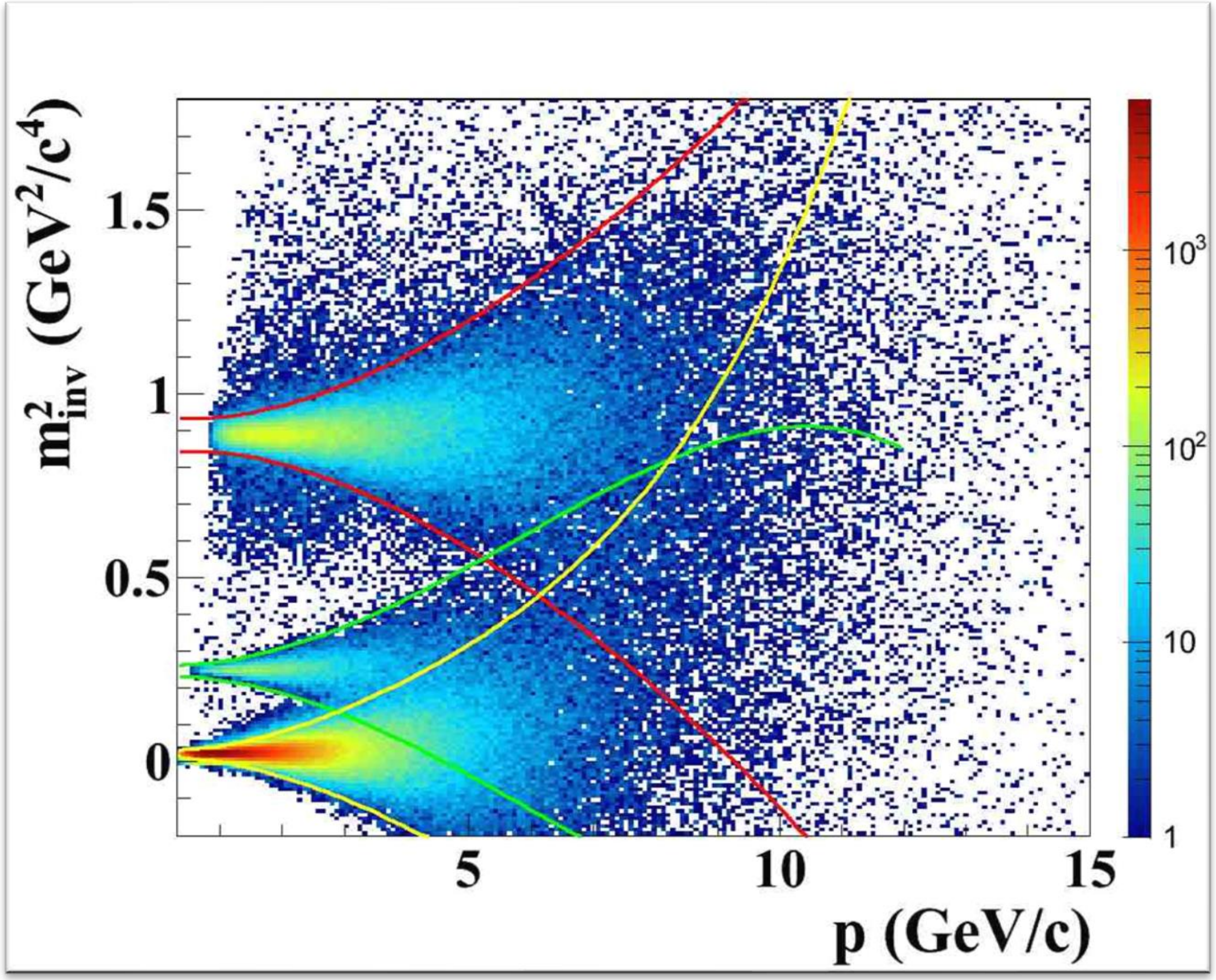

CBM simulation

Distance to target: L=6m

System time resolution: 80 ps

π – K separation up to 3 GeV/c

Generalities of Arrival Time Measurement

Timing resolution

$$\sigma_t = \frac{\sigma_{noise}}{\left.\frac{dS}{dt}\right|_{S_{threshold}}} \approx \frac{t_{rise}}{S/N}$$

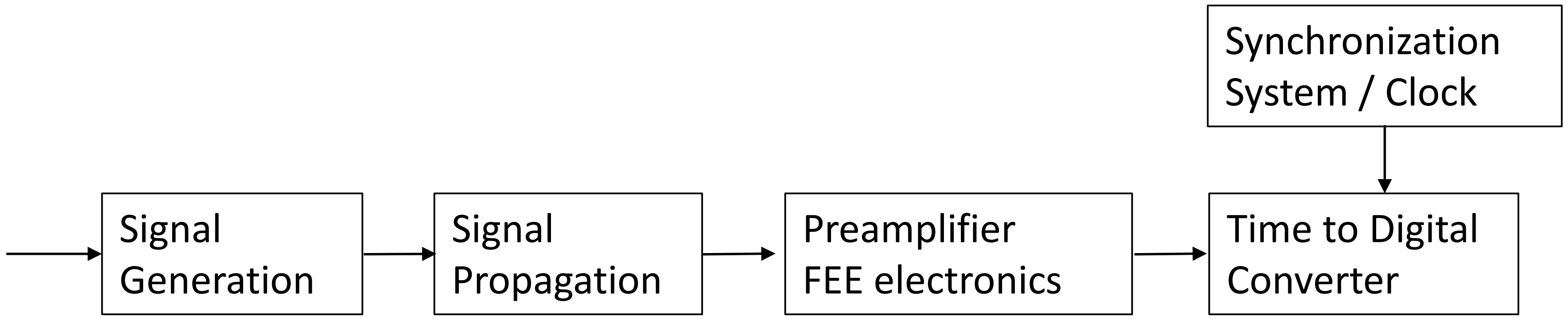

$$\sigma_t^2 = \sigma_{generation}^2 \oplus \sigma_{transport}^2 \oplus \sigma_{conversion}^2 \oplus \sigma_{digitization}^2$$

Example: plastic slat counter

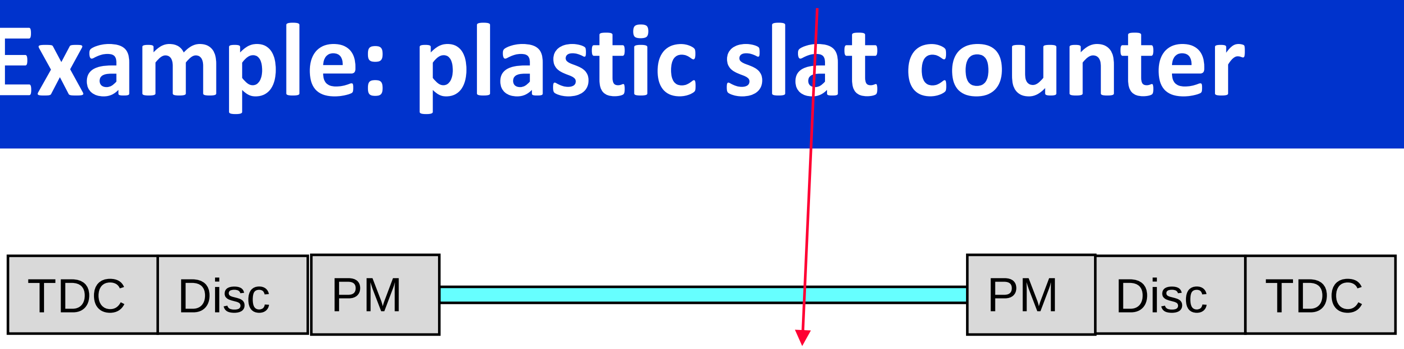

1) Ionization by Bethe-Bloch, scintillation process with decay time τ ~ 2 ns

2) Photon propagation, refractive index n = 1.58

3) Light conversion in photomultiplier with transient time spread

4) Discrimination for varying pulse heights (walk or slewing correction needed)

5) Digitization with clock synchronization

Note: Timing resolution in single ended readout is limited by plastic size: $\sigma_t = L \cdot n/(c\sqrt{12})$

Double sided readout:

$$t = \tfrac{1}{2}(t_1 + t_2) - L \cdot n / c$$

$$\sigma_t = \tfrac{1}{\sqrt{2}} \sigma_{t_i}$$

Signal Generation in Plastic Scintillators

Organic scintillators (plastic, liquid) use a solvent
+ large concentration of primary fluor
+ smaller concentration of secondary fluor
+ ......

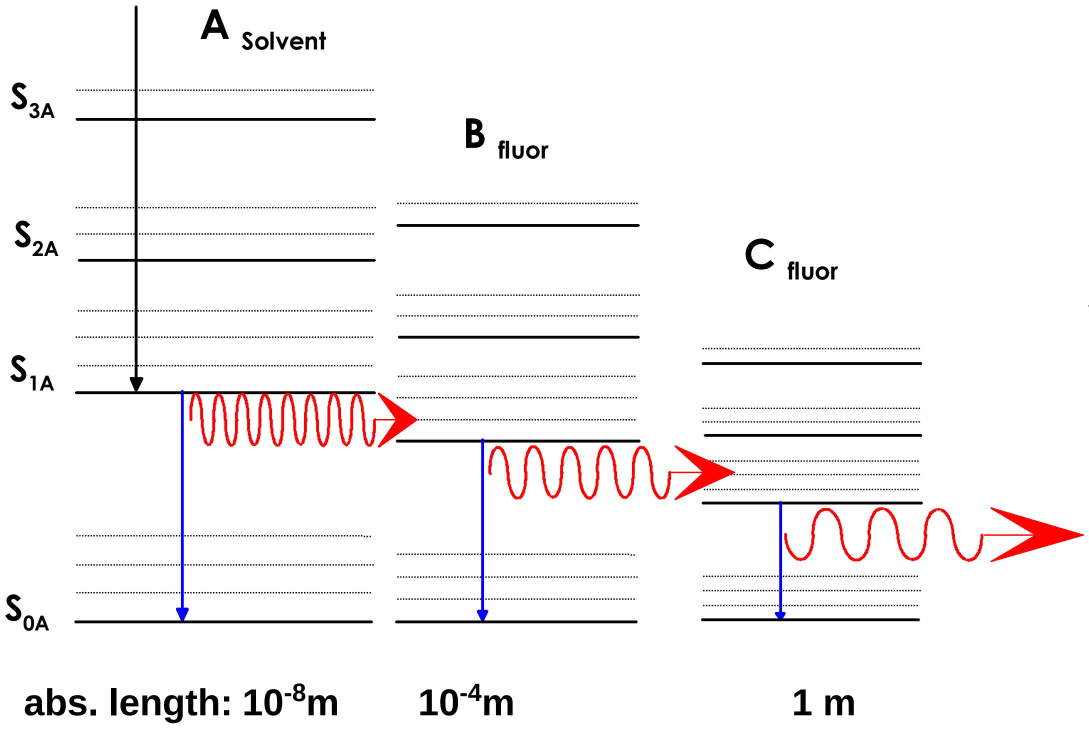

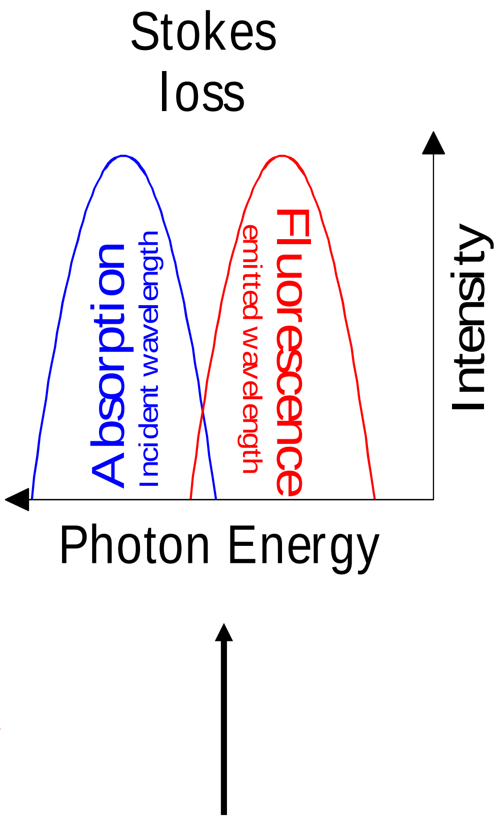

Fast energy transfer via non-radiative dipole-dipole interactions (Förster transfer).

→ shift emission to longer wavelengths

→ longer absorption length and better matching to photocathode efficiency

Properties of Plastic Scintillators

Scintillator material	Density [g/cm^3]	Refractive Index	Wavelength [nm] for max. emission	Decay time constant [ns]	Photons/MeV
NE102*	1.03	1.58	425	2.5	$2.5 \cdot 10^4$
NE104*	1.03	1.58	405	1.8	$2.4 \cdot 10^4$
NE110*	1.03	1.58	437	3.3	$2.4 \cdot 10^4$
NE111*	1.03	1.58	370	1.7	$2.3 \cdot 10^4$
BC400**	1.03	1.58	423	2.4	$2.5 \cdot 10^2$
BC428**	1.03	1.58	480	12.5	$2.2 \cdot 10^4$
BC443**	1.05	1.58	425	2.2	$2.4 \cdot 10^4$

* Nuclear Enterprises, U.K.

** Bicron Corporation, USA

Typical numbers:
Energy deposition of MIP in 1 cm plastic (Bethe – Bloch)

$\Delta E \sim 1.7$ MeV

$\Rightarrow$ ~ 50.000 photons

Only directly propagating photons contain relevant timing information!

Light propagation in plastic slat / fibre

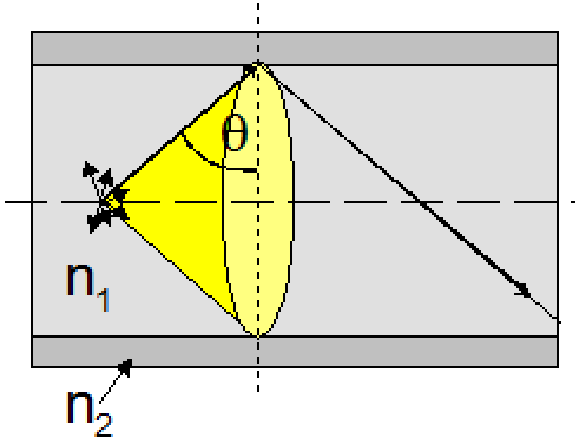

Total internal reflection

$$\theta \geq \arcsin\frac{n_2}{n_1} = \arcsin\frac{1}{1.58} = 39.3°$$

$$\frac{\Delta\Omega}{4\pi} = 18\%$$ best case, when surface is perfect

Light attenuation (absorption): $N_{ph} = N_0 e^{-\frac{d}{\lambda}}$

Example for 3 x 2 cm^2

(bulk counter wrapped with Teflon tape to optimized light yield)

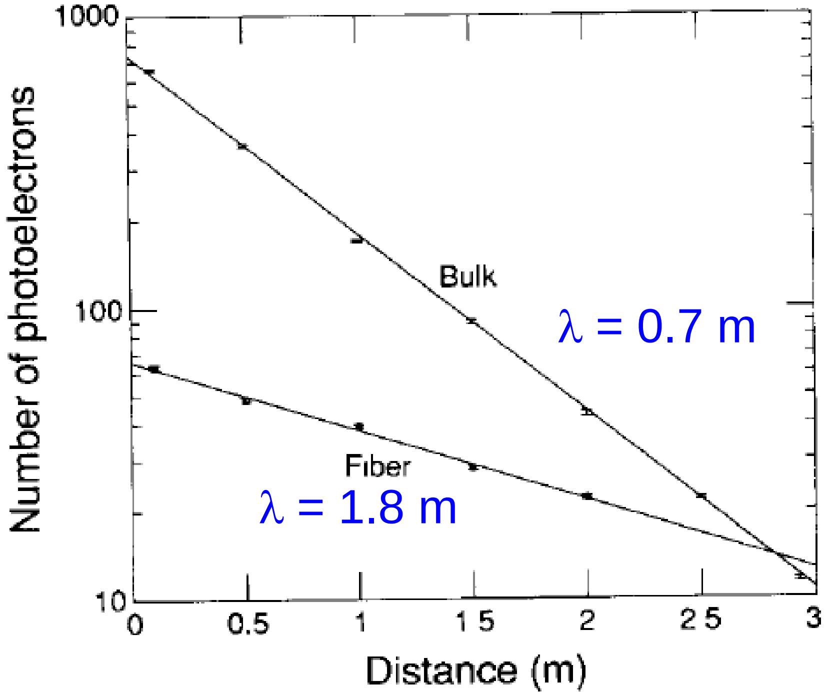

M. Kuhlen et al., NIM A301(1991)223

Impact on light propagation on timing

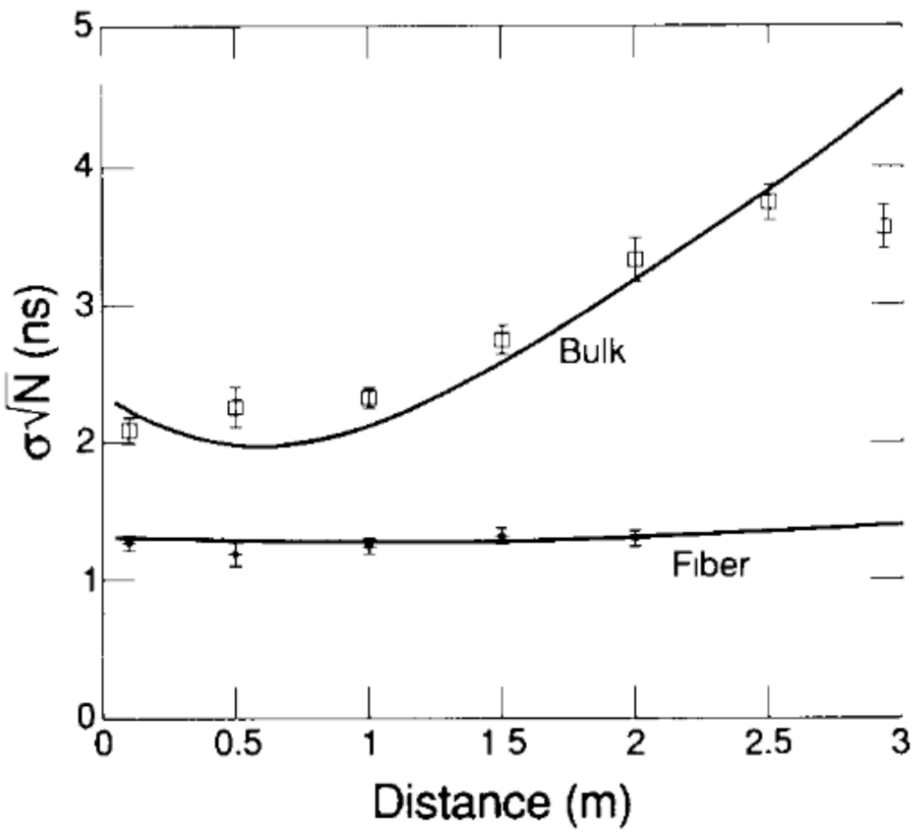

Fig. 10. Normalized time resolution for the fiber and the bulk counters. The lines show the fit to the data.

M. Kuhlen et al., NIM A301(1991)223

Timing information is carried by the early photons.
→ design systems with well defined propagation path length.

Photosensors

PMT

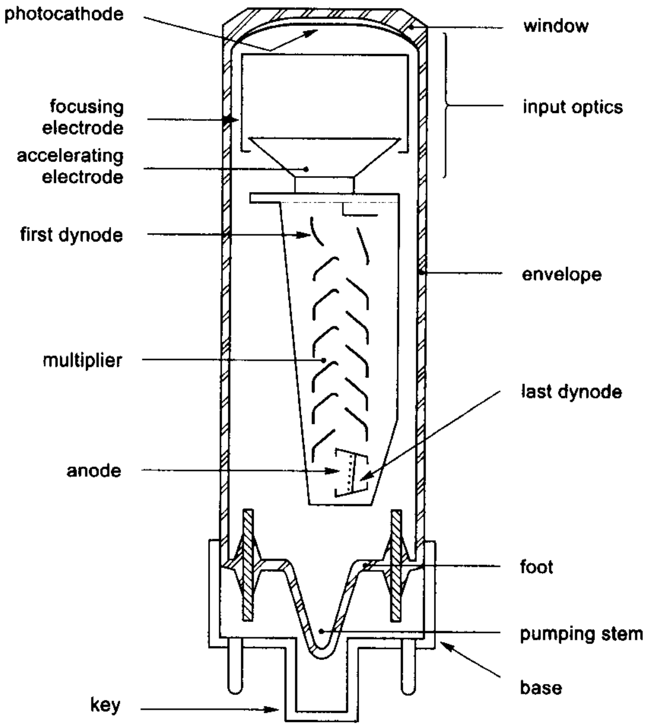

key feature for timing
path length variation from photoelectrode to first dynode
→ transient time spread

Micro channel plate (MCP)

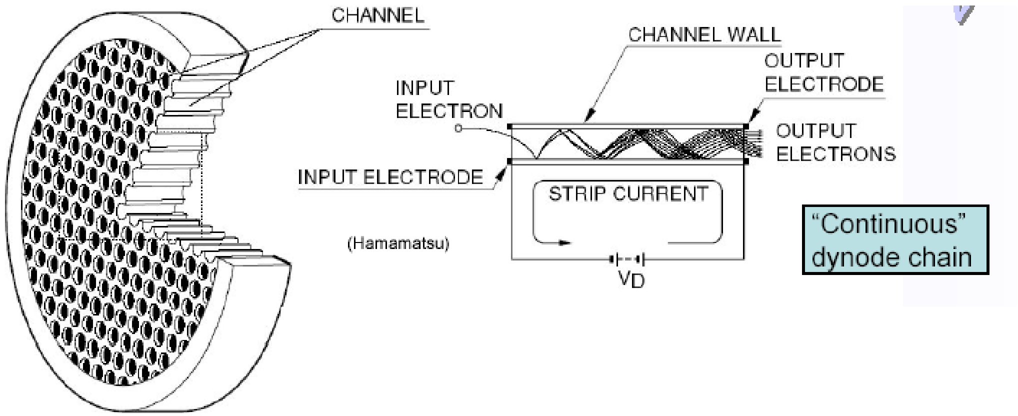

Hybrid photo diodes (HPD)

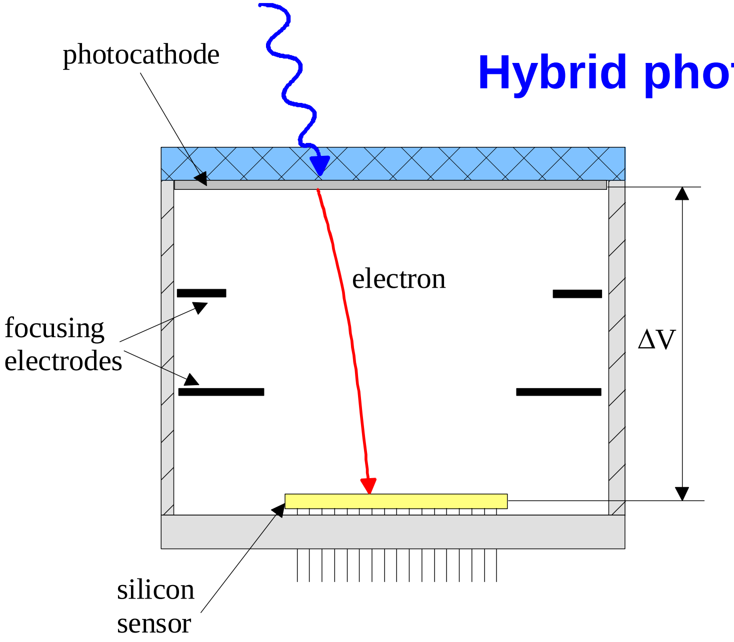

photo cathode + p.e. acceleration + silicon det. (pixel, strip, pads)

ΔV 10-20 kV

Photon detection

https://pdg.lbl.gov/2021/reviews/rpp2021-rev-particle-detectors-accel.pdf

P.A. Zyla *et al.* (Particle Data Group), Prog. Theor. Exp. Phys. **2020**, 083C01 (2020) and 2021 update.

Table 35.2: Representative characteristics of some photodetectors commonly used in particle physics.

Type	λ (nm)	$\epsilon_Q\,\epsilon_C$	Gain	Risetime (ns)	Single photon time resol. (ps)	Area (mm^2)	1-p.e noise (Hz)	HV (V)
PMT *	115–1700	0.15–0.25	10^5–10^7	0.7–10	$\sim$200	10^2–10^5	10–10^4	500–3000
MCP-PMT*	115–650	0.01–0.10	10^3–10^7	0.15–0.3	$\sim$20	10^2–10^4	0.1–200	500–3500
HPD*	115–850	0.1–0.3	10^3–10^4	$O(1)$	$\sim$1000	10^2–10^5	10–10^3	$\sim 2\times10^4$
HAPD*	115–850	0.1–0.3	10^4–10^5	$O(1)$	$\sim$30	10^2–10^5	10–10^3	$\sim 1\times10^4$
GPD*	115–500	0.15–0.3	10^3–10^6	$O(0.1)$	$\sim$100	$O(10)$	10–10^3	300–2000
APD	300–1700	$\sim$0.7	10–10^8	$O(1)$	- †	10–10^3	1–10^3	400–1400
SiPM	125–1000	0.15–0.4	10^5–10^6	$\sim$ 1	$\sim$50	1–10	$O(10^5)$	30–60

*These devices often come in multi-anode configurations. In such cases, area and noise are to be considered on a "per readout-channel" basis.

†No single photon detection possible.

Commercially available timing sensors (PMT, MCP) with suitable rise times (< 1 ns) are very expensive: ~ 1000 € / channel except for SiPM

Solid State Photosensors: SiPM

Avalanche photo diode (APD)

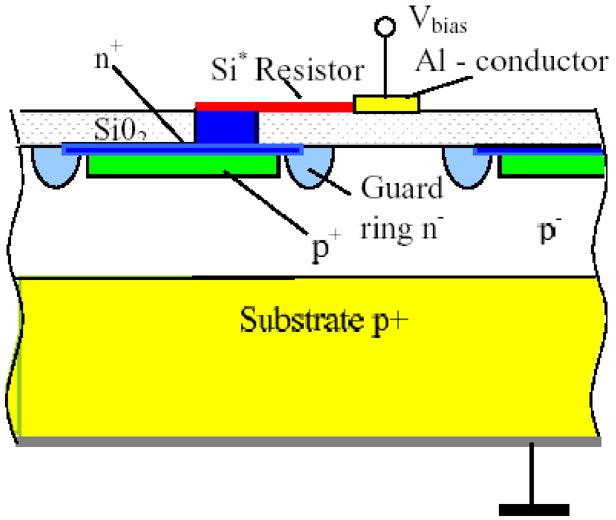

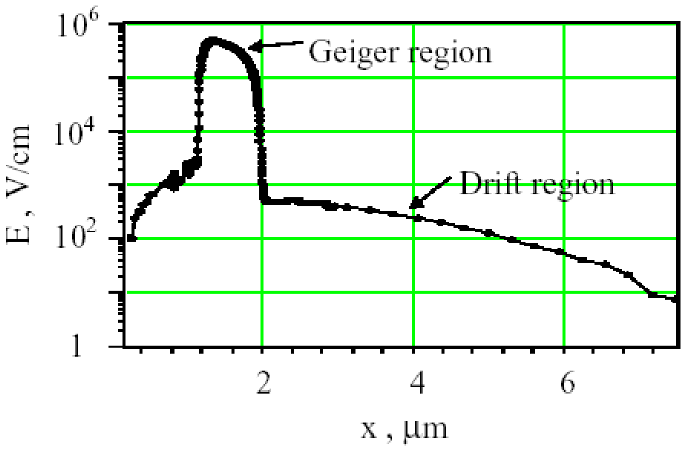

SiPM = Array of APDs
(photon counter)

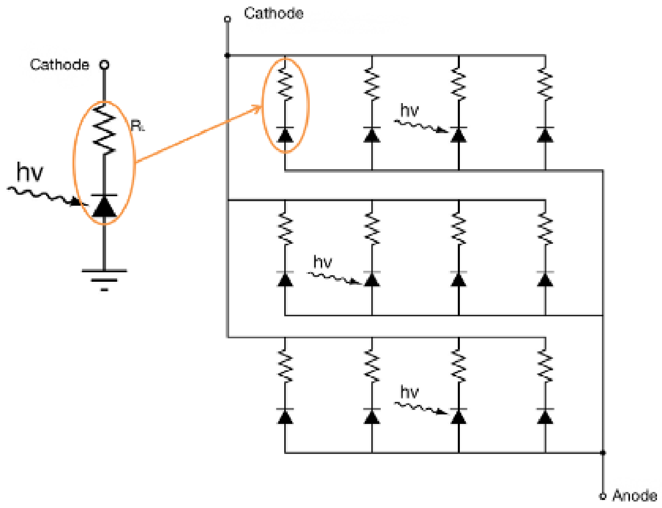

Working principle:

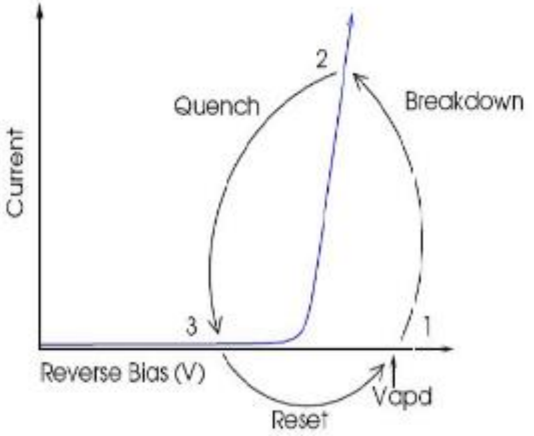

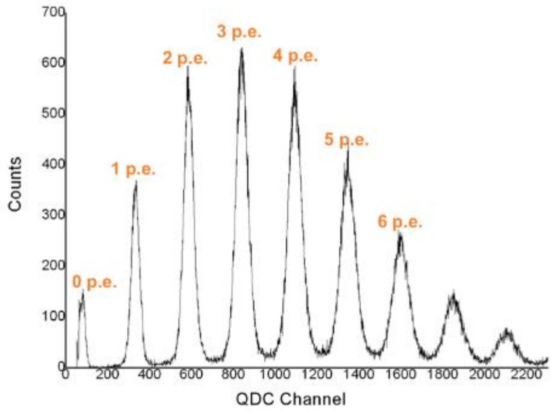

Example of SiPM

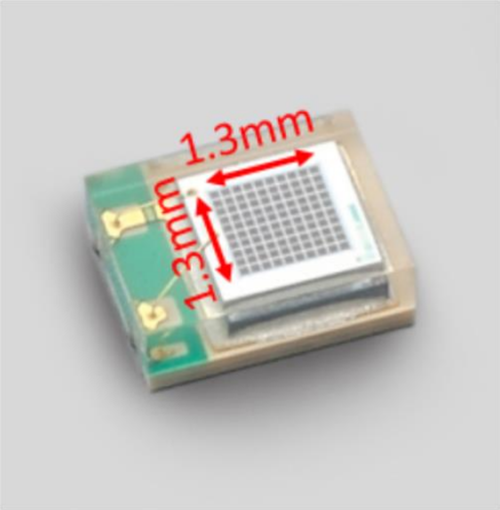

Hamamatsu MPPC-S13360-1325PE SiPM.

Parameter	Hamamatsu MPPC-S13360-1325PE
Photosensitive Area	$1.3\,\mathrm{mm} \times 1.3\,\mathrm{mm}$
Number of Pixels	2668
Pixel Pitch	$25\,\mu\mathrm{m}$
Spectral Acceptance Range	320 nm - 900 nm
Peak Sensitivity Wavelength	450 nm
Typical Breakdown Voltage at 25 °C	48 V - 58 V
Recommended Operation Voltage	$V_{breakdown} + 5\,\mathrm{V}$
PDE (at Peak Sensitivity Wavelength)	25 %
Typical Gain	7.0×10^5

Pixel recovery time: ~ 10 ns

MMPC – Multi Pixel Photon Counter

(used in AHCAL prototype, thesis D. Heuchel (2022))

Timing Characteristics of SiPM

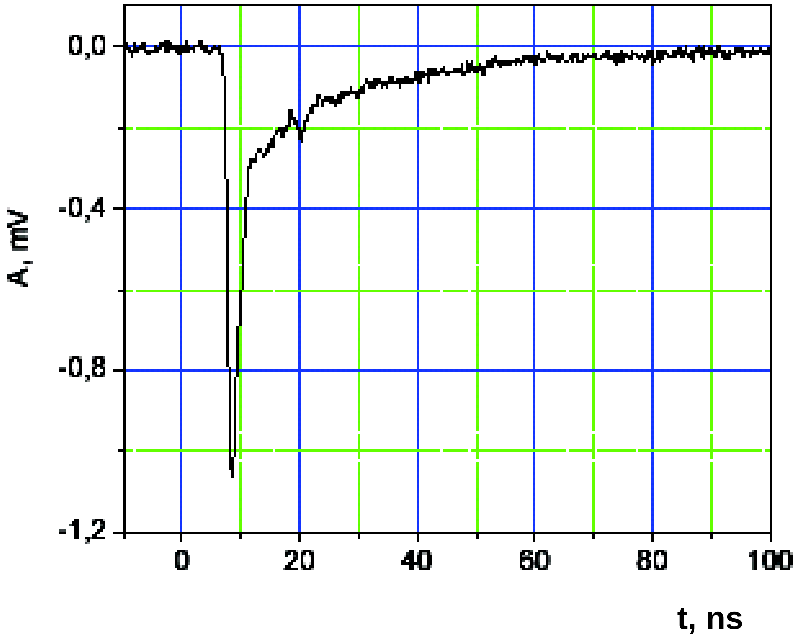

- Fast Geiger discharge development

  t_{rise} < 500 ps

- Discharge is quenched by current limiting with polysilicon resistor in each pixel I<10μA

- Pixel recovery time

  ~ $C_{pixel}R_{pixel}$=10 - 500ns

Low noise, high bandwidth electronics required.

Plastic & SiPM

A. Stoykov et al., NIM A 695 (2012) 202

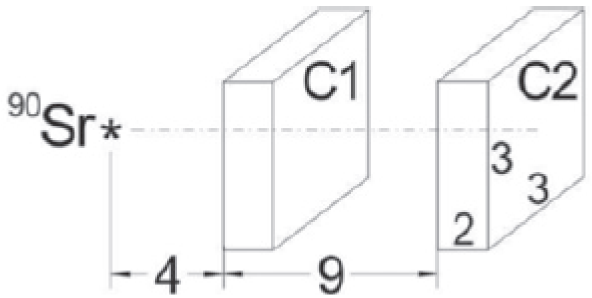

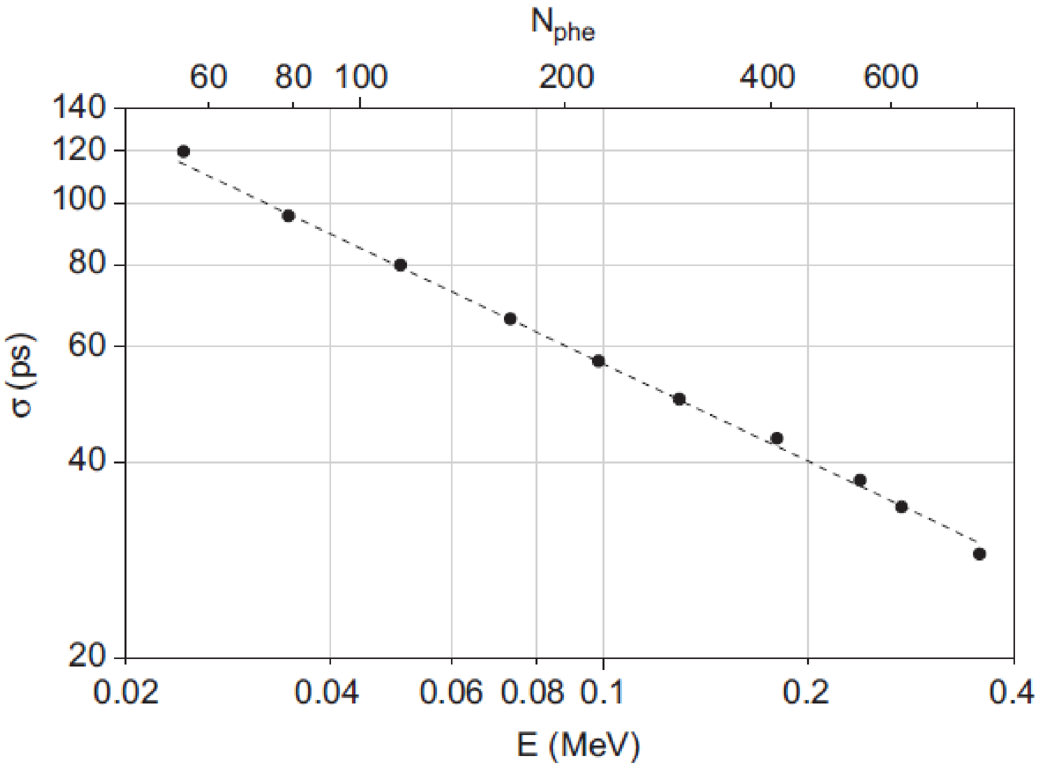

Scintillators coupled to
Hamamatsu MPPC
S10362-33-050
(3 x 3 mm^2, 3600 pixel)

Achieved time resolution: as good as for PMT!

$$\sigma_t = 18\,ps / \sqrt{E / 1\ \mathrm{MeV}}$$

Electron TOF counter with Plastic & SiPM

P.W. Cattaneo et al. (MEGII), arXiv:1402.1404v2 [physics.ins-det]

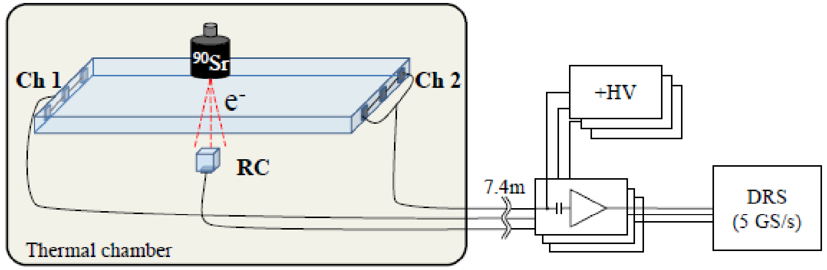

Fig. 1. Test setup for measurements of the counter time resolution. RC denotes the reference counter. See the text for details.

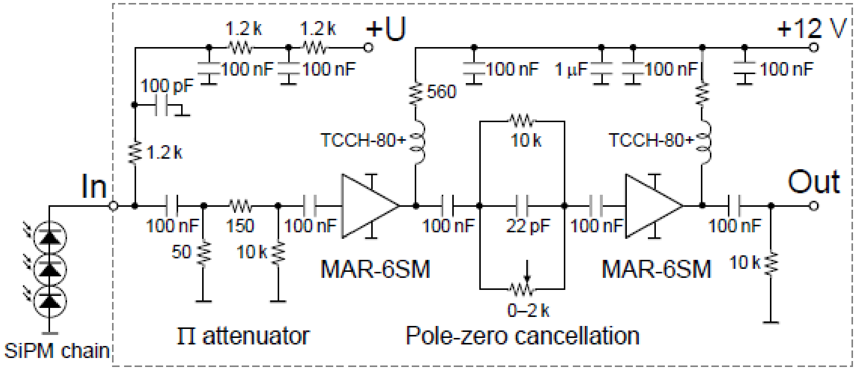

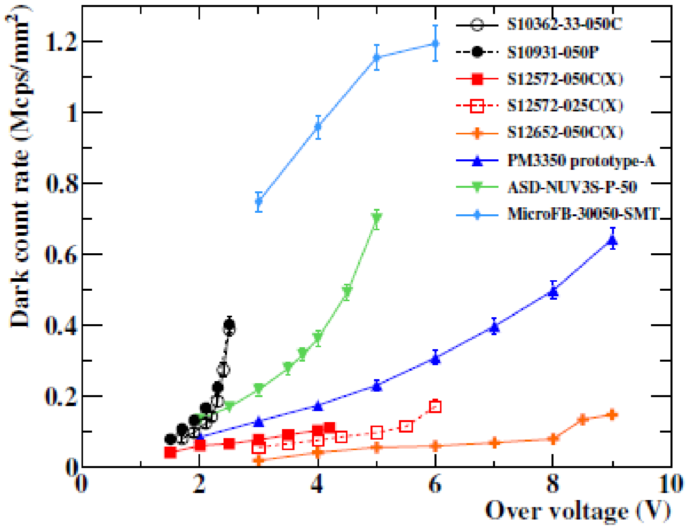

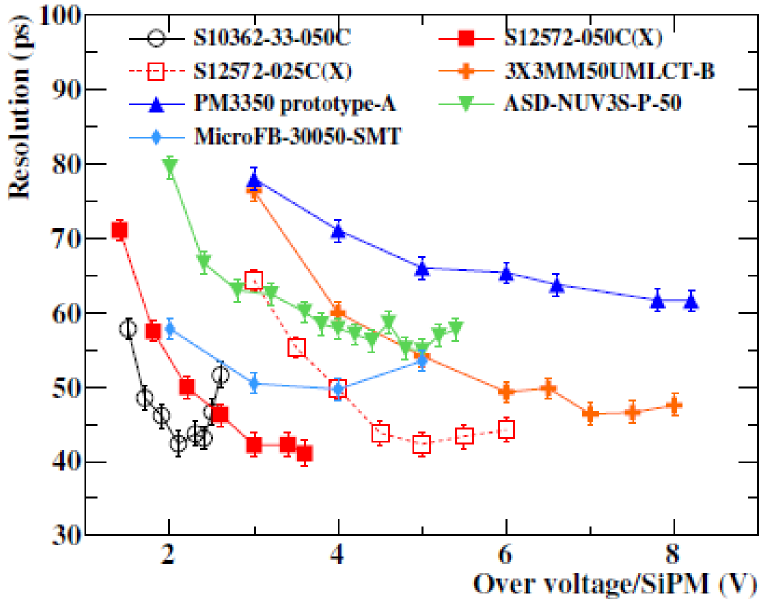

SiPM usage

Recent review: F. Simon, Silicon photomultipliers in particle and nuclear physics, Nuclear Inst. and Methods in Physics Research, A 926 (2019) 85–100

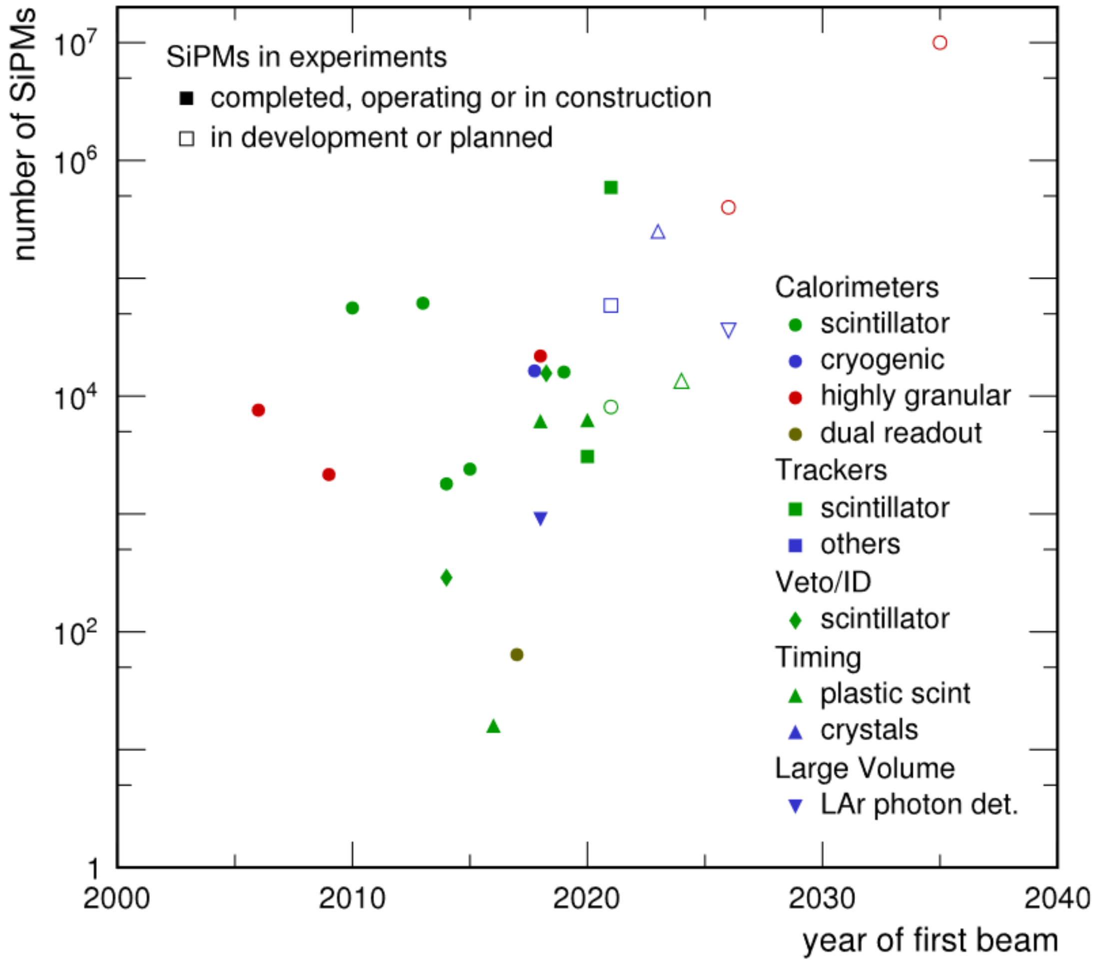

Neutron TOF counter with Plastic & SiPM

T.P. Reinhardt et al. (R3B), NIM A816 (2016) 16

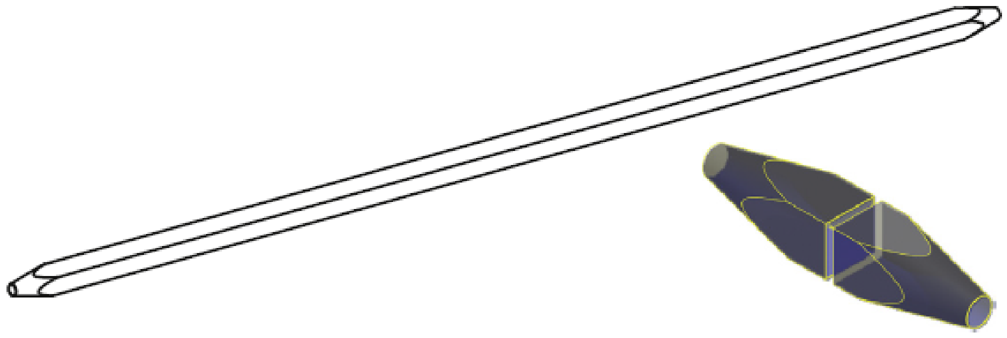

Fig. 1. NeuLAND bar. The left side shows the entire, 270 cm long NeuLAND bar. The right side shows the two tapered sides converting from 5×5 cm^2 square shape to $d = 2.5$ cm circular shape.

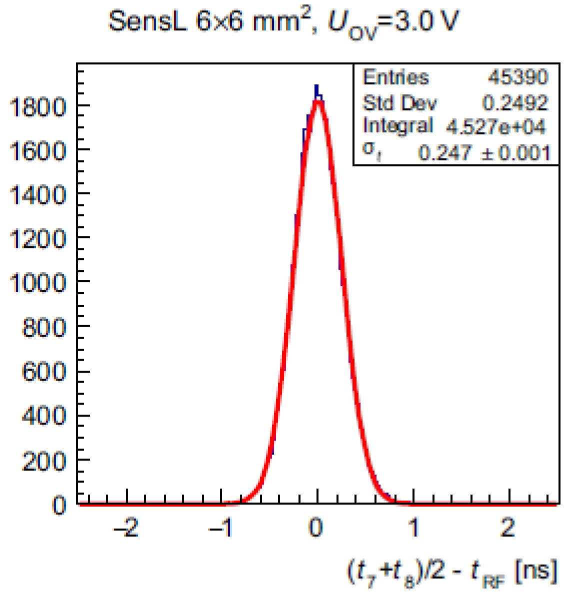

Test beam results with
30 MeV e$^-$ @ ELBE

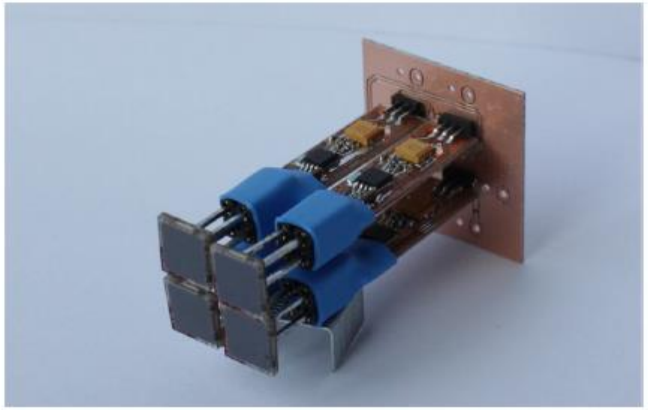

Fig. 2. Photograph of the preamplifier board, complete with four 6×6 mm^2 SiPMs. When in use, the SiPMs are separated from the board by a neoprene layer that is penetrated by the pin connectors of the SiPMs.

Performance better than with PMT
(although not all the area was covered with sensors)

Efficiency: 99 +/- 1 %
Timing resolution: σ_t = 136 +/- 2 ps

Radiation damage of SiPM

E. Garuti, Yu. Musienko, arXiv:1809.06361 [physics.ins-det]

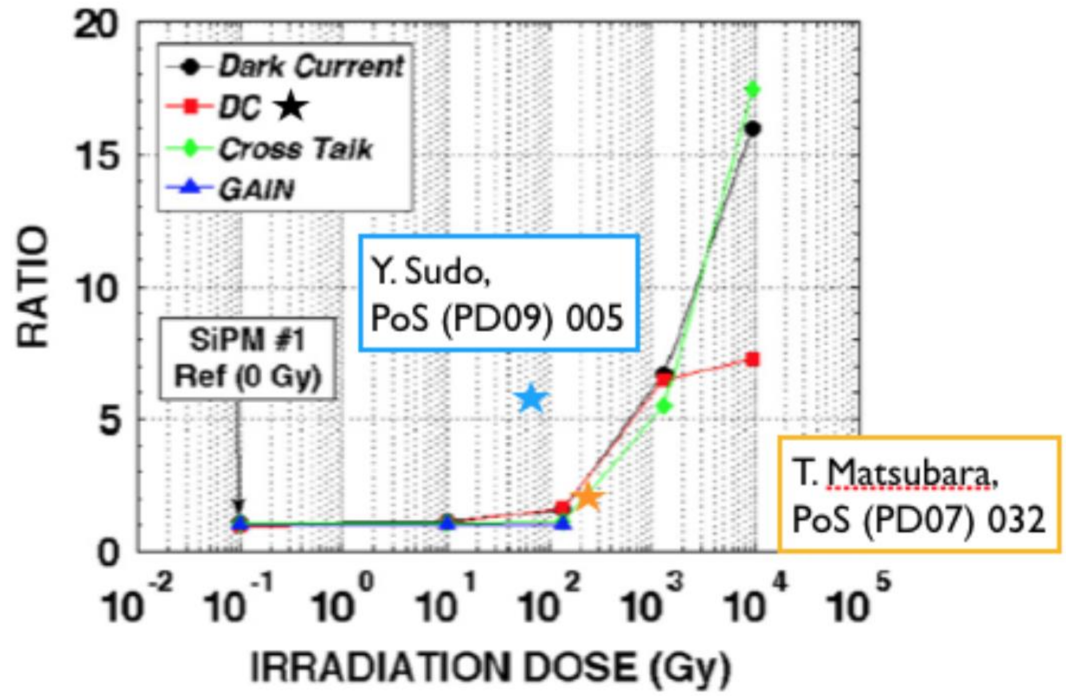

Figure 12: Ratio of measured quantities vs. irradiation dose. Modified from [31]. The red squared indicate the Dark Counts (DC) from [31] taken at $\Delta V = 3$ V ($\Delta V/V_{bd} = 11\%$). The two additional star points indicate measurements from [29] (orange) and [32] (blue).

Limiting feature:

strong increase of dark current and dark count rate after irradiation

Active research field!

Radiation Level of CBM

A. Senger, CBM – TN 18001

Fluka calculation for 2 month running with 10^9 Hz Au beam

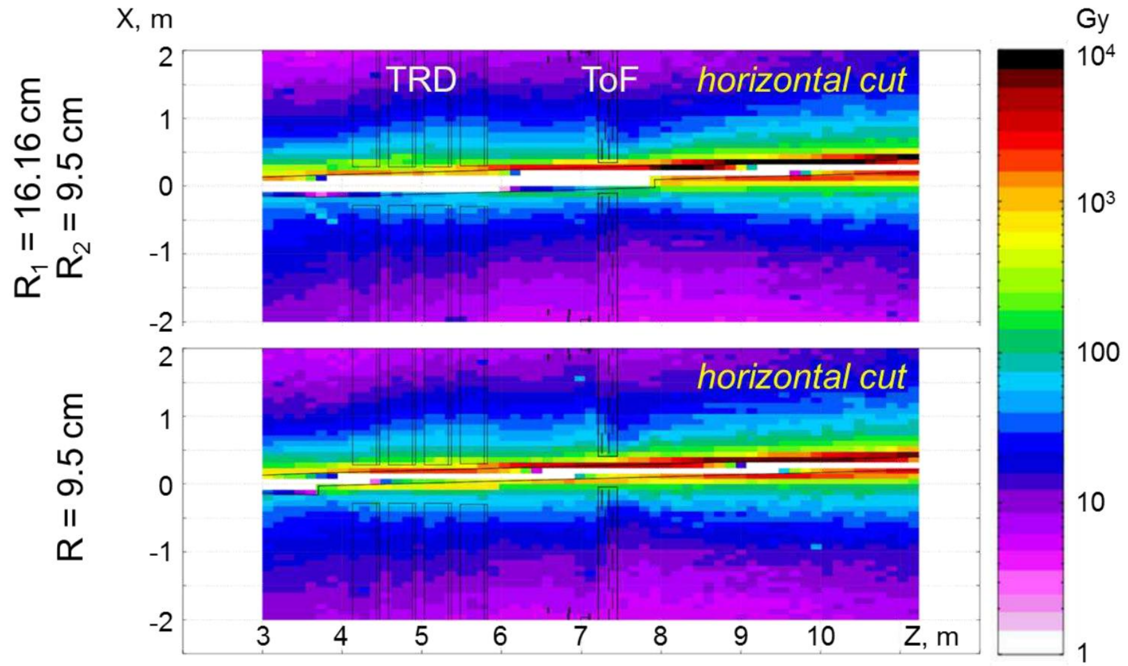

Fig.12: Ionizing dose in the CBM cave for the two beam pipe options (see text).

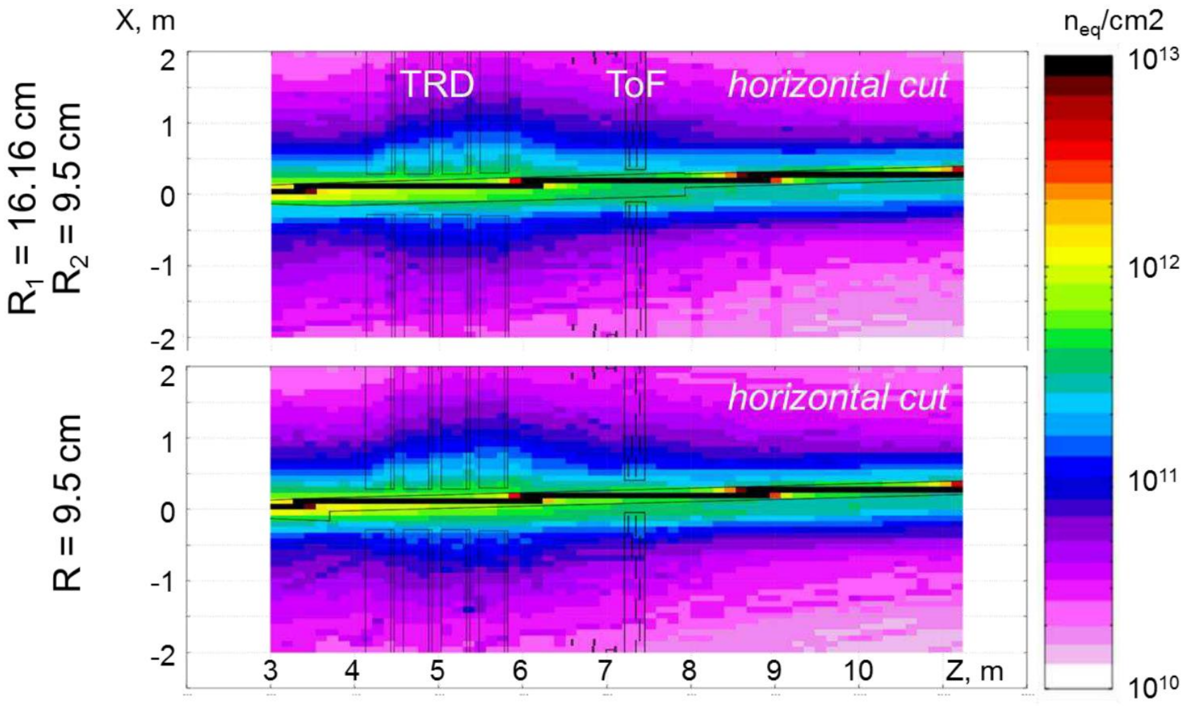

Fig.13: Non-ionizing dose in the CBM cave for the two beam pipe options (see text).

STAR Event Plane Detector

J. Adams et al., arXiv:1912.05243 [physics.ins-det]

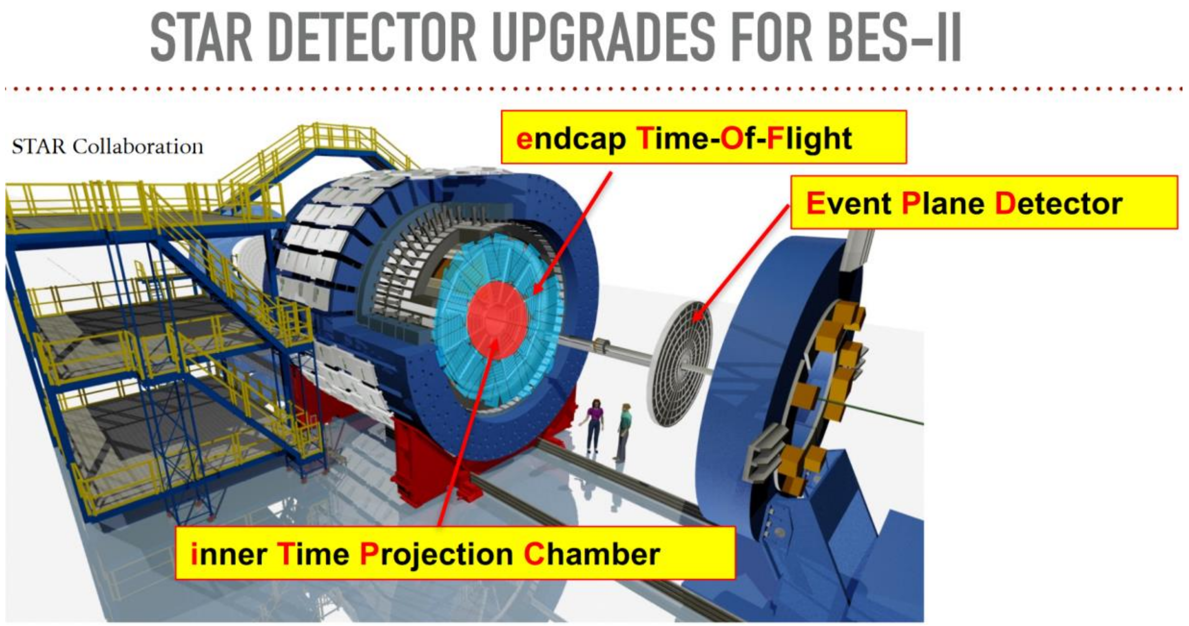

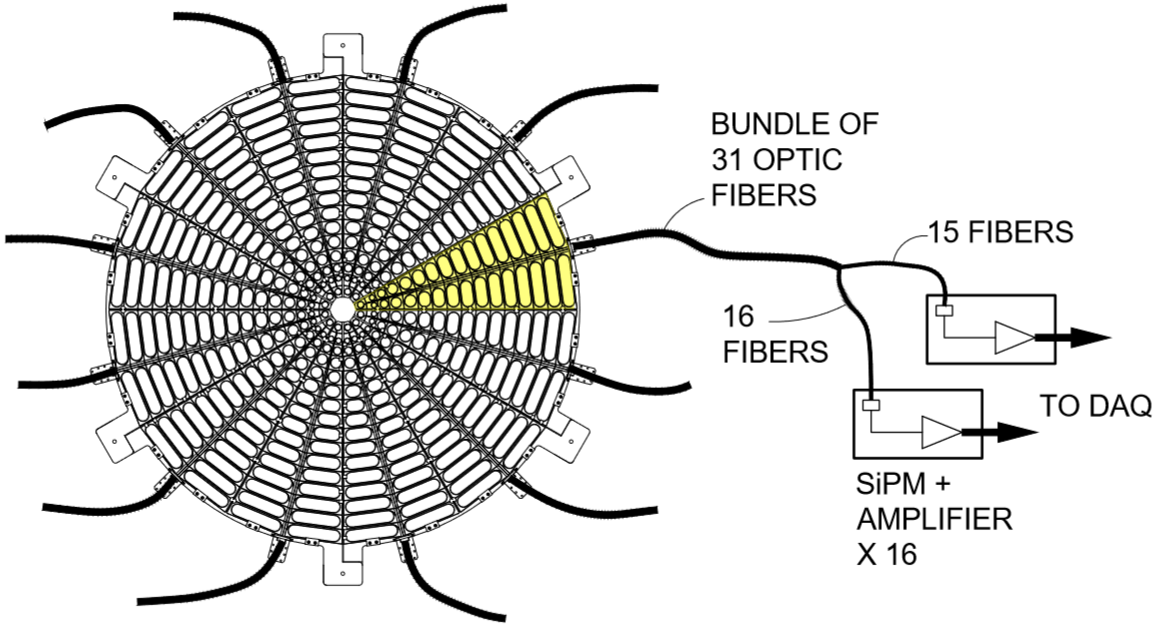

1.2 cm thick plastic scintillator (Eljen EJ-200) planes
Radius of scintillator wheel: 85 cm
WLS fibers to outer rim
Optical fibre length ~5m
Hamamatsu S13360-1325PE MPPC located
3m away from beam pipe behind iron shield (magnet yoke)

Timing with Gas Counters

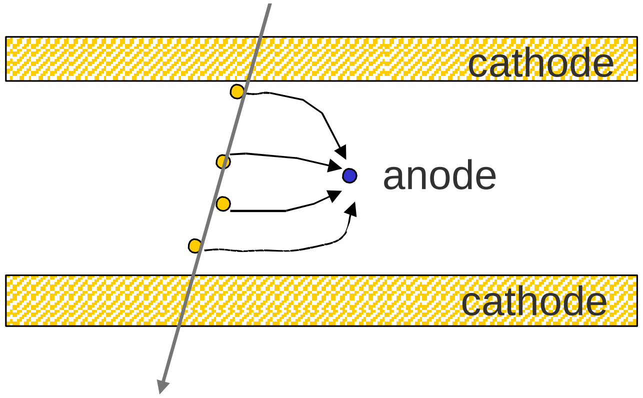

Problem:
"slow" drift of electrons from primary ionization to amplification region
$v_{drift} \sim 10\ \mu m/ns$

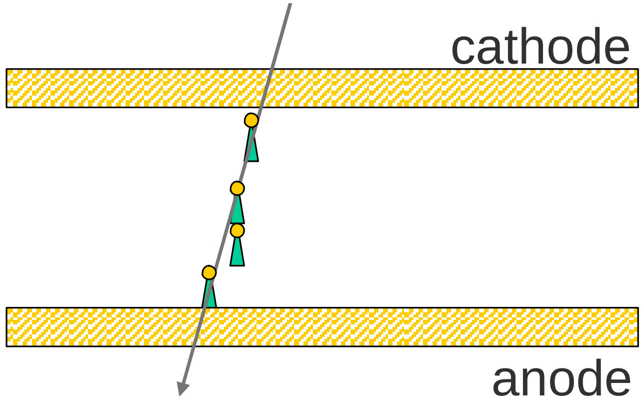

Concept:
detect avalanches directly,
large E-field in whole detector volume

Electron multiplication

Cloud chamber picture of electron avalanches in parallel plate counter

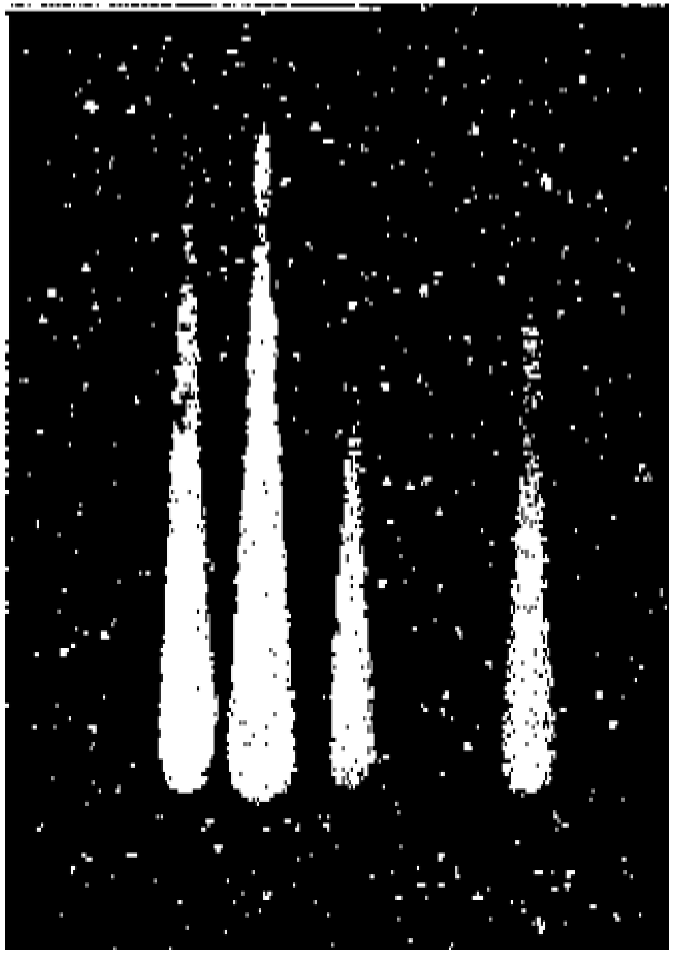

W. Legler, Z. Naturforschung 16a, 253 (1961)

$$\frac{d\bar{n}}{dx} = \underbrace{(\alpha - \eta)}_{\alpha_{eff}} \bar{n}$$

$$\frac{d\bar{p}}{dx} = \alpha \bar{n}$$

$\bar{n}$ - average electron number
$\bar{p}$ - average positive ion number

α – Townsend coefficient

η – attachment coefficient
(electron can get attached to an atom forming a negative ion)

$$\bar{n}(0) = 1,$$
$$\bar{n}(x) = e^{(\alpha-\eta)x}$$

$$\bar{p}(0) = 0$$
$$\bar{p}(x) = \frac{\alpha}{\alpha - \eta}\left(e^{(\alpha-\eta)x} - 1\right)$$

Avalanche growth

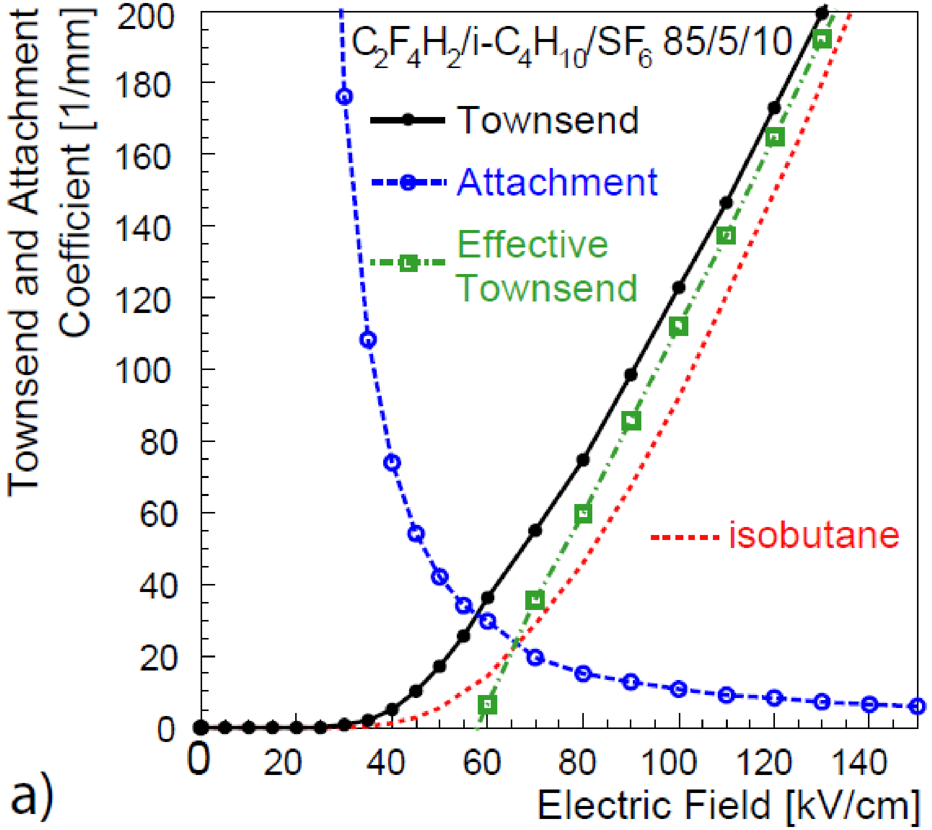

W. Riegler, C. Lippmann, R. Veenhof

NIM A500 (2003) 144

IMONTE calculation: S. Biagi (CERN)

Operating point:

E=100 kV/cm

α_{eff} = 100 / mm

Over a distance of 0.2 mm
a single electron would generate
$5 \cdot 10^8$ electrons (Q=80pC).

However: space charge effects!
Raether limit: multiplication $M < 10^8$, $\alpha x < 20$

Timing with Parallel Plate Counters

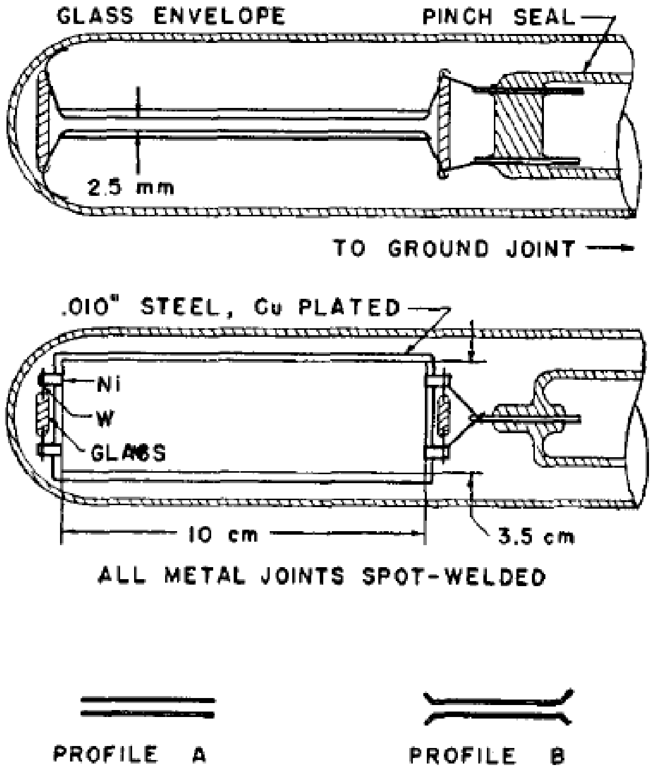

FIG. 2. Schematic drawing of the experimental parallel-plate counters.

J. W. Keuffel, Rev. Sci. Instr. 20, 202 (1949)

Time resolution: ~ 1ns

Rate capability: ~ 20 Hz

Done at CalTec, Pasadena, California

Local Discharge Spark Counter

A Picosecond Time-of-flight Spectrometer For The Vepp-2m
Based On Local - Discharge Spark Counter
Yu.N. Pestov, G.V. Fedotovich, SLAC-TRANS-0184, IYF-77-78 (1978)

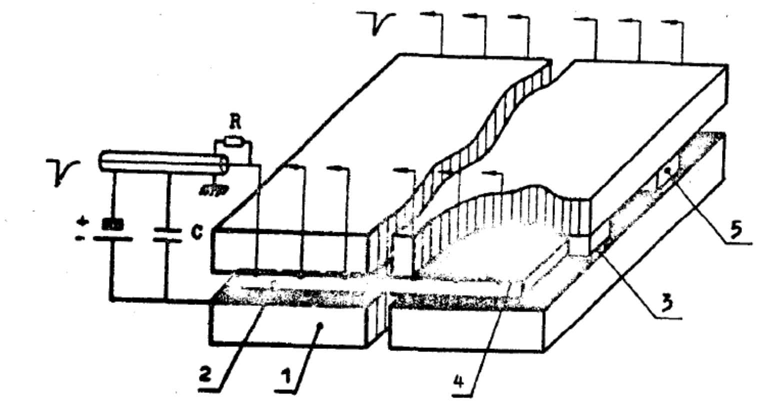

FIGURE 2: Diagram of spark counter:
1, Negative electrode; 2, Electrode of semiconducting glass; 3, Steel inserts determining gap between electrodes; 4, Copper strips; 5, Optical glass inserts

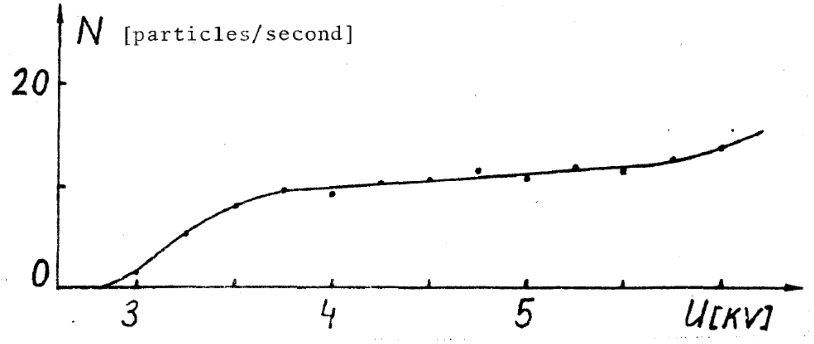

FIGURE 3: Counting characteristic of spark counter

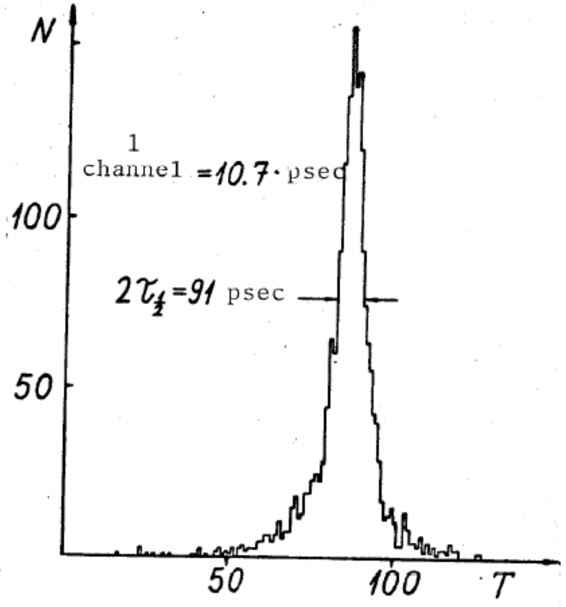

FIGURE 4: Diagram of fluctuations in time delay between operation of two spark counters upon passage of individual cosmic ray particles

Pestov - counter

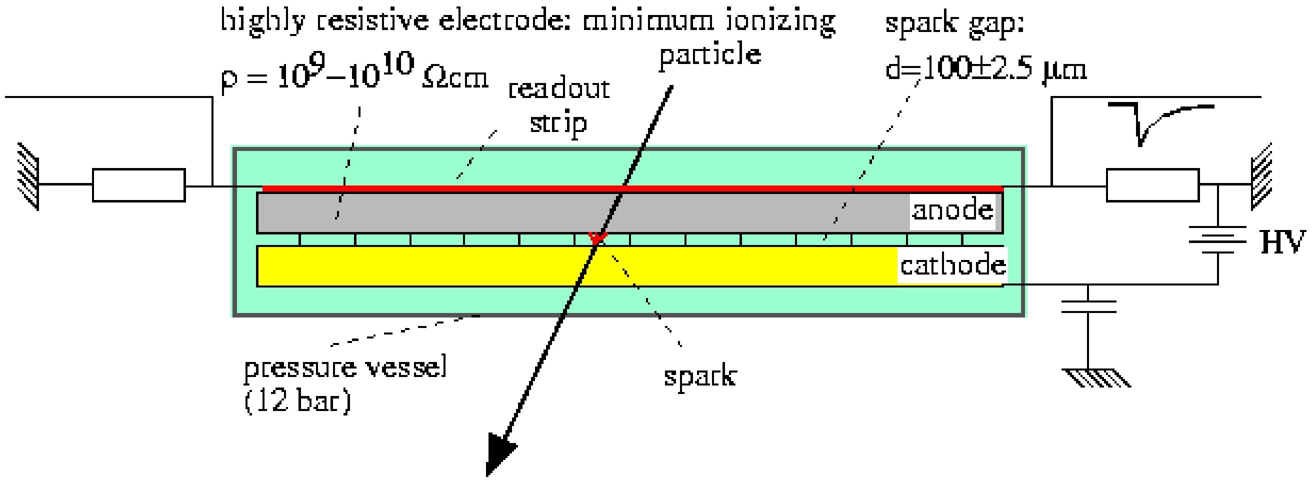

A. Devismes et al., (FOPI)
NIM A 482, 179 (2002)

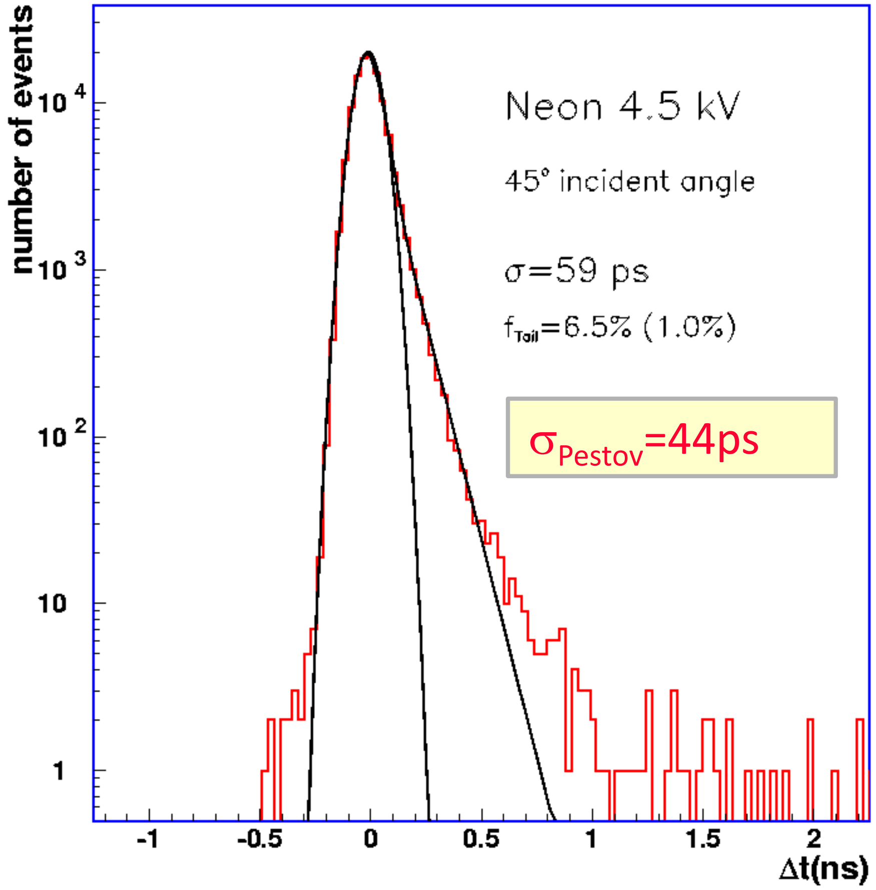

Developed for SPS NA49 and ALICE
Still used in NA61 SHINE

Signal pulse height: several V
Works without preamplifier.

Technologically too challenging,
Resistive electrode could not be produced industrially.

Resistive Plate Chamber

“Trigger RPC” R.Santonico, R. Cardarelli, NIM 187 (1981) 377-380

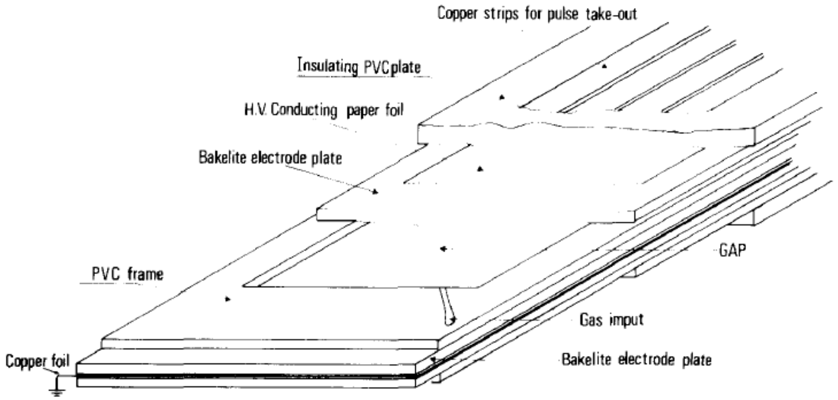

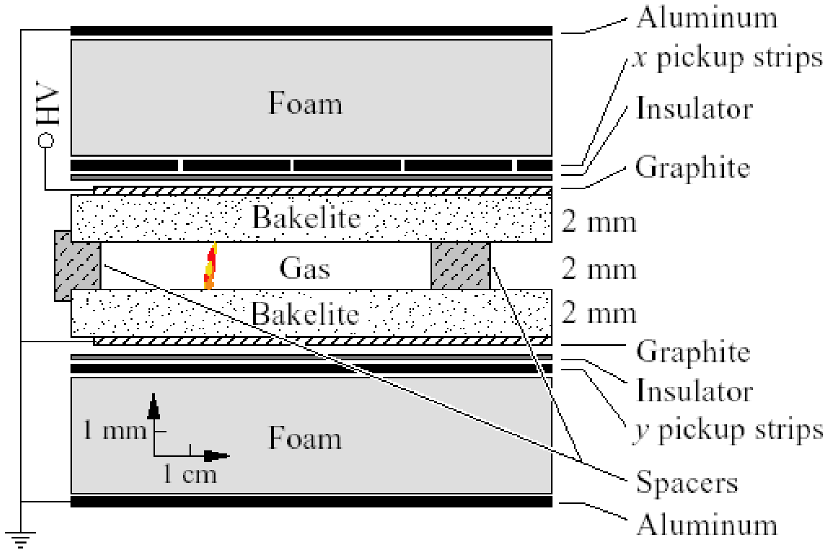

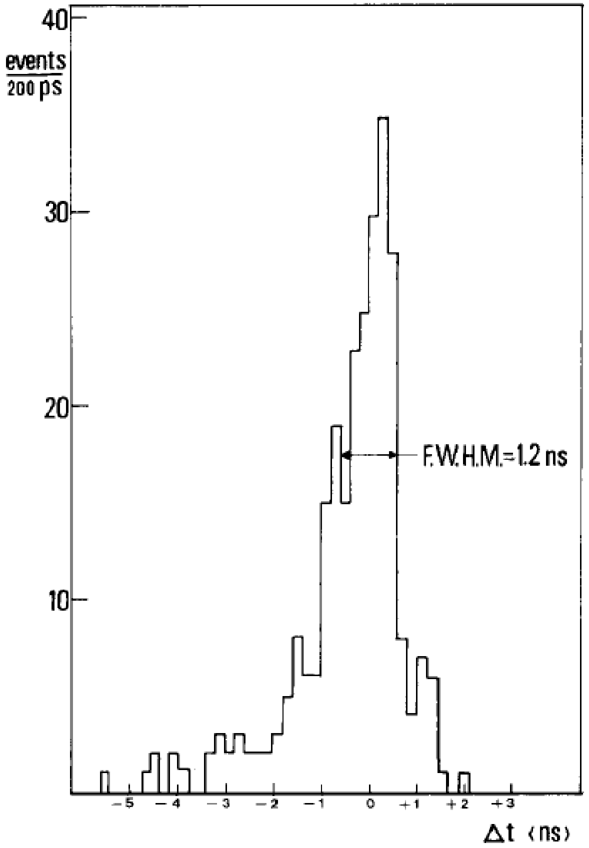

Fig. 5. Distribution of the relative delay Δt between the RPC and a small scintillation counter (T4) viewed by an XP 2020 photomultiplier. The fwhm of the distribution is 1.2 ns. The short tail on the left originates from delayed pulses of the RPC.

BaBar type Bakelite RPC
Streamer mode: low cost electronic
Problems due to electrode surfaces (linseed oil)
Time resolution ~ 5 ns => Trigger RPC

Multigap RPC

E.C. Zeballos et al., A new type of Resistive Pate Chambers : The Multigap RPC, Nucl. Inst. and Methods A 374 (1996) 132

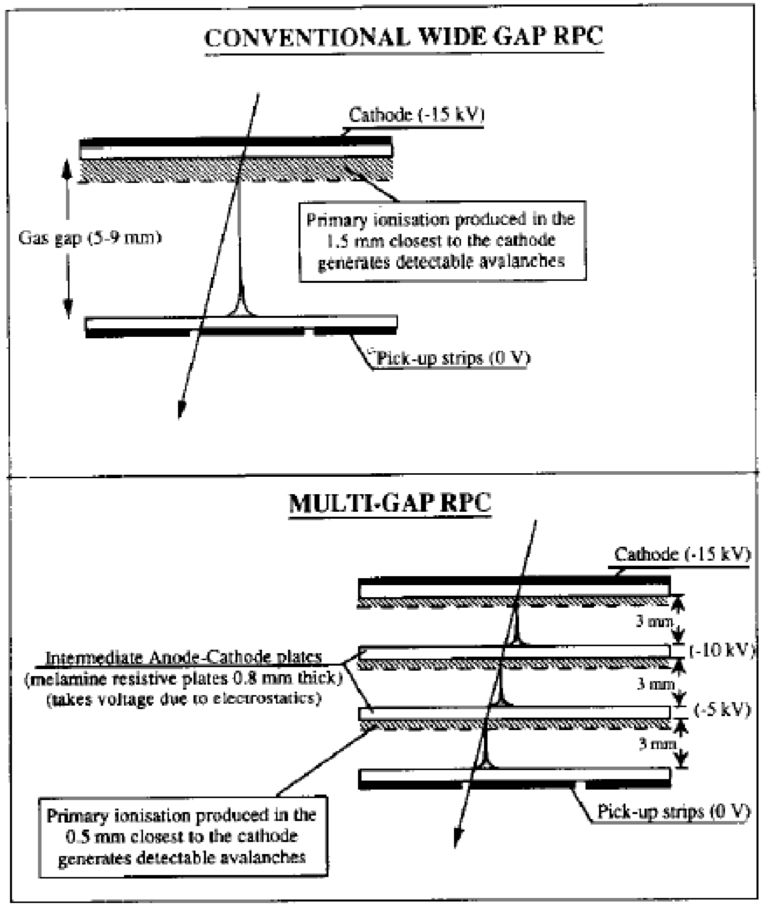

Fig. 1. Schematic diagram and principle of operation of multi-gap RPC compared to a conventional 9 mm single gap RPC.

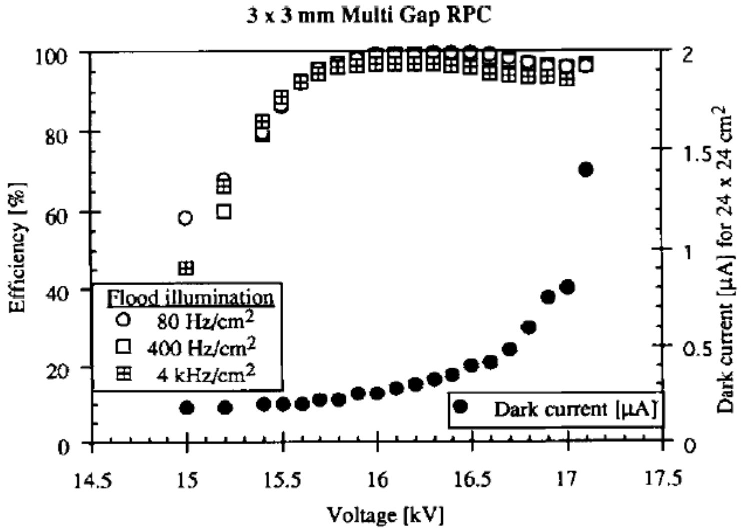

Fig. 2. Efficiency versus high voltage for various fluxes. The beam was defocused, thus the whole active area of the chamber exposed. The gas mixture was 86% argon, 8.5% CO_2, 0.5% C_4F_{10} and 5% DME.

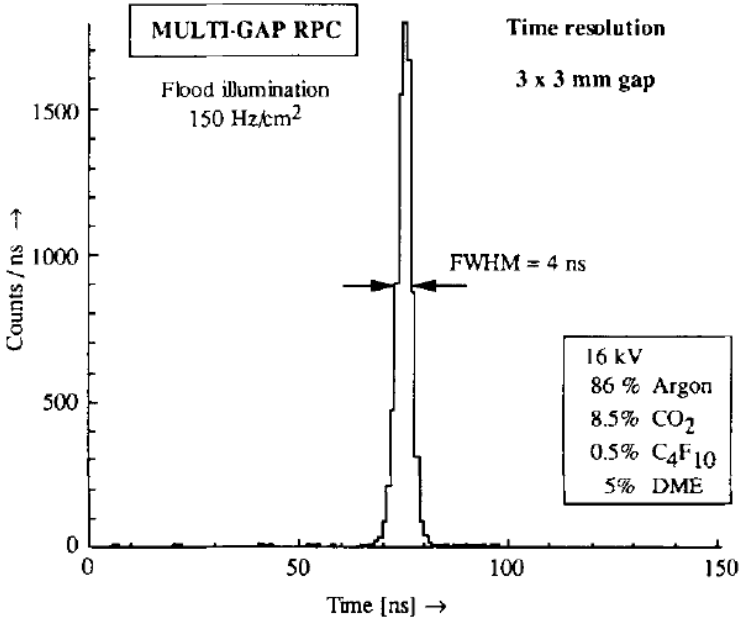

Fig. 3. Time spectra of the average of the leading and trailing edge timing at 16 kV (200 V above the knee of the efficiency plateau).

Timing Multigap RPC

P. Fonte, A. Smirnitski, M.C.S. Williams,
A new high-resolution TOF technology, Nucl. Inst. and Methods A 443 (2000) 201-204

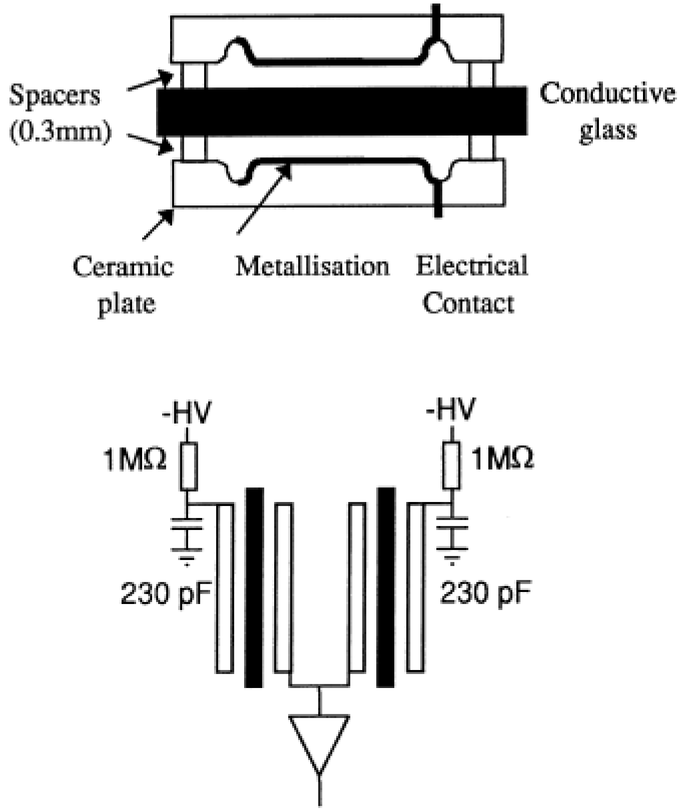

Fig. 1. Schematic representation of the structure of a single RPC cell, made with two metallised, profiled, ceramic plates placed on each side of a central glass plate. Two of such cells are electrically connected in parallel to form a single detector.

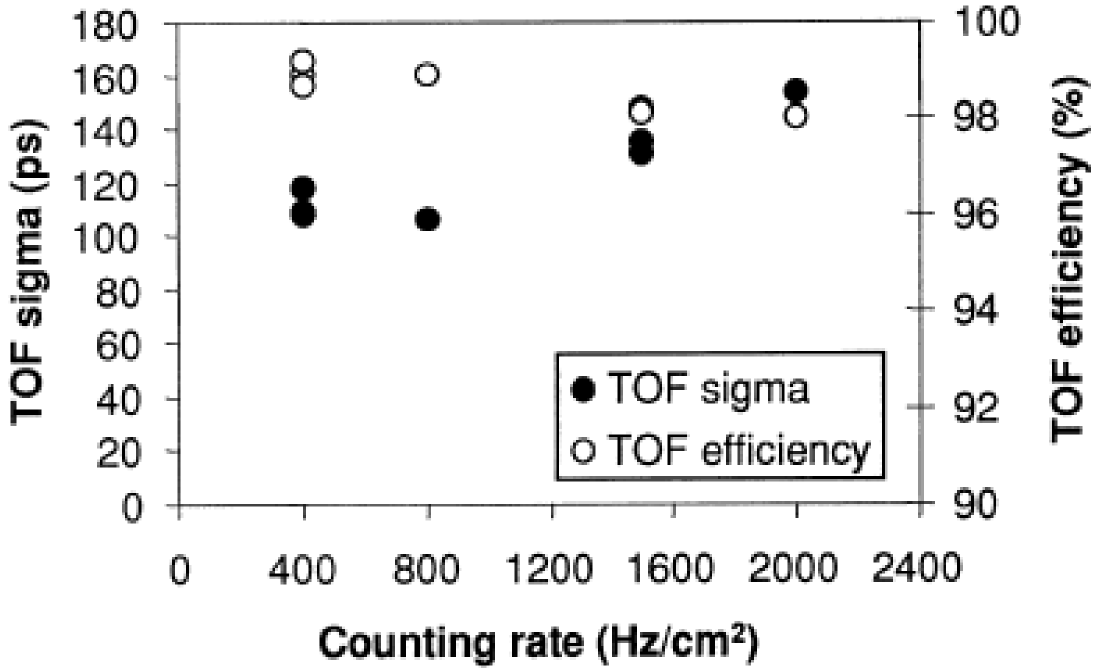

Fig. 5. Timing resolution and efficiency as a function of the counting rate per unit area. For counting rates below 800 Hz/cm^2 a resolution better than 120 ps sigma was achieved with efficiency above 98%.

Multi-gap Resistive Plate Chamber (MRPC)

floating resistive glass electrodes with gas gaps

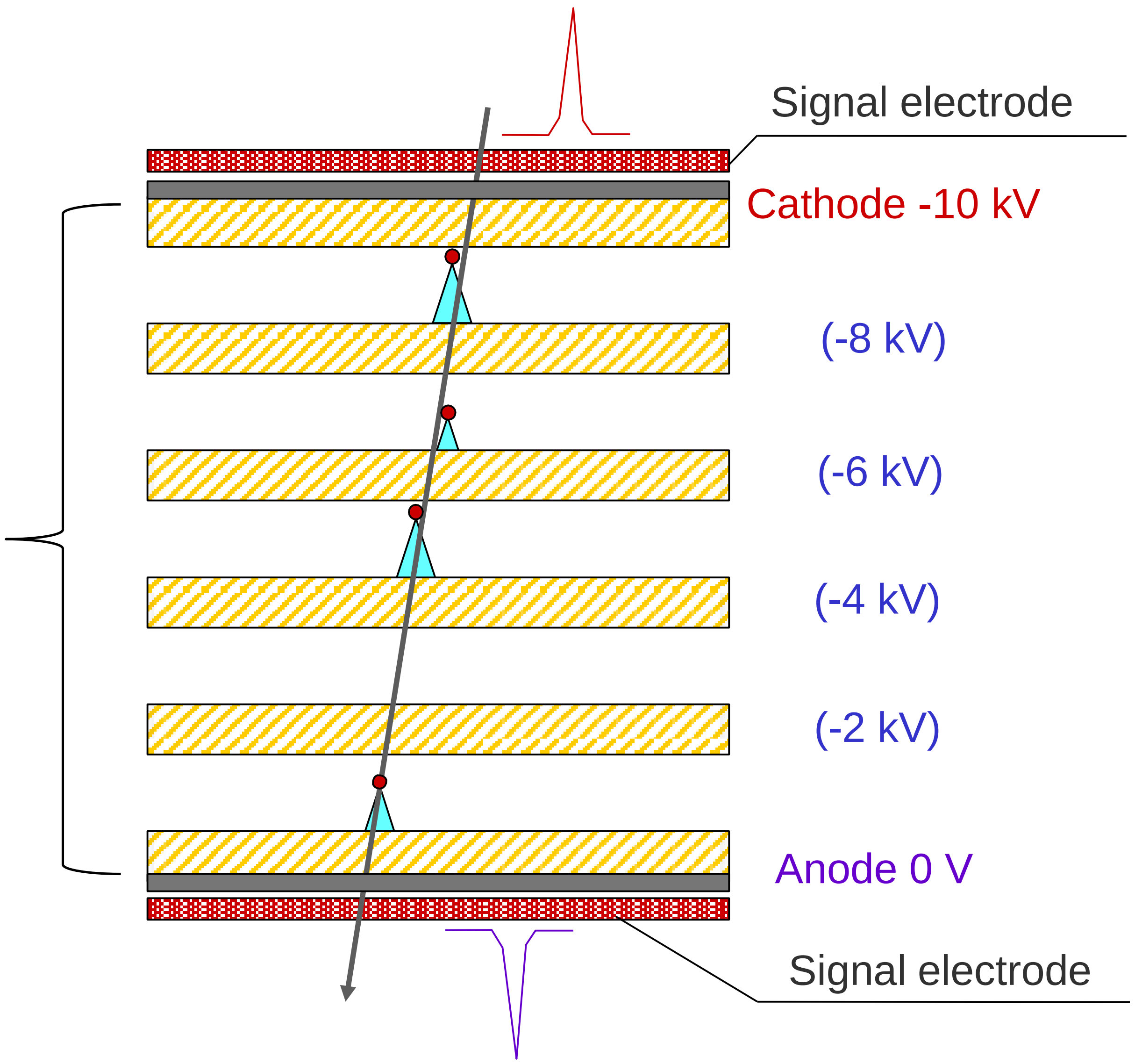

Stability of MRPC operation

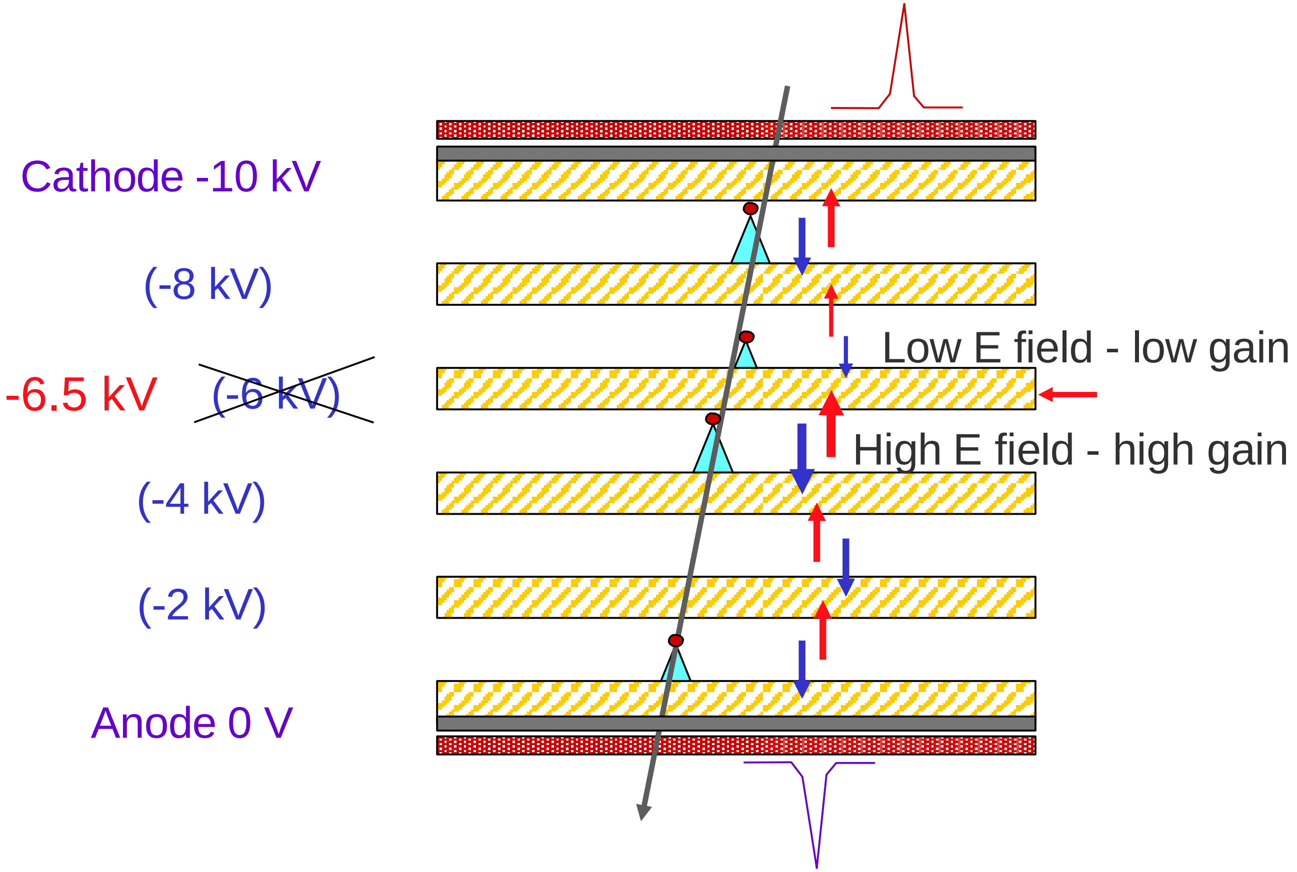

Avalanche gain dependence automatically corrects potentials on the resistive plates – stable situation is ”equal gains in all gas gaps”

RPC signal generation

W. Riegler, NIM A491, 258 (2002)

Mechanism: **Induction**

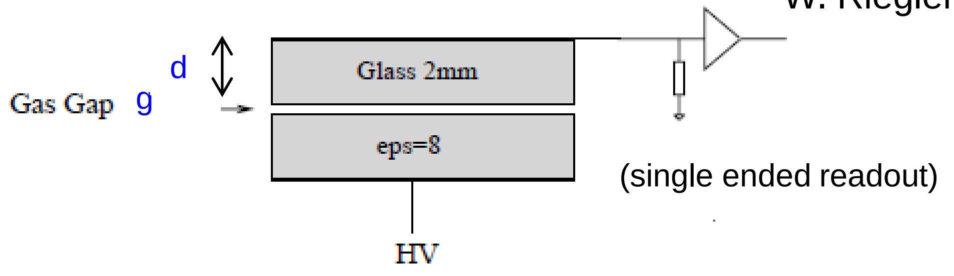

Shockley – Ramo - theorem:

Assume perfectly conducting electrodes:

$$I(t) = Q\vec{E}(\vec{x}) \cdot \dot{\vec{x}}(t)$$

electrons generate the signal

$$\vec{E}(\vec{x}) - \text{static electric field}$$

with resistive elements;

$$I(t) = \frac{E_W \cdot \mathrm{v}_{\mathrm{drift}}}{V_W} e_0 N(t)$$

N(t) – number of electrons in avalanche

$$E_{\mathrm{W}} - \text{weighting field, } V_W - \text{weighting potential}$$

$$\frac{E_W}{V_W} = \frac{\varepsilon_r}{2d + g\varepsilon_r}$$

$$\text{from } \sum_{i=1}^{b} E_i d_i = V_W\,, \qquad \text{with } \varepsilon_i \;\; E_i = \varepsilon_j \;\; {}_{\mathrm{j}}E_j \text{ for neighbouring layers}$$

Intrinsic timing resolution

Timing determined by crossing
a discriminator threshold

- sufficiently fast amplifier
- low threshold,
- no saturation effects

$$i(t) = Ae^{(\alpha-\eta)vt} = A_{thr}$$

W. Riegler et al., NIM A500, 144 (2003)

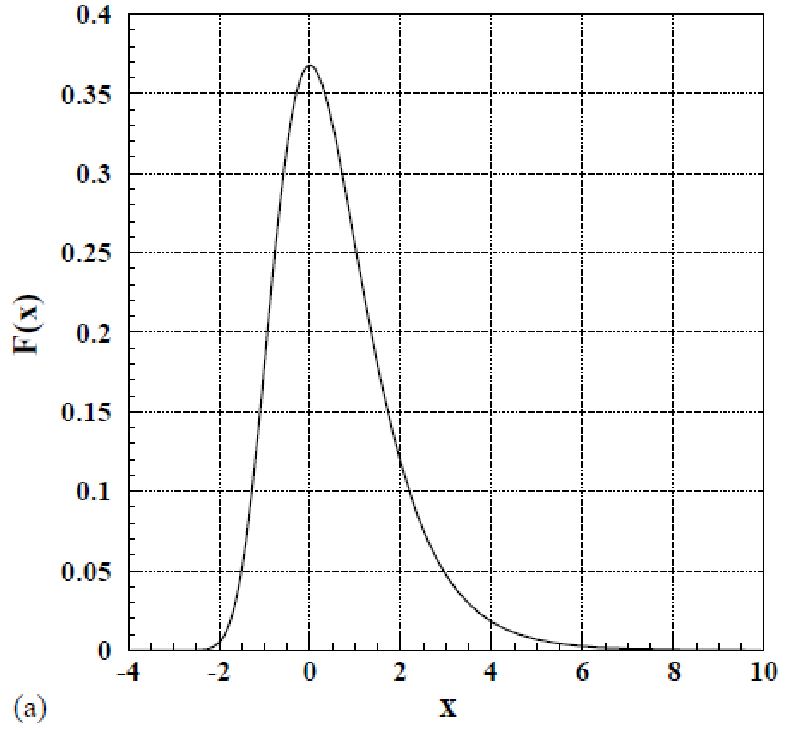

Probability to cross threshold at time t:

$$P(t) = (\alpha-\eta)vF((\alpha-\eta)vt)$$

$$F(x) = \exp(x - \exp(-x))$$

Time resolution of single gap:

$$\sigma_t = \frac{1.28}{(\alpha-\eta)v}$$

Operating point:
E=100 kV/cm
α_{eff} = 100 / mm
v = 200 μm/ns
=> σ_t = 64 ps

20 ps MRPC timing device

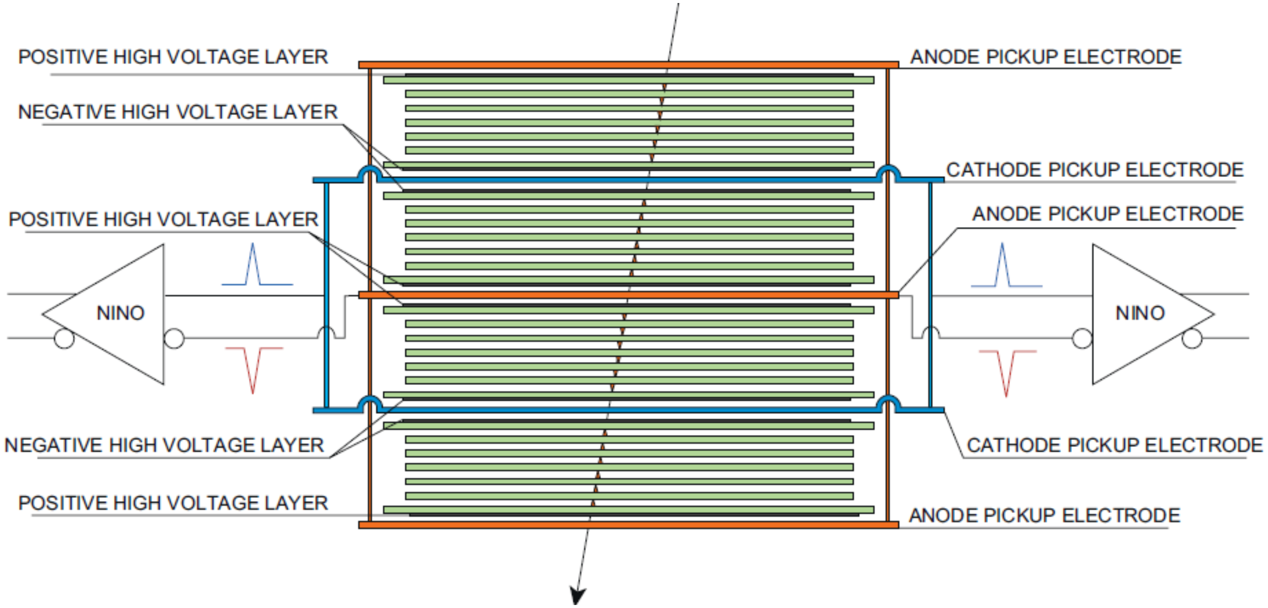

S. An et al., NIM A594, 39 (2008)

24 gaps of 160 μm

10 ps resolution possible with 10GHz oscilloscopes as DAQ system

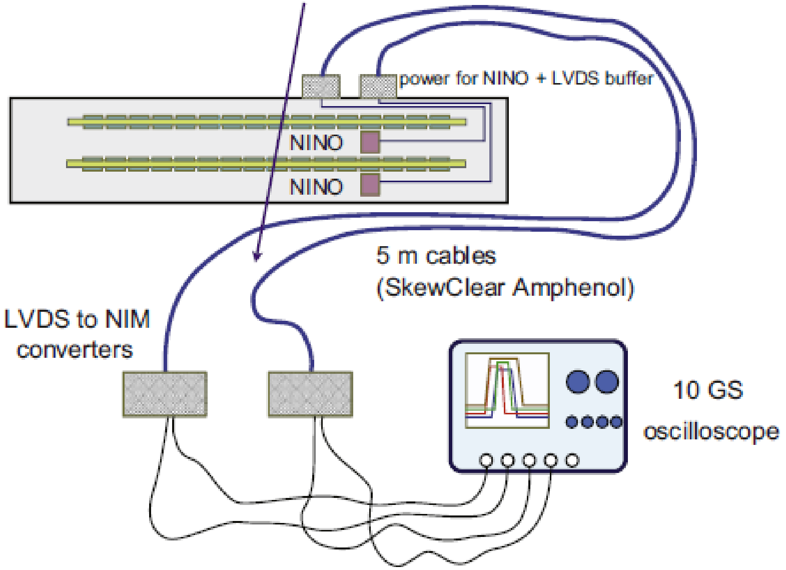

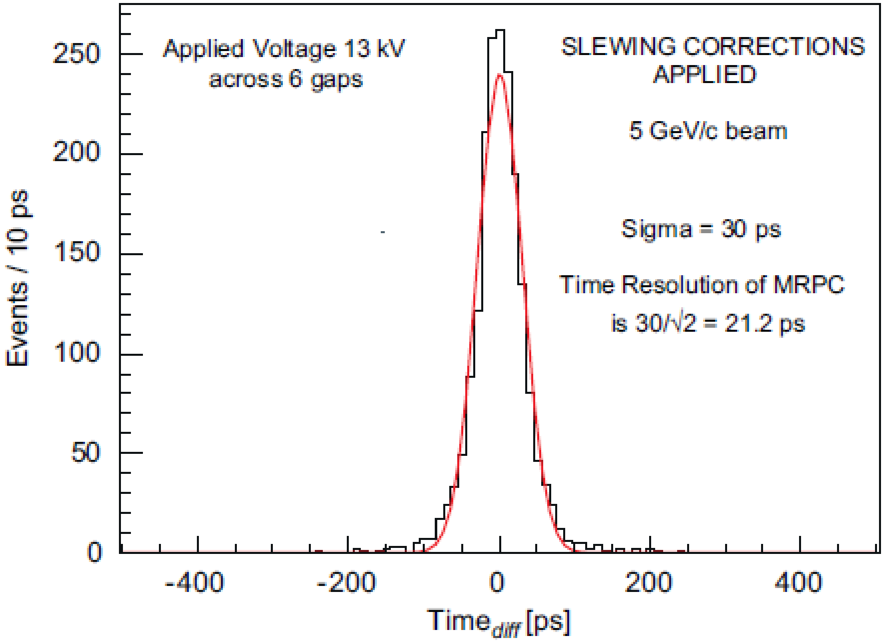

ALICE TOF

barrel radius: 3.7 m,
divided into 18 sectors,
each sector contains 5 modules in z direction
1674 MRPC 'strips' with two rows of 48 pickup pads of 3.5 × 2.5 cm^2 pickup pads,
160 m^2, 160.000 channels

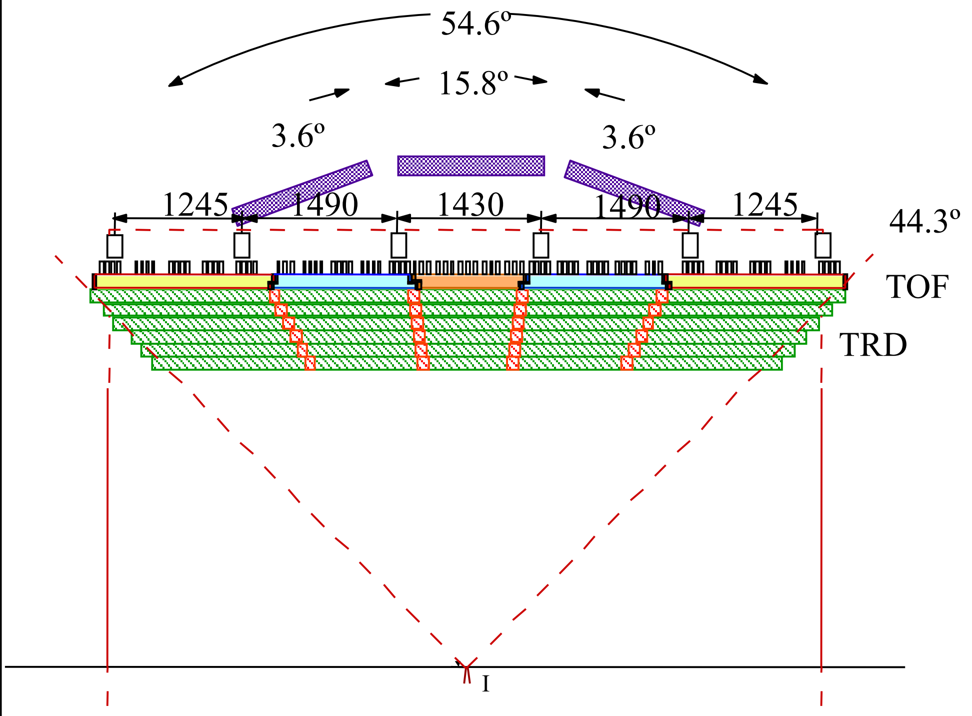

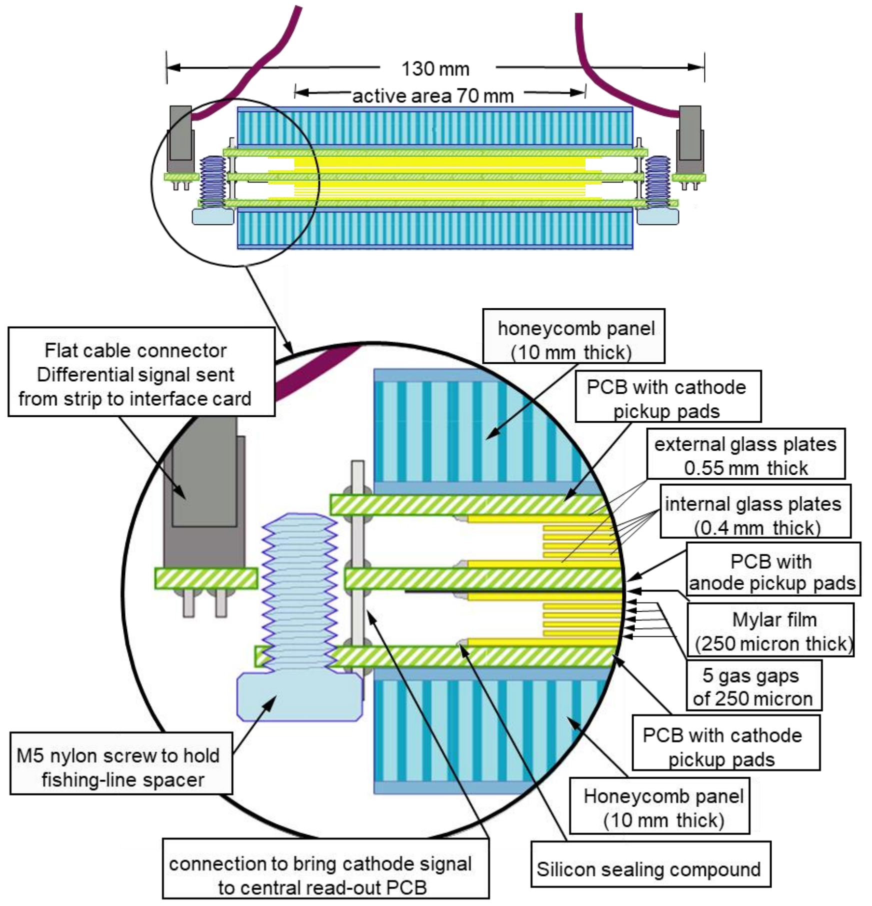

Double stack
- each stack has 5 gaps
  (i.e. 10 gaps in total)

250 micron gaps with spacers made from nylon fishing line

Resistive plates
soda lime glass

400 micron internal glass
550 micron external glass

Resistive coating
5 MΩ/square

ALICE TOF

F. Carnesecchi et al. (ALICE), arXiv:1806.03825v1

Max. charged particle flux at surface of detectors: 60Hz/cm^2

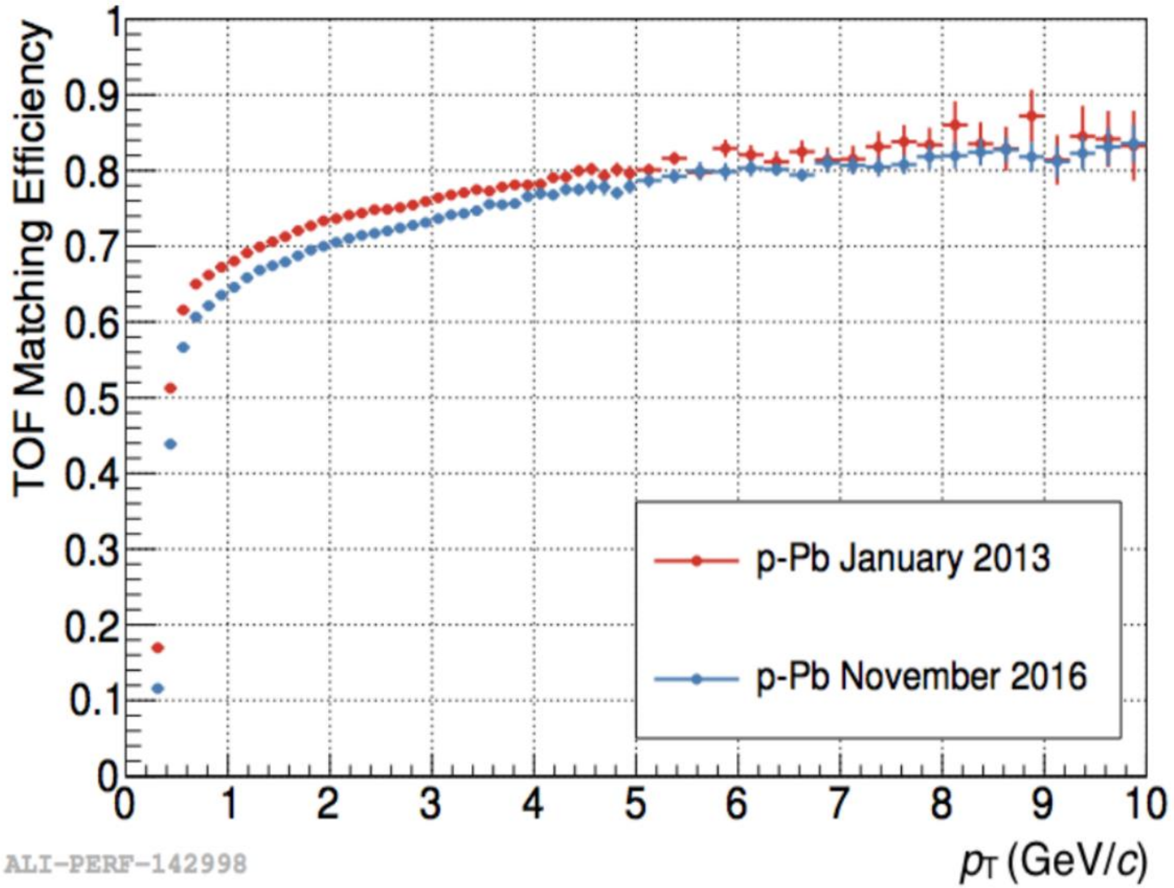

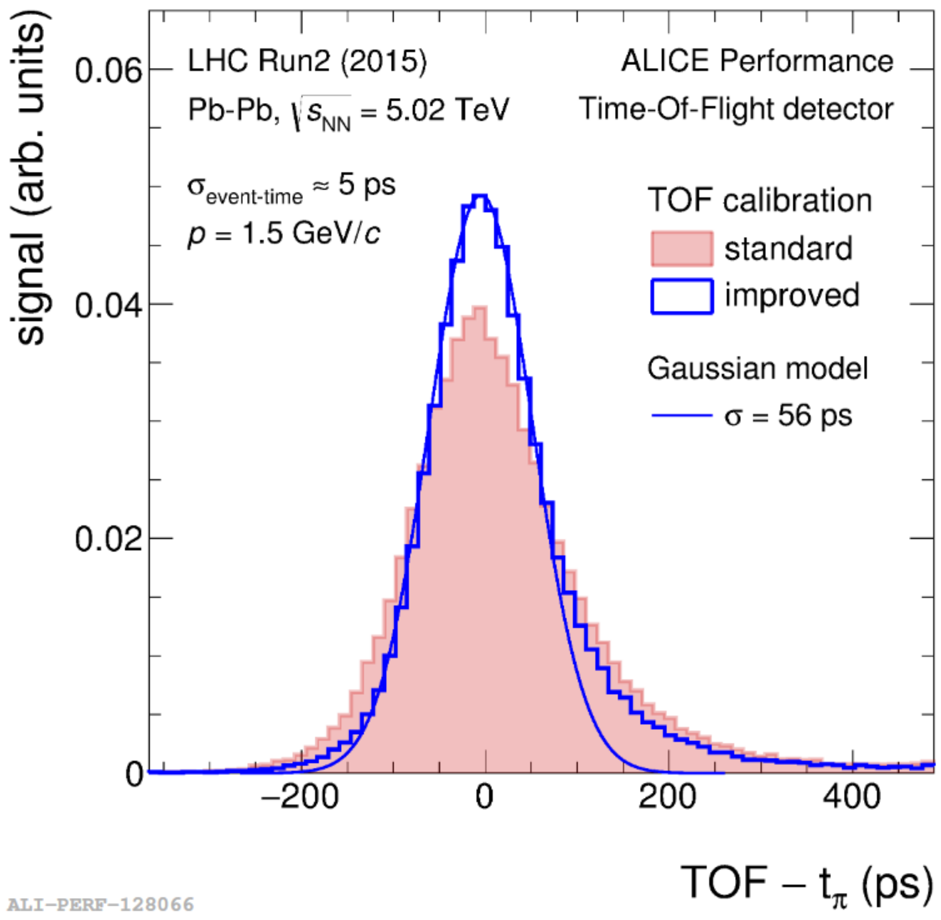

Timing resolution:

$$\sigma^2_{TOT} = \sigma^2_{TOF} + \sigma^2_{trk} + \sigma^2_{event}$$
$$= \sigma^2_{MRPC} + 2\,\sigma^2_{TDC} + \sigma^2_{FEE} + \sigma^2_{clock} + \sigma^2_{Cal} + \sigma^2_{trk} + \sigma^2_{event}$$

PID with ALICE TOF

F. Carnesecchi et al. (ALICE), arXiv:1806.03825v

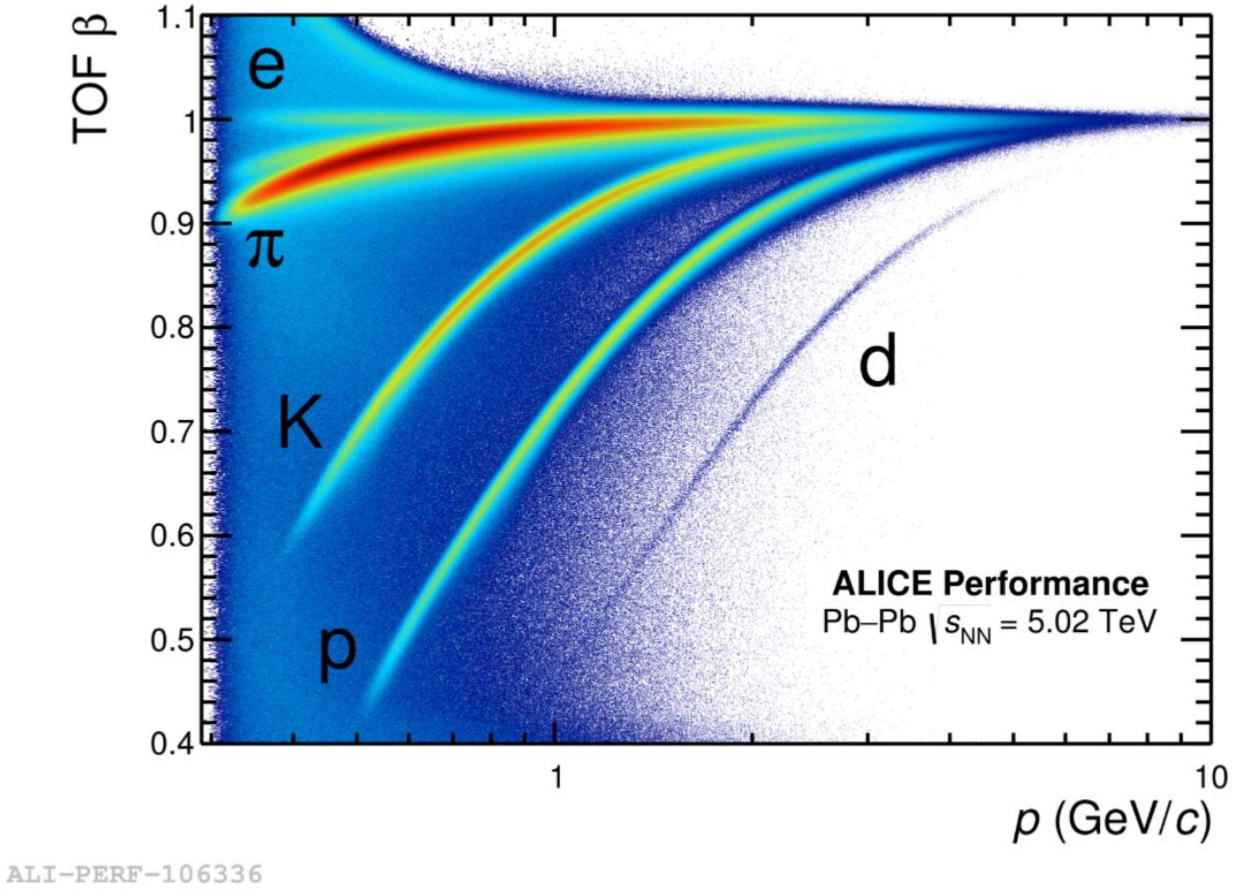

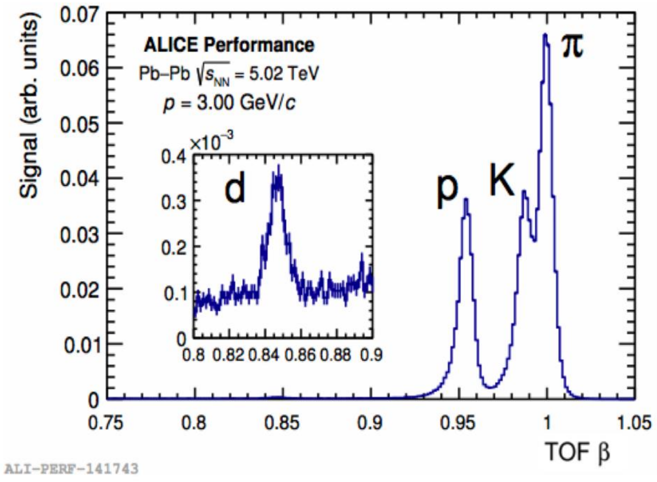

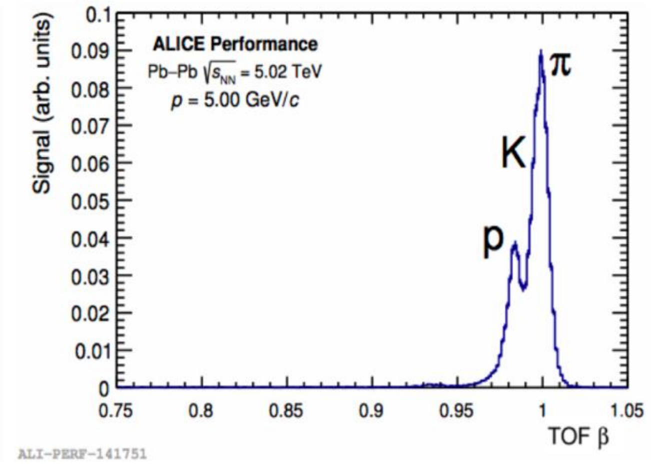

Multistrip Multigap RPC (MMRPC)

1. full size prototype, Oct 2003

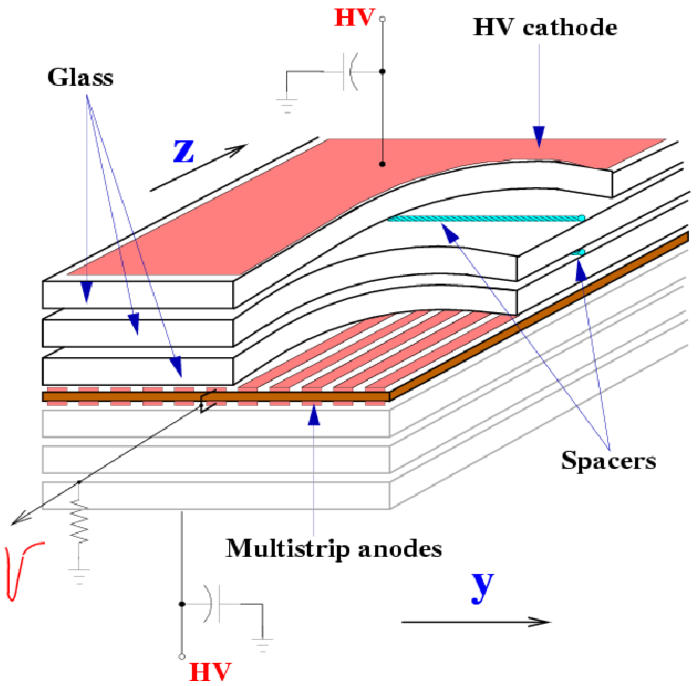

Multi-Strip Multi-Gap-RPC

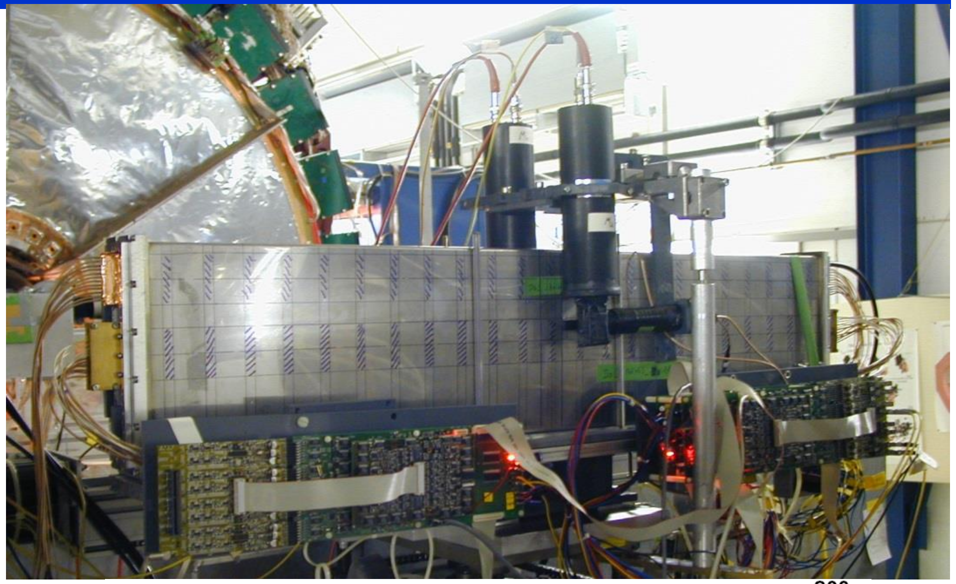

Gap-size:	250-300 μm
High voltage:	~3kV/gap
Length:	90 cm
Pitch:	2.54 mm

Performance:

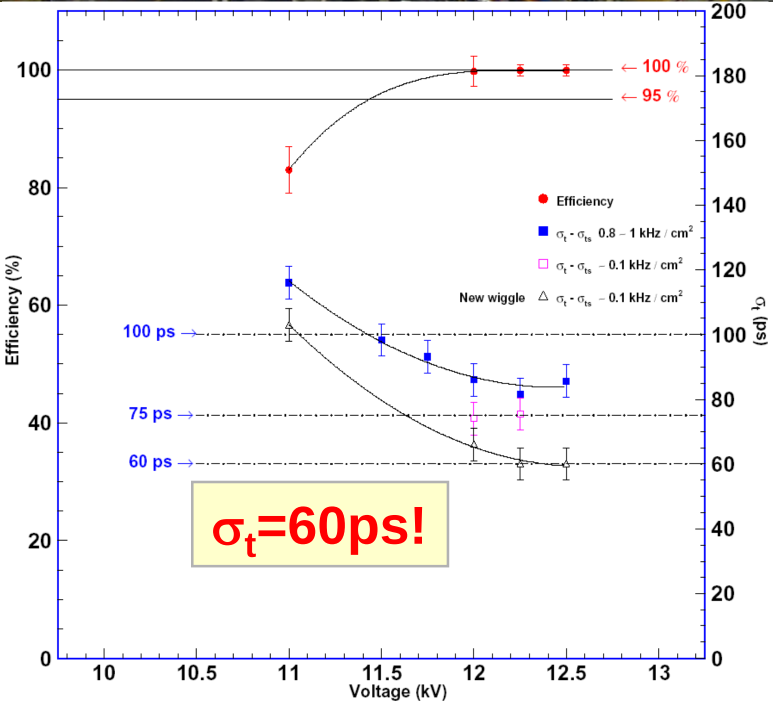

Signal propagation in strip counters

W. Riegler, D. Burgarth, NIM A481 (2002) 130

$$\frac{\partial}{\partial z}U(z,t) = -\hat{R}I(z,t) - \hat{L}\frac{\partial}{\partial t}I(z,t)$$

$$\frac{\partial}{\partial z}I(z,t) = -\hat{G}U(z,t) - \hat{C}\frac{\partial}{\partial t}U(z,t)$$

with

$$I(z,t) = \begin{pmatrix} I_1(z,t) \\ \dots \\ I_N(z,t) \end{pmatrix}, \qquad U(z,t) = \begin{pmatrix} U_1(z,t) \\ \dots \\ U_N(z,t) \end{pmatrix},$$

$\hat{C}, \hat{L}, \hat{R}, \hat{G}$ are capacitance, inductance, resistance and transconductance N x N matrices per unit length

I and V are vectors of the voltages and currents on each line

The pulse running along one conductor is a superposition of N times the same pulse - shape $I_0(t)$ running with N different velocities v_i.
Signal dispersion even for a lossless transmission line is called ***modal dispersion***.

Multistrip Multigap RPC

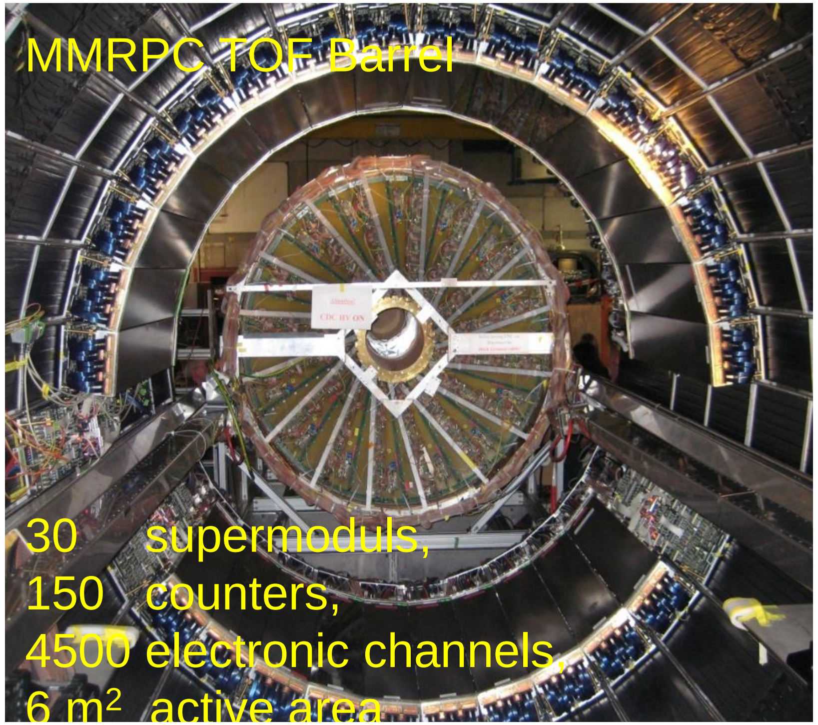

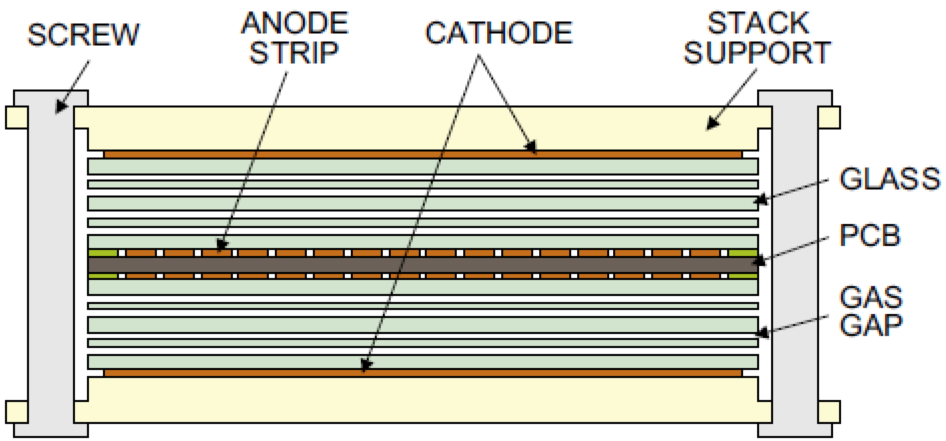

M. Kis et al. (FOPI), NIM A 646, 27 (2011)

Multistrip – Multigap – RPC

Developed	2001 – 2005
Construction	2005 – 2007
Operation	2007 - 2011

Features:
8 gaps of 250 μm
length: 90 cm
pitch: 2.54 mm
Impedance: 50 Ω
16 readout strips per counter
single ended readout

Signal distributed on several strips
→ high demands on preamplifier
→ PADI chip development

Walk (slewing) correction

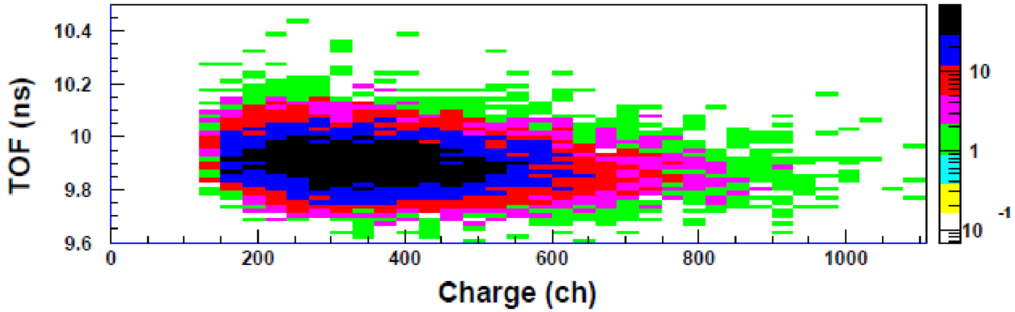

Measured correlation TOF vs. Charge

Mean deviation:
t_{meas} - t_{exp}

after correction
t_{meas} - t_{exp}

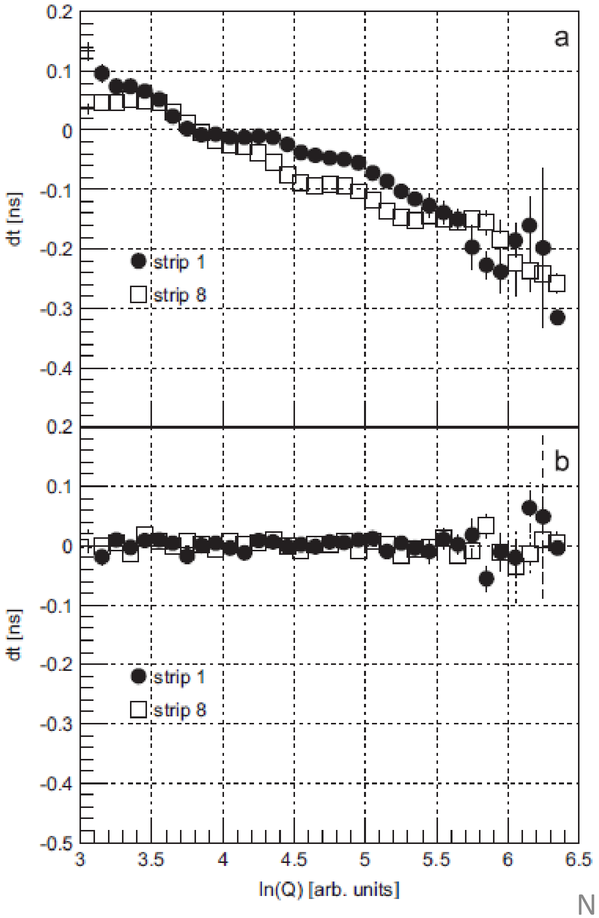

Leading edge discriminator

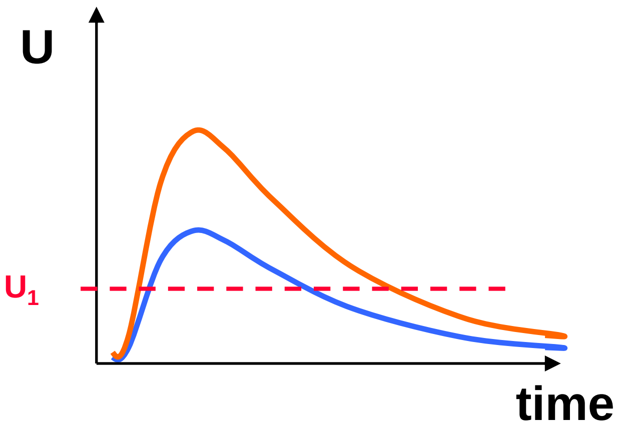

Corrections done individually for each strip (~ 2400)

Final result;
RPC – RPC coincidences

$\sigma_{\Delta t}$ = 94.9 ps
↓
σ_{RPC} = 67.1 ps

Gas ionization

Ionization (Bethe – Bloch) produces electron clusters in gas gap.

C. Lippmann, PhD thesis (2003)

HEED:

http://consult.cern.ch/writeup/heed/main.html

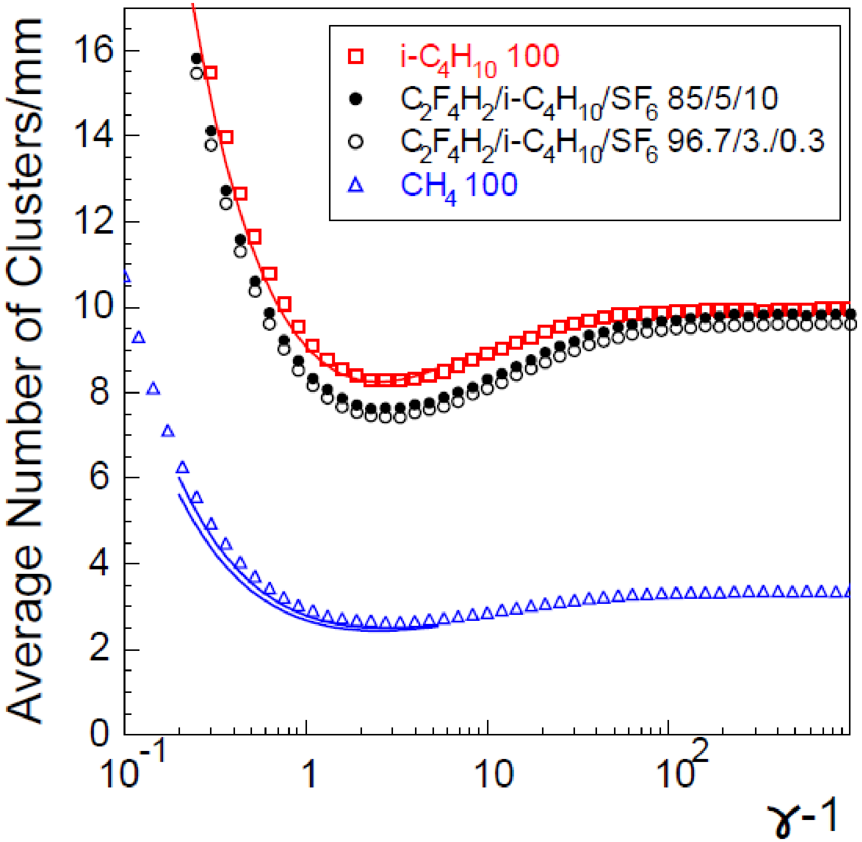

Ionization by 7 GeV/c pion

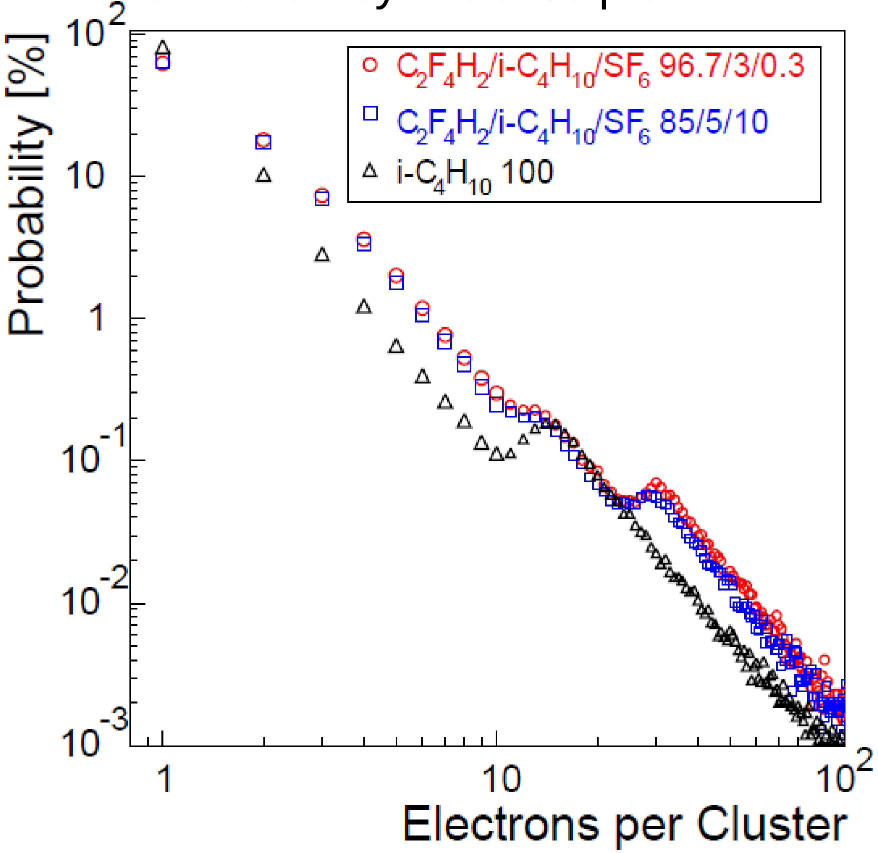

Detection efficiency

Ionisation is a statistical process.

$$\bar{n} = 8/mm$$

$$d = 0.2mm$$

$$\Downarrow$$

$$m = 1.6$$

$$P(m,n) = \frac{m^n}{n!} e^{-m}$$

$$P(0) = e^{-1.6} = 20.2\%$$

homogeneous
E-field

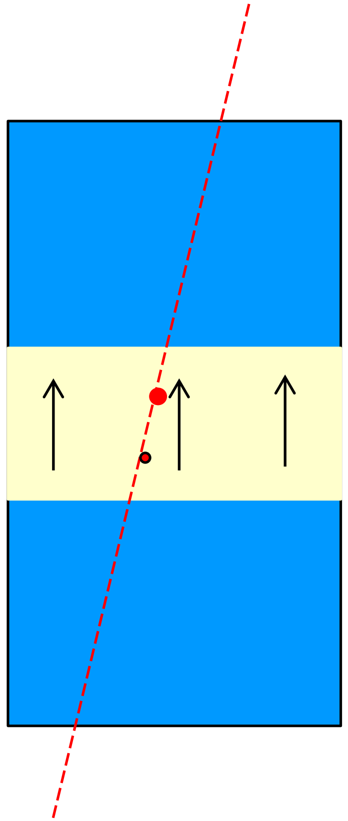

Single gas gap of 0.2 mm has a maximum efficiency of 80%
(if all electron clusters are registered).

RPC - Efficiency

Induced charge has to pass threshold:

For single primary electron:

$$Q_{ind}(x) = \frac{E_W}{V_W} \frac{e_0}{\alpha - \eta} e^{(\alpha-\mu)(d-x)} - 1$$

$$\Downarrow$$

$$\varepsilon = 1 - e^{-\left(1-\frac{\eta}{\alpha}\right)\frac{d}{\lambda}} \left[1 + \frac{V_W}{E_W} \frac{\alpha - \eta}{e_0} Q_{thr}\right]^{\frac{1}{\alpha\lambda}}$$

(λ is average distance of primary clusters.)

Single gap efficiency at operating point
ε = 80 %
→ multigap configuration needed.

Note: explicit dependence on α and η
-> gas mixture

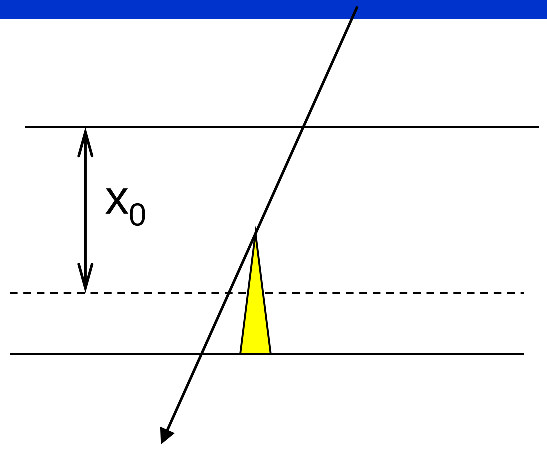

W. Riegler, NIM A **508** (2003) 14

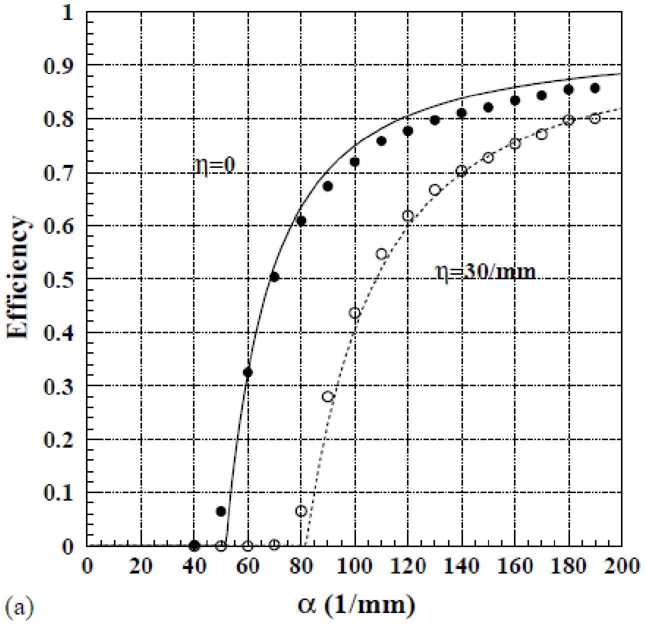

Rate capability of RPCs

M. Abbrescia, NIM A533, 7(2004)

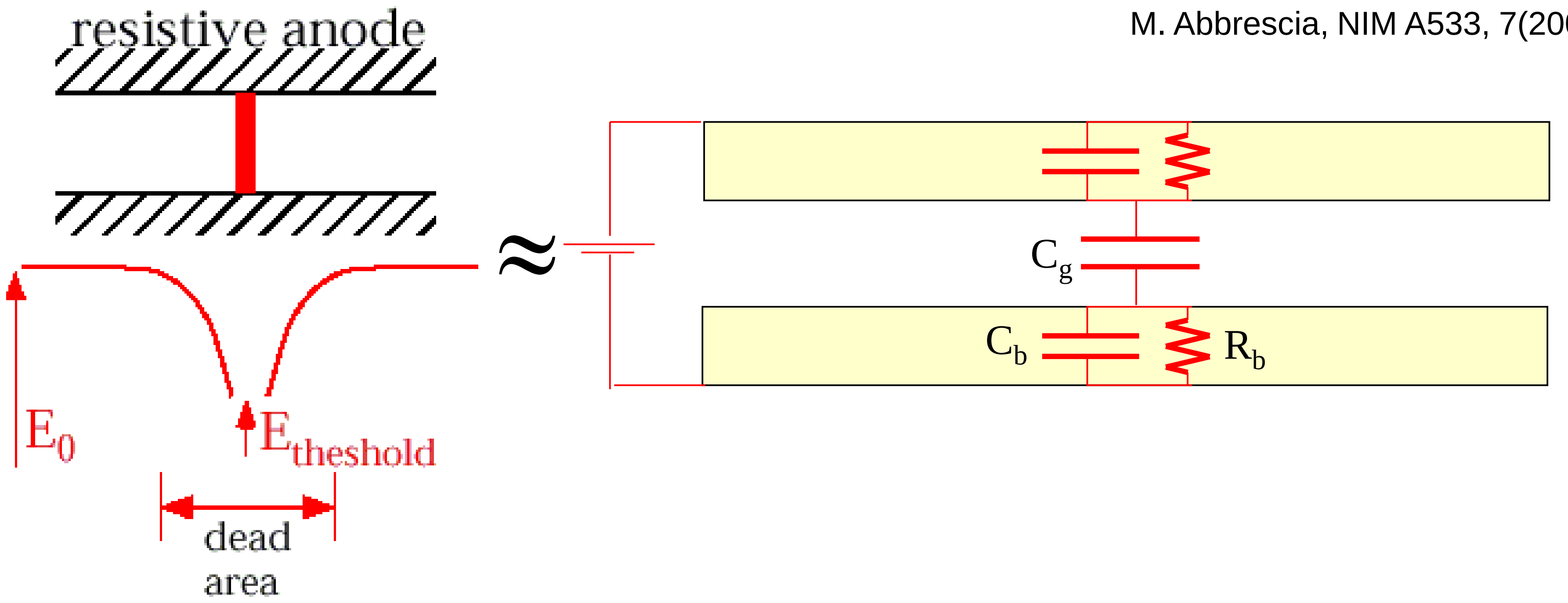

Recovery time from local field breakdown: $\tau = 2R_b\left(2C_b + C_g\right) = 2\rho_b\varepsilon_0\left(2\varepsilon_r + \frac{b}{g}\right)$

Estimate for counter with window glass electrodes:
$\rho_b = 10^{13}\ \Omega\text{cm}$, $\varepsilon_0 = 8.85\ 10^{-12}\ \text{Fm}^{-1}$, $\varepsilon_r = 6.5$, b=1mm, g=0.2mm $\rightarrow$ $\tau = 31$s.

Low resistivity glass

Resistive glass for high-rate MRPCs is developed in Beijing, China

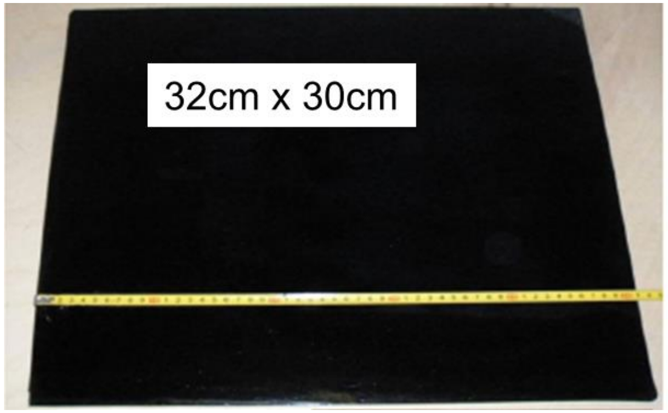

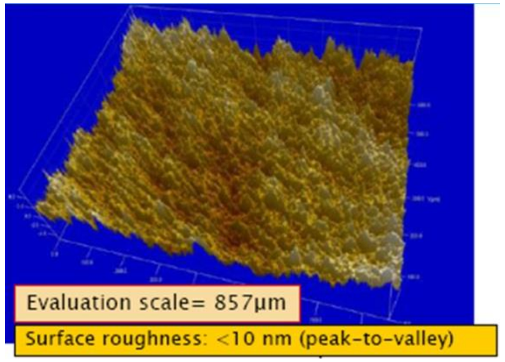

Maximal dimension	32cm × 30cm
Bulk resistivity	10^{10} Ωcm
Standard thickness	0.7, 1.1mm
Thickness uniformity	20 µm
Surface roughness	< 10nm
Dielectric constant	7.5 - 9.5
DC measurement	Ohmic bebavior stable up to 1 C/cm^2

Raw resistive glass material for 400 m²

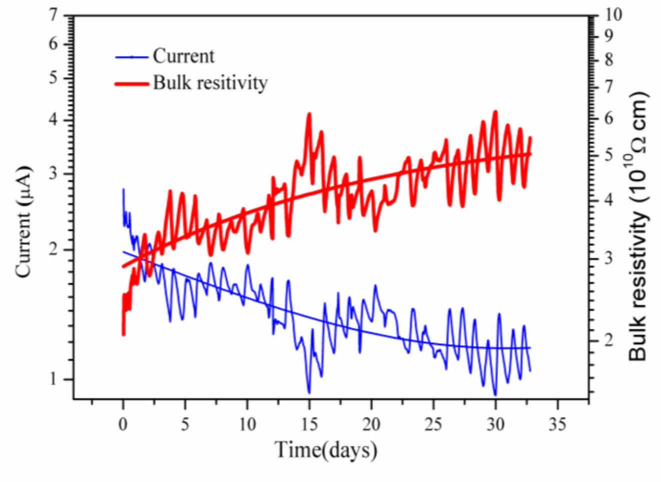

Aging tests

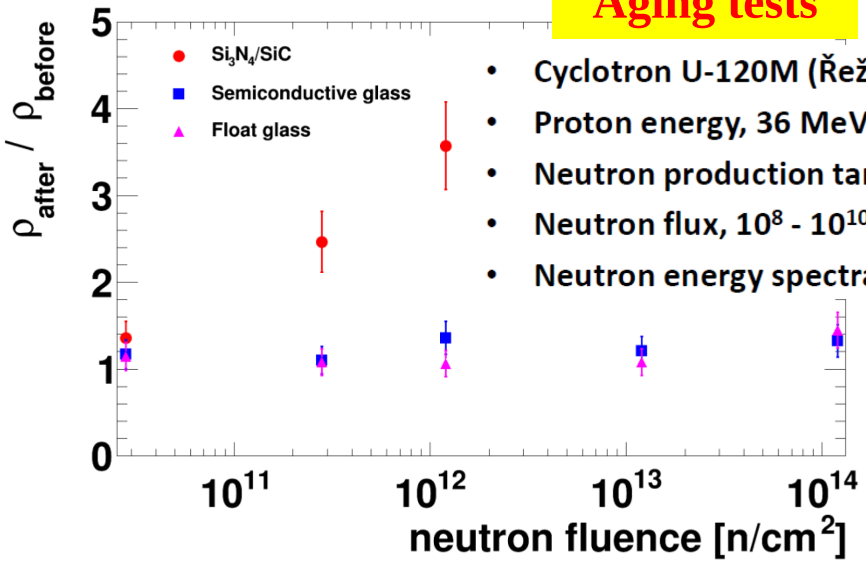

- Cyclotron U-120M (Řež)
- Proton energy, 36 MeV
- Neutron production target, Be
- Neutron flux, 10^8 - 10^{10} n/cm²/s
- Neutron energy spectra, 1 – 36 MeV

Rate capability of MRPCs

DC model

$$\overline{V}_{drop} = V - \overline{V}_{gap} = \overline{I}R = \overline{q}\phi\rho d.$$

Parametrization of time resolution σ_T and efficiency ε

$$\sigma_T = \sigma_0 + K_T\overline{q}\phi\rho d$$
$$\epsilon = \epsilon_0 - K_\epsilon\overline{q}\phi\rho d$$

V: external applied high voltage
$\bar{I}$: average current in the glass
$\bar{q}$: average charge per avalanche
ϕ: incident ch. particle flux
ρ: electrode bulk resistivity
d: electrode thickness

Def. rate capability: an efficiency drop no more than 5% compared to ε_0 and an increase in time resolution no more than 20 ps compared to σ_0

Nuclear Instruments and Methods in Physics Research A 661 (2012) 121 - 124

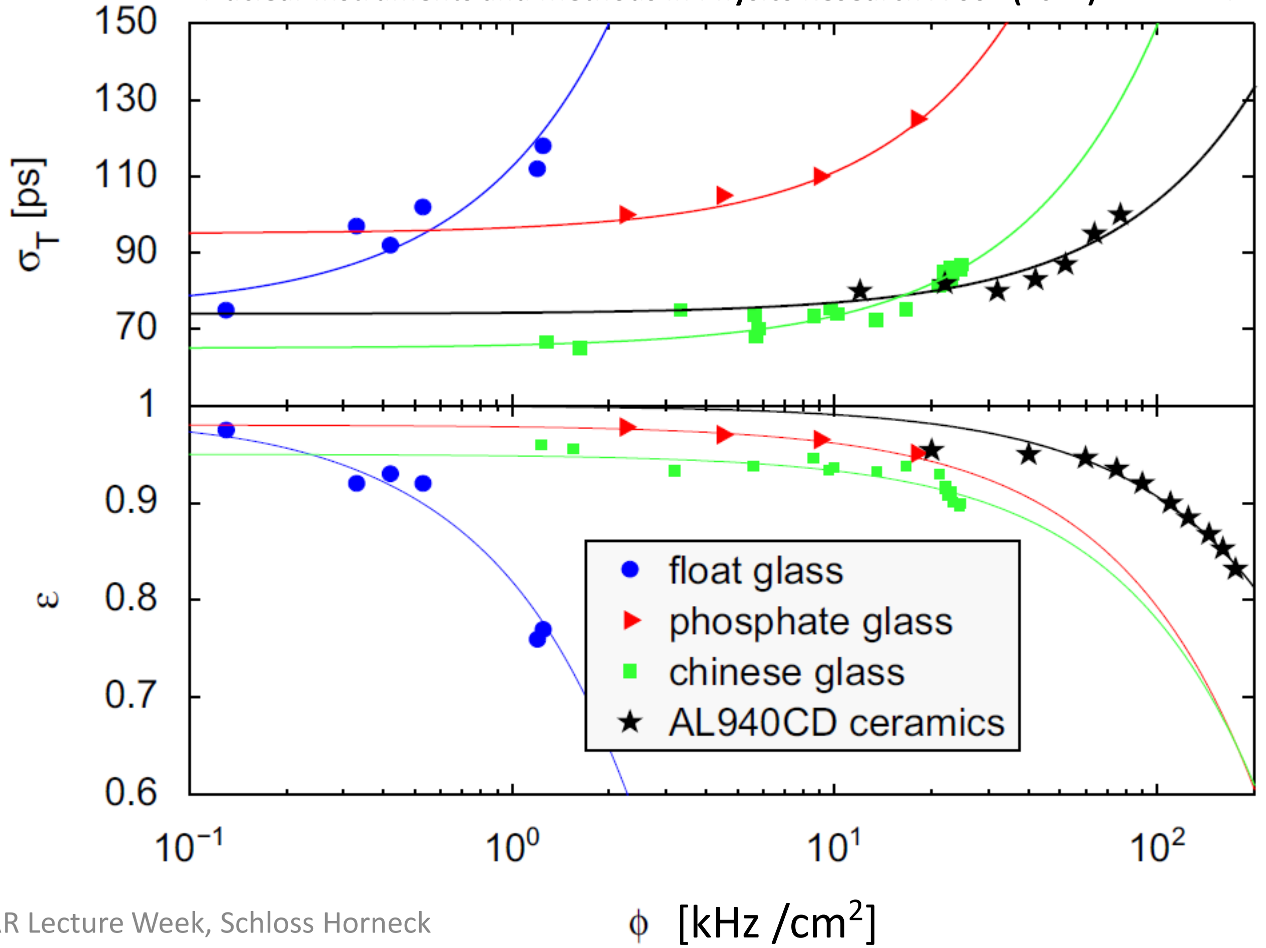

Ceramic composites

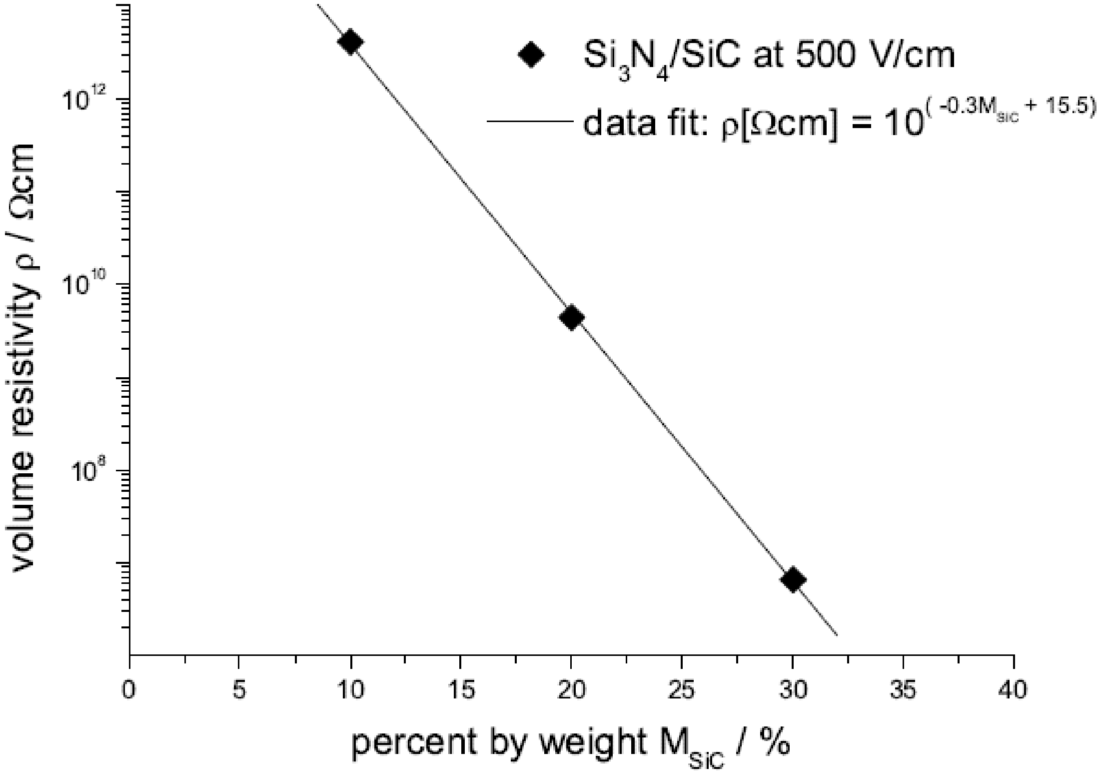

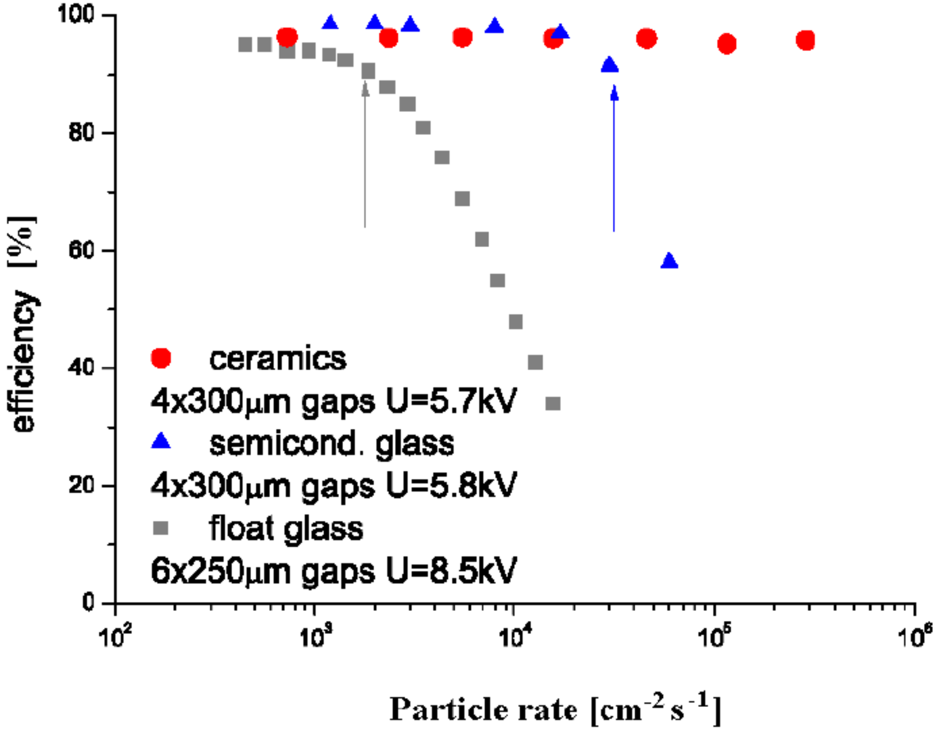

Resistivity can be adjusted by SiC fraction.

$\rho_{ceramic} \sim 10^9\ \Omega cm$

RPC – cost

Differential single stack MRPC with 8 gaps

vs.

Differential double stack MRPC with 2 x 4 gaps

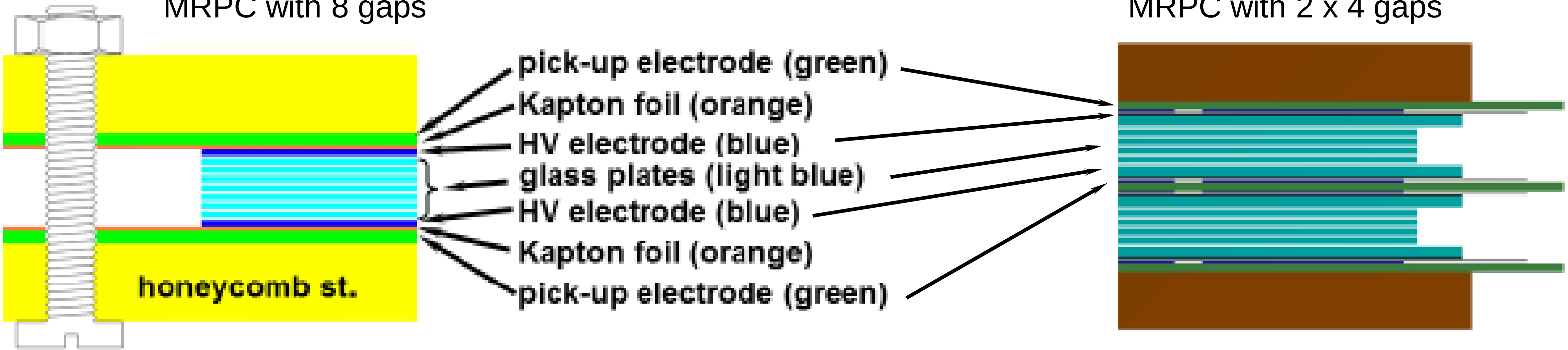

All MRPCs for CBM are double stacks

Advantages
- simpler construction
- symmetric signal path
- fewer glass plates (#9)
- lower weight
- impedance matched to 100 Ω (easy)

Disadvantages
- higher High Voltage (> ±10 kV)
- bigger cluster size

Advantages
- lower High Voltage (< ±6 kV)
- smaller cluster size
- impedance matched to 100 Ω with novel technic

Disadvantages
- more complex construction
- non-symmetric signal path
- more glass plates (#10)

CBM – TOF counter menue

Ingo Deppner, PI

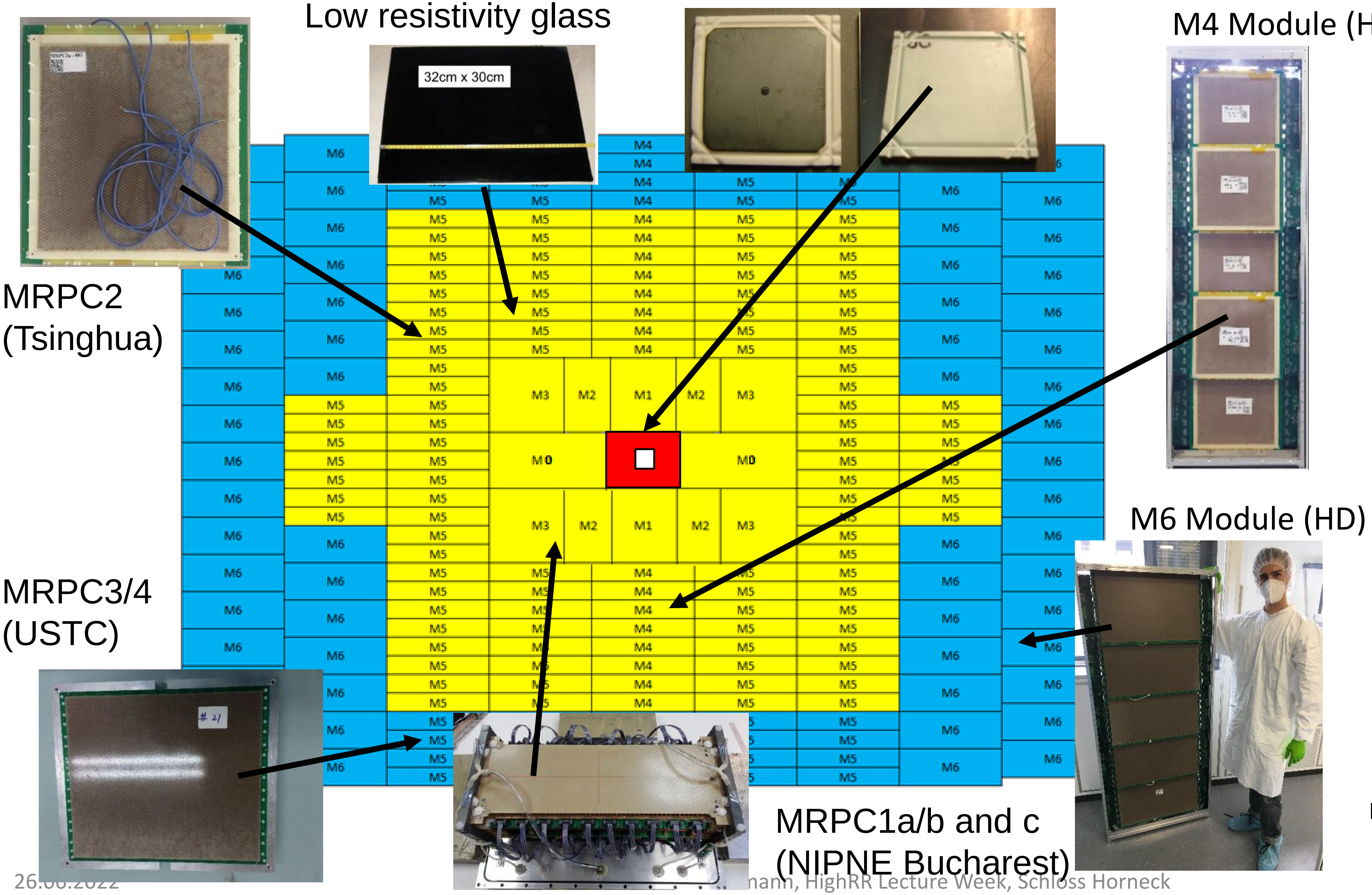

- **Full size counter with close to final design for all regions build and tested**
- **M4 and M6 full size modules constructed and installed at mCBM**

- **thin float glass, $\rho \approx 10^{12}\ \Omega$ cm** (blue)
- **low resistivity glass, $\rho \approx 10^{10}\ \Omega$ cm** (yellow)
- **ceramic $\rho \approx 10^{9}\ \Omega$ cm** (red)

≈ 230 + 20* modules
≈ 1400 MRPCs
≈ 90000 channels

BFTC* - Beam Fragmentation T0 Counter

CBM TOF MRPCs

	MRPC1a	MRPC1b	MRPC1c	MRPC2	MRPC3	MRPC4
# Gaps	2 x 5	2 x 5	2 x 5	2 x 4	2 x 5	2 x 5
Gap size	200 µm	200 µm	200 µm	250 µm	230 µm	230 µm
Glass type	Low res.	Low res.	Low res.	Low res.	Float	Float
Glass thickness	700 µm	700 µm	700 µm	700 µm	230 µm	230 µm
MRPC size	30 cm x 6 cm	30 cm x 10 cm	30 cm x 20 cm	32 cm x 27 cm	32 cm x 27 cm	32 cm x 53 cm
# Strips	32	32	32	32	32	32
Strip length	6 cm	10 cm	20 cm	27 cm	27 cm	53
Pitch	0.90 cm	0.90 cm	0.90 cm	1.0 cm	1.0 cm	1.0 cm
Impedance	100 Ω	100 Ω	100 Ω	50 Ω	50 Ω	50 Ω
Developed at	IFIN-HH (RO)	IFIN-HH (RO)	IFIN-HH (RO)	Tsinghua (CH)	USTC (CH)	USTC (CH)
Needed for CBM	0	132	168	580	200	310

MRPC testing site: mCBM @ SIS18

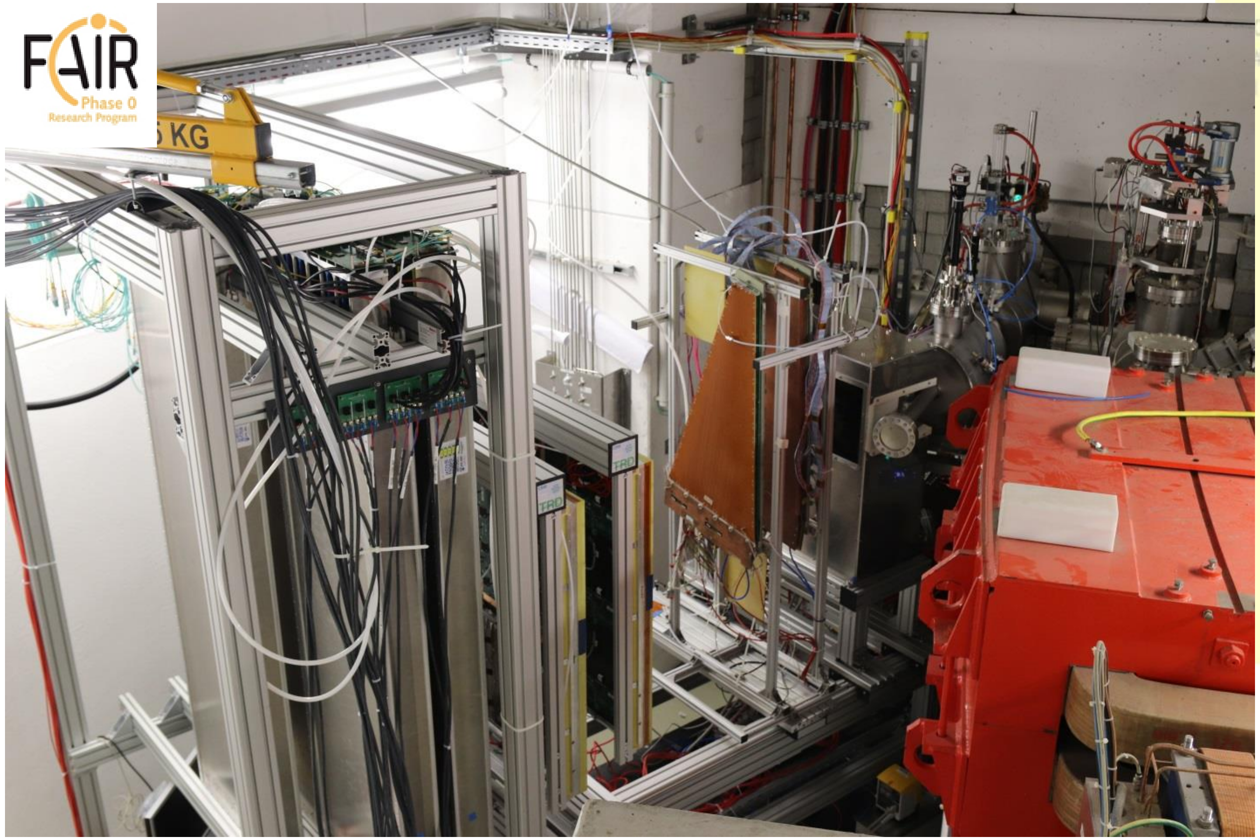

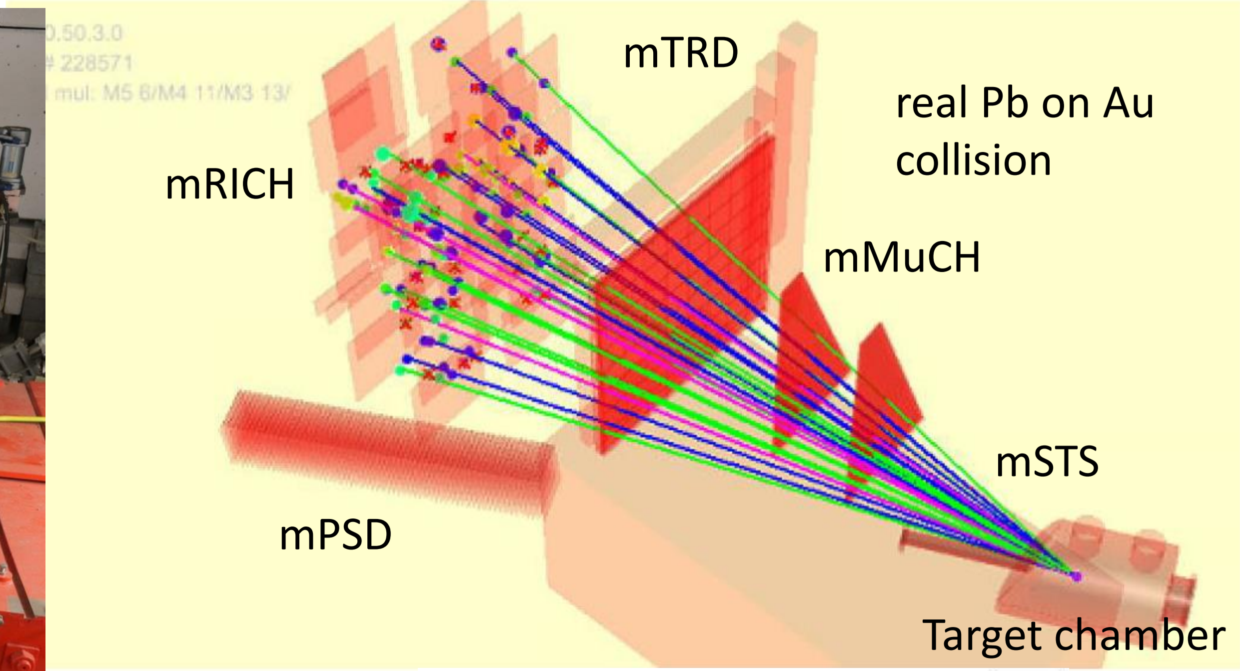

Simulation: Au+Au @ 1.24 GeV mbias

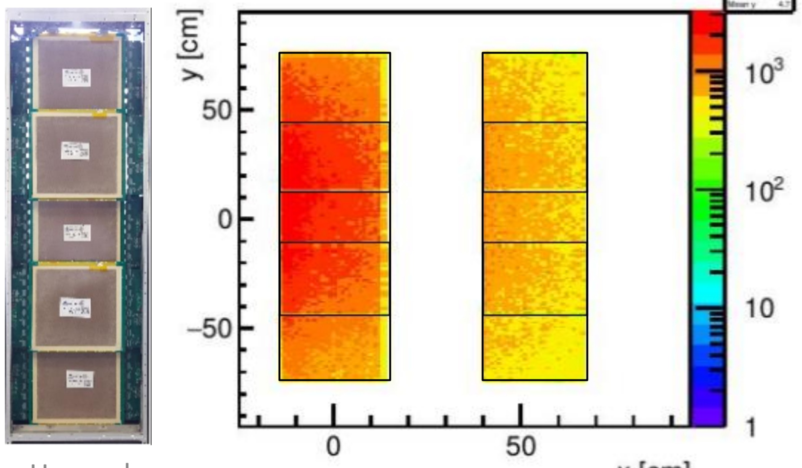

- mCBM is a full system test setup installed at SIS18/GSI dedicated for high rate detector and readout test including free streaming data acquisition and online event selection
- Charged particle fluxes of up to 30 kHz/cm^2

mCBM beamtime results 2021

MRPC1a (low resistivity glass counter)

Run **1470 – 1478 → high voltage scan**

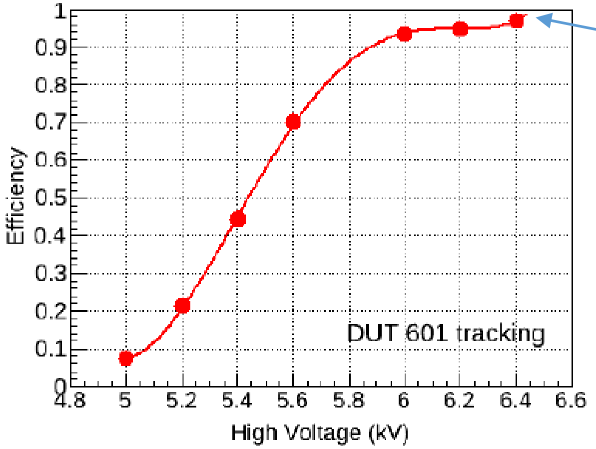

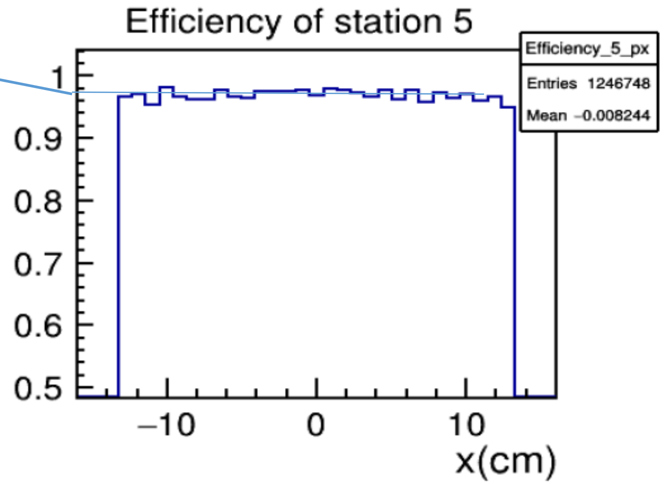

Run **1454 – 1460 → beam intensity scan**

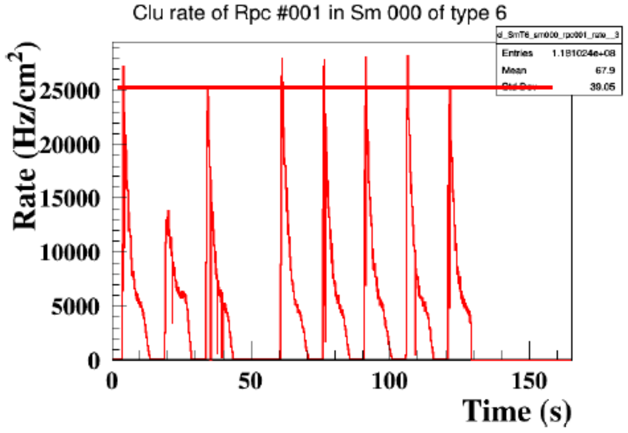

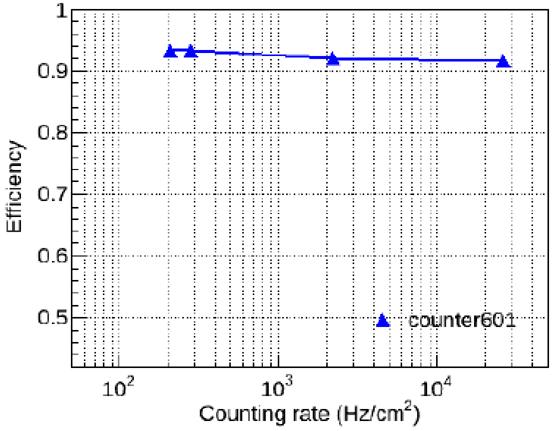

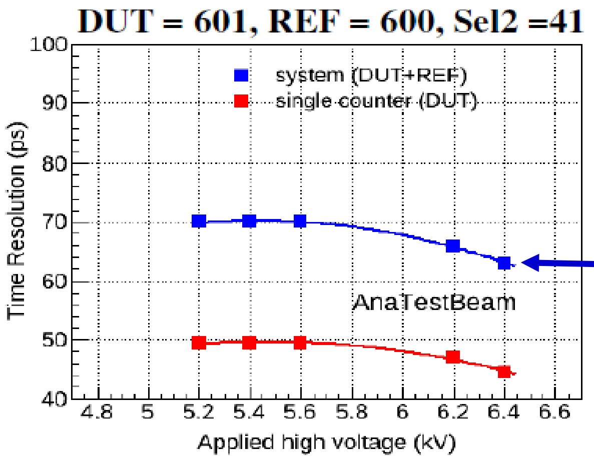

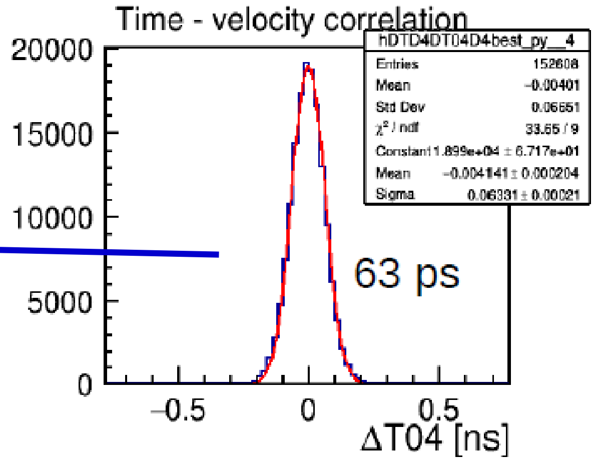

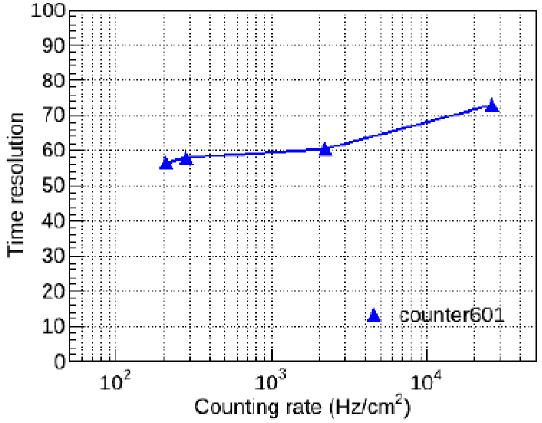

mCBM beamtime results 2021

MRPC3 (thin float glass counter)

Efficiency as function of incident ch. particle flux

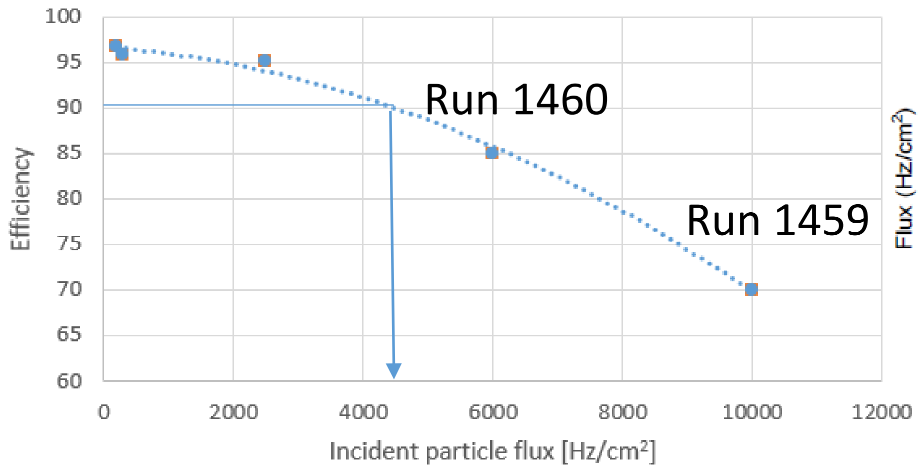

Time resolution as function of incident ch. particle flux

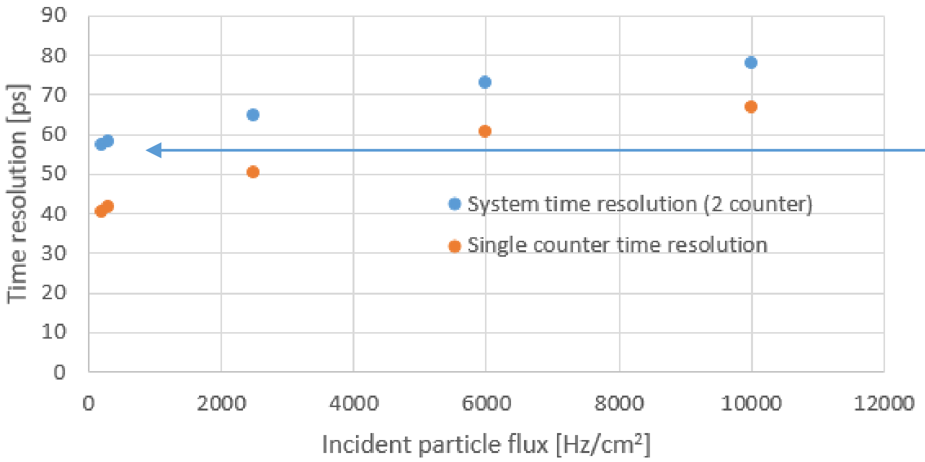

Data loss issues (faced during beam time)

- Bandwidth limitations
- Get4 dropouts
- Time slice losses

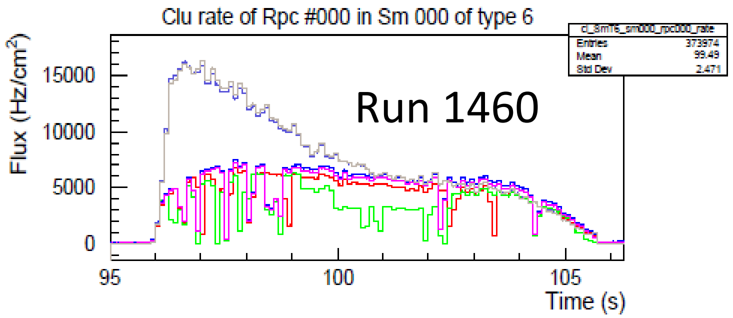

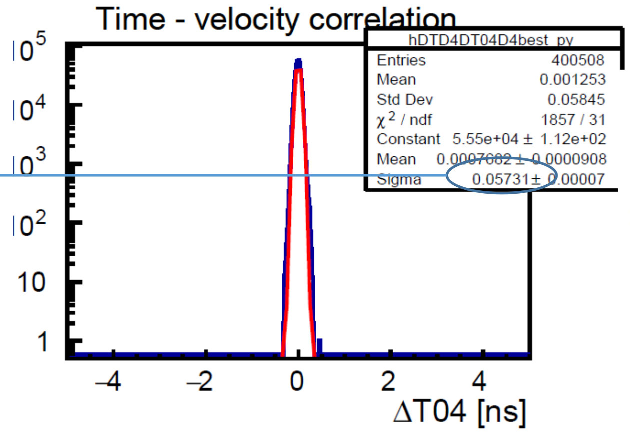

Memory effect

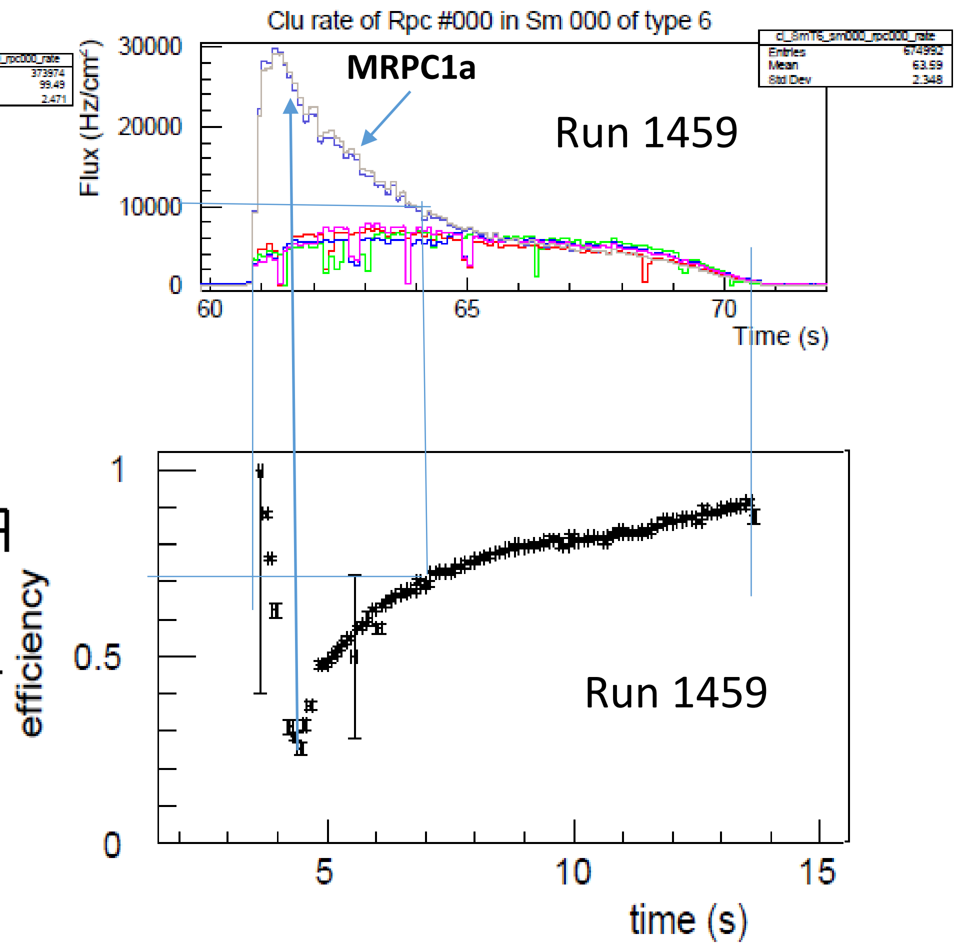

MRPC gas pollution and aging

Observations: continuous increase in dark rate (permanent aging)

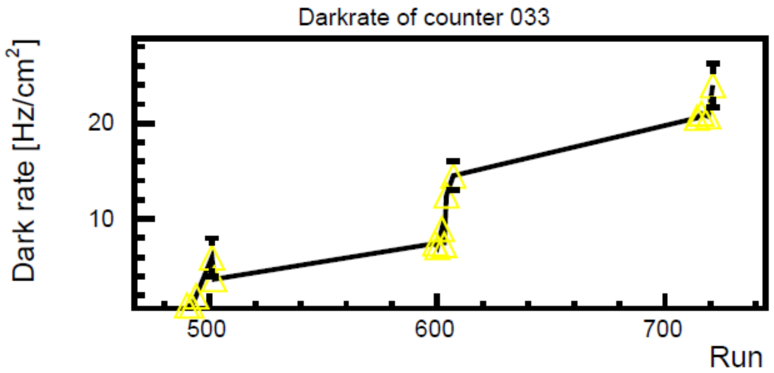

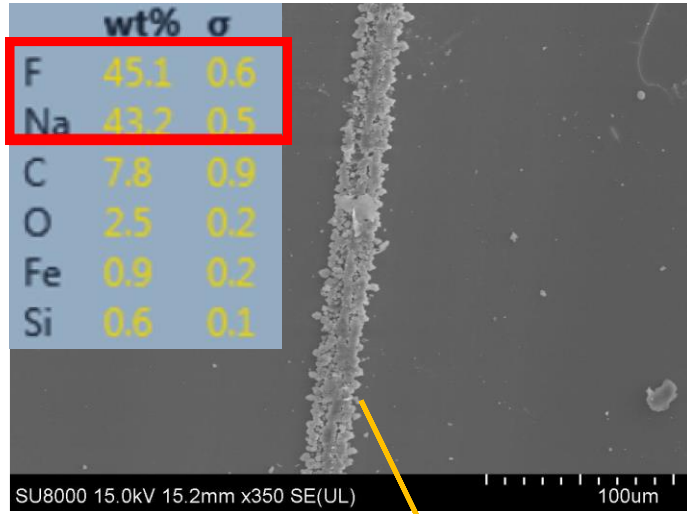

	wt%	σ
F	45.1	0.6
Na	43.2	0.5
C	7.8	0.9
O	2.5	0.2
Fe	0.9	0.2
Si	0.6	0.1

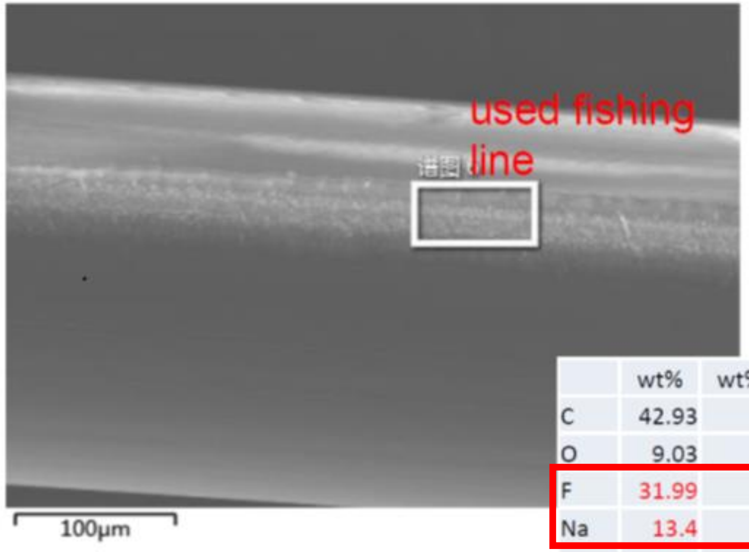

	wt%	wt% Sigma
C	42.93	0.21
O	9.03	0.15
F	31.99	0.18
Na	13.4	0.1
Si	2.36	0.04
Pt	0.28	0.07

- Traces of NaF was found on the glass surface
- Dark rate (noise) is generated entirely on spacers
- Electrical field simulations performed

Electrical field simulations

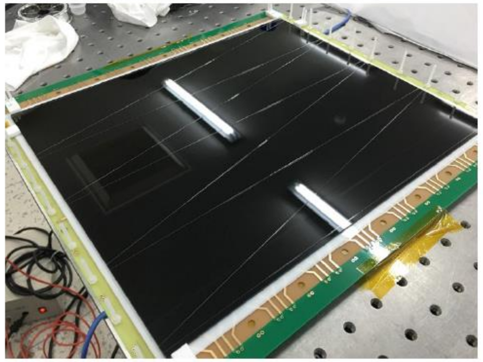

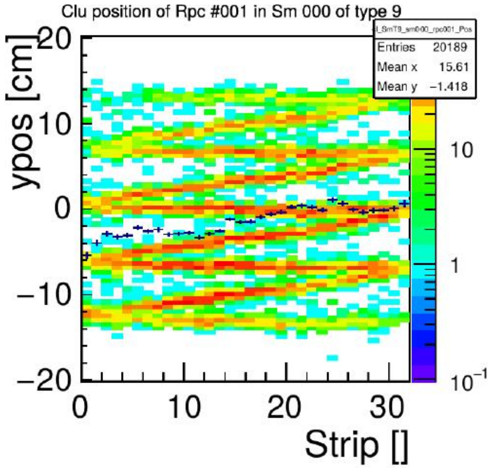

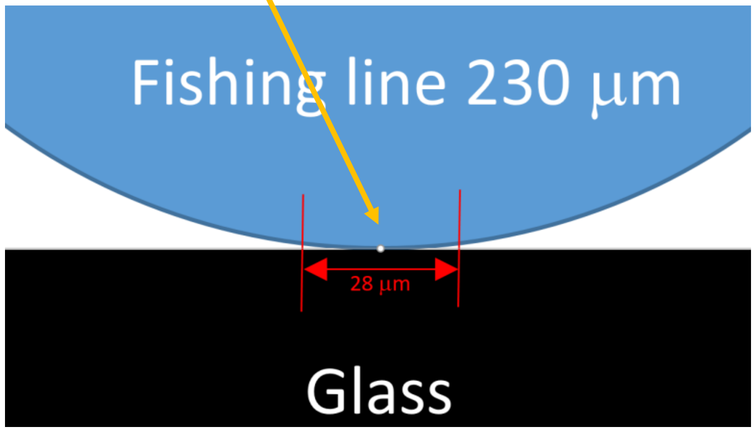

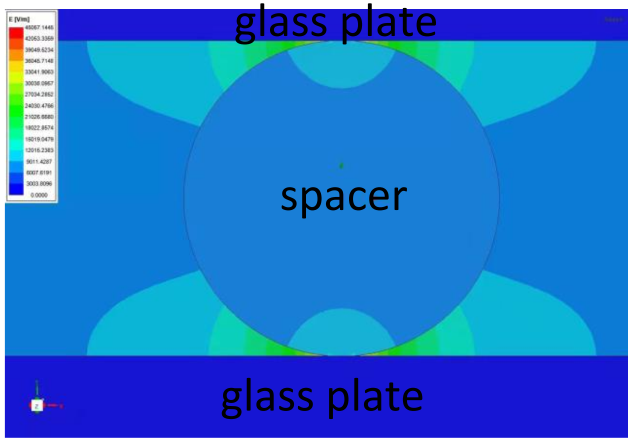

MRPC mitigation of aging & gas pollution

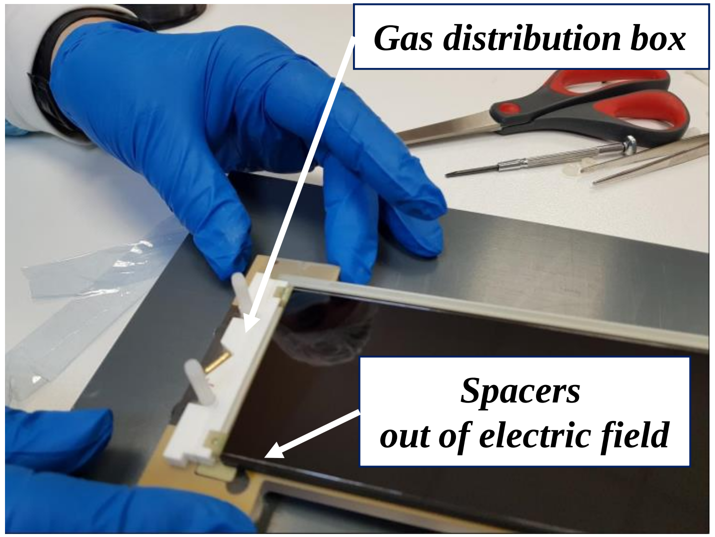

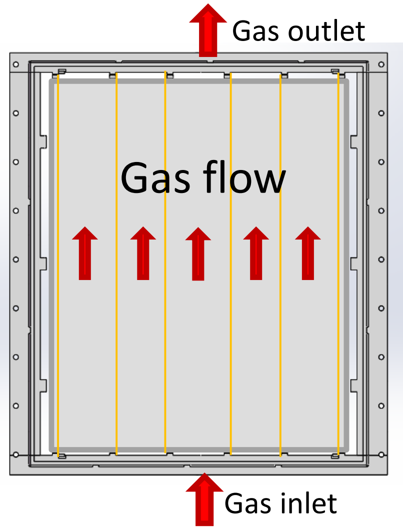

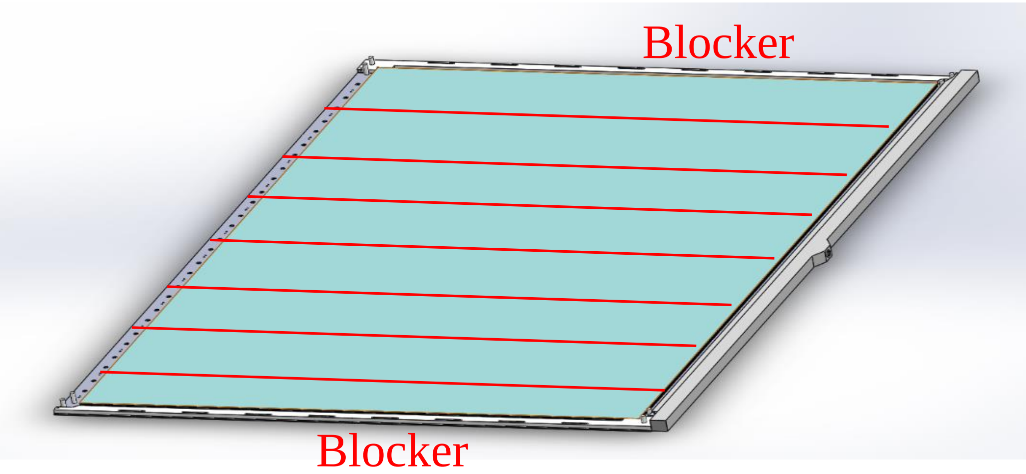

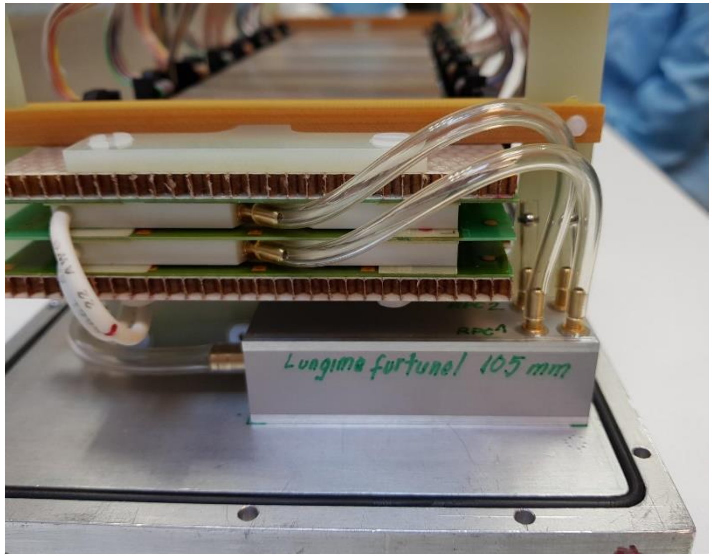

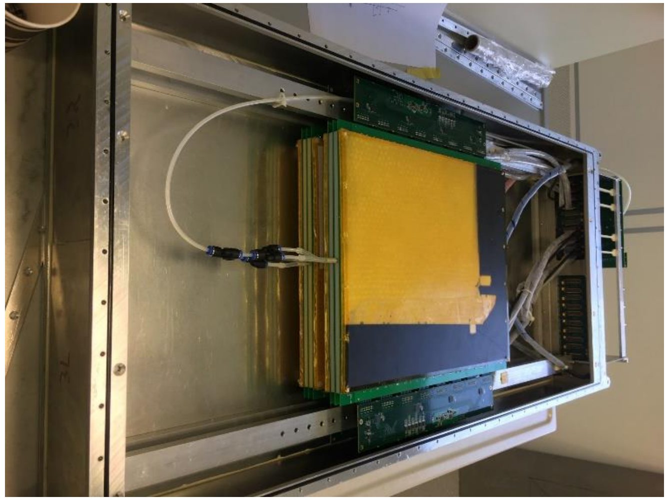

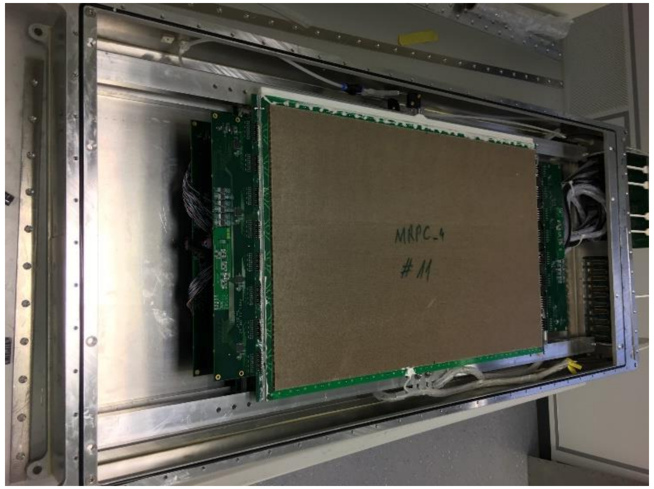

T0 – determination

Large multiplicities, central events, high energies:

- use fastest particles within an event and calculate T0 from measured momenta

Low multiplicities, semicentral and peripheral events, moderate beam intensities:

- measure each beam particle

- available technologies

  diamond - detector

  Low Gain Avalanche Diode (LGAD) – detector

Diamond

Physical Property at 300 K	*Diamond*	*Silicon*
band gap [eV]	5.45	1.12
Electron mobility [cm^2 /Vs]	2200	1500
Hole mobility [cm^2 /Vs]	1600	600
Breakdown field [V/m]	10^7	$3x10^5$
Resistivity [Ω cm]	$>10^{13}$	$2.3x10^5$
Dielectric constant ε_r	5.7	11.9
Thermal conductivity [W/cm K]	20	1.27
Lattice constant [Å]	3.57	5.43
Energy to remove an atom from the lattice [eV]	80	28
Energy to create an e-h pair [eV]	13	3.6

Favorable material parameter

- mechanical hardness
- high thermal conductivity
- Insensitive to visible light
- No cooling needed
- No p-n junction needed
- Fast signal rise time
- Radiation hardness

Availability:
Single-crystal CVD diamond plate, max. size: 5×5 mm^2, d=50,100,200,300μm
Polycrystalline CVD diamond plate, max. size: 50×50 mm^2, d=50,100,200,300μm

Diamond Beam Detector

Principle:

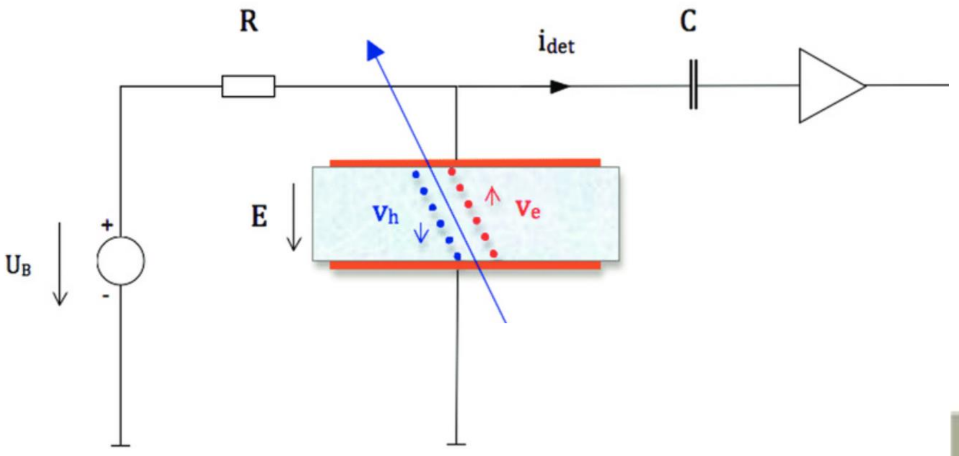

Example: M. Ciobanu *et al.*, "In-Beam Diamond Start Detectors," in *IEEE Transactions on Nuclear Science*, 58 (2011) 2073-2083

Key issue: fast electronics

$$\sigma_t = \frac{\sigma_{noise}}{\left.\frac{dS}{dt}\right|_{S_{threshold}}} \approx \frac{t_{rise}}{S/N}$$

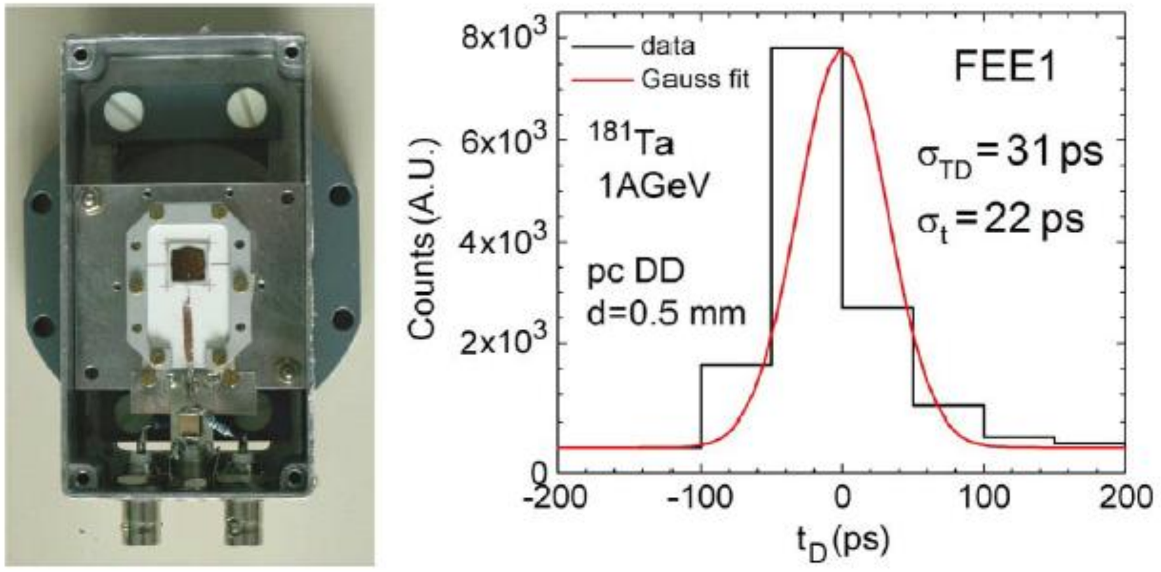

Fig. 13. The pcDD set used in a ^{181}Ta beam of 1 A GeV (left). The time difference spectrum measured between two identical detectors (right). The time resolution is 22 ps.

Diamond Beam Detector

https://hades.gsi.de/?q=node/32

Example: HADES

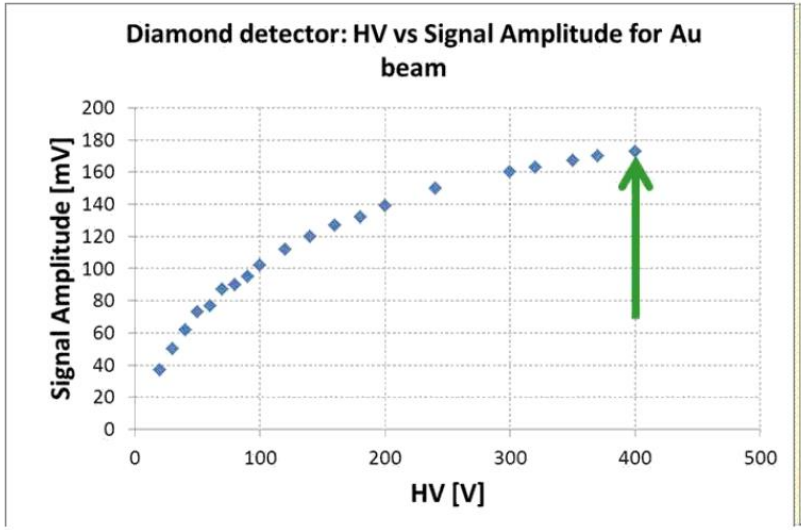

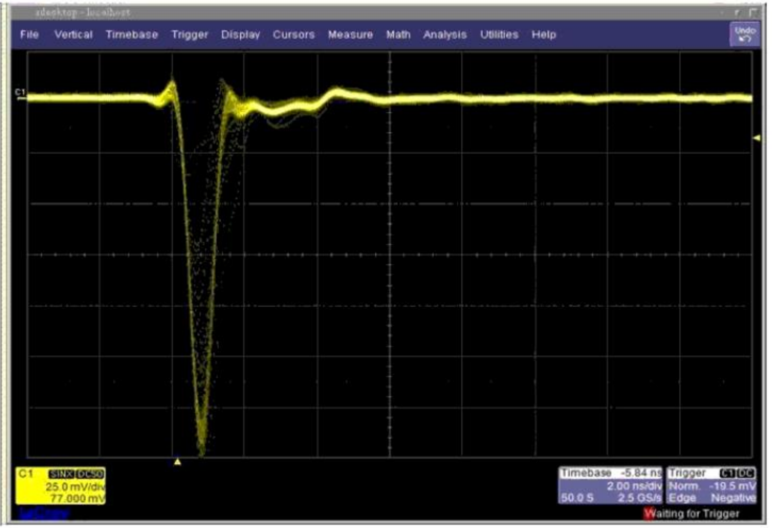

horizontal: 40 ps /div

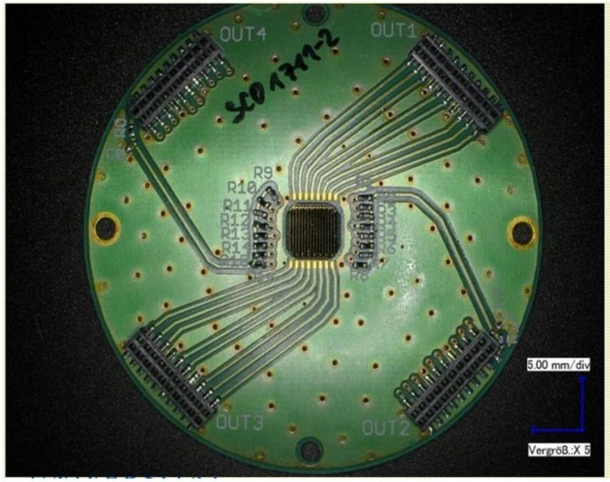

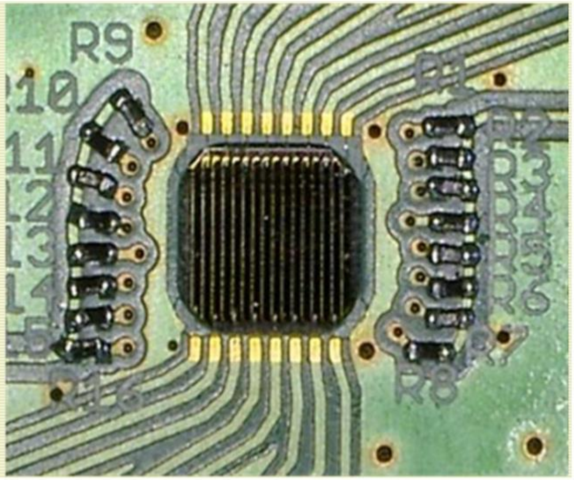

scCVD diamond
Rate capability: 2-3 10^6/s/mm^2

Size: 4.7mm x 4.7mm
16 strips

In Au+Au reactions at 1.23 AGeV
timing resolution < 50 ps

Diamond Beam Detector for protons

J. Adamczewski-Musch et al., Eur. Phys. J. A (2017) 53: 188

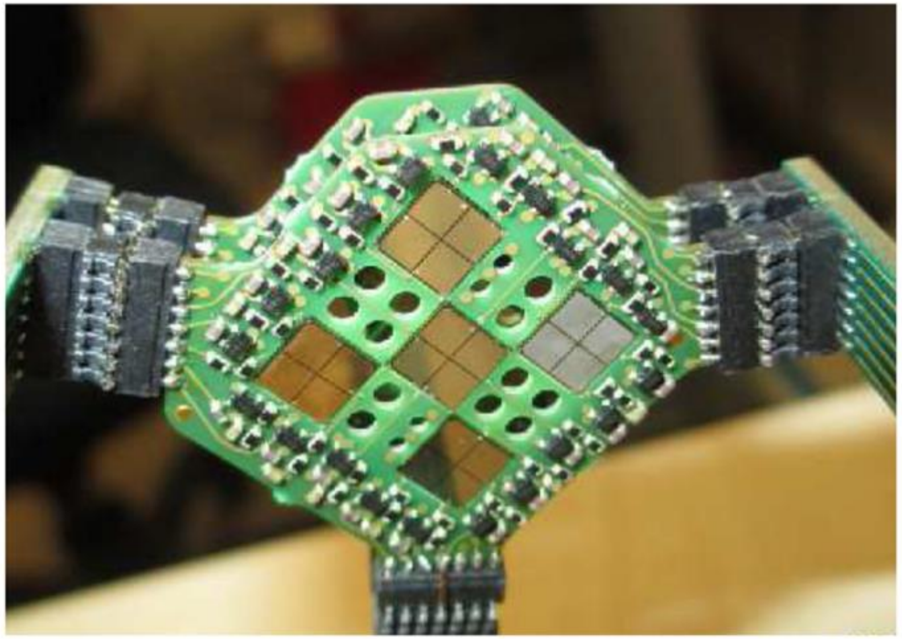

Fig. 14. Photograph of the T_0 detector. Nine metallized sc-CVD diamond sensor plates with fourfold segmented read-out electrodes are mounted on 2 attached PCBs arranged such as to build a 3×3 matrix structure. Read-out, LV and HV supply are mounted on 3 holding PCB rods.

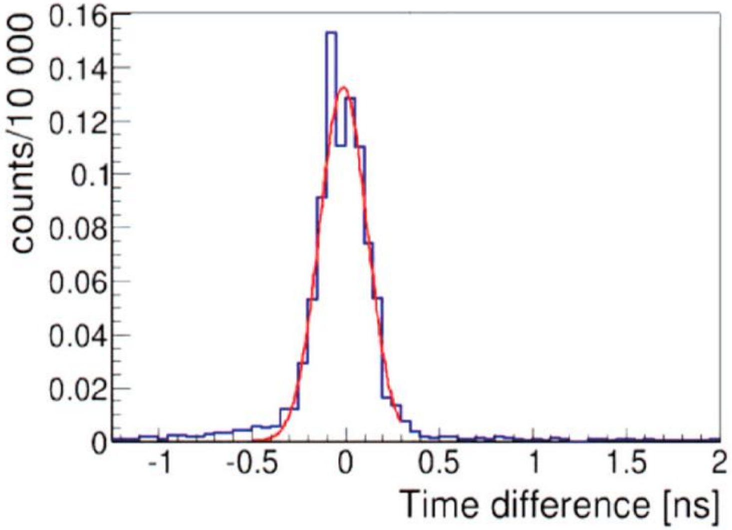

Fig. 15. Two detector timing distribution for correlated signals from protons at 2.95 GeV. The timing precision of individual sensors is $\delta t = 127\,\text{ps}/\sqrt{2} = 91\,\text{ps}$.

1) Bias voltage $U_{bias} = 200\,\text{V}$.
2) Rise time (10%–90%): 1.35 ns.
3) Signal/RMS noise ratio: 30:1.
4) Expected timing precision: $< 100\,\text{ps}$.
5) Preamplifier power consumption: 1.65 mW/channel, in total: 60 mW.
6) Horizontal and vertical pixel resolution (σ): 0.7 mm each.

Low Gain Avalanche Diode (LGAD)

N. Cartiglia et al., NIM A796(2015)141–148

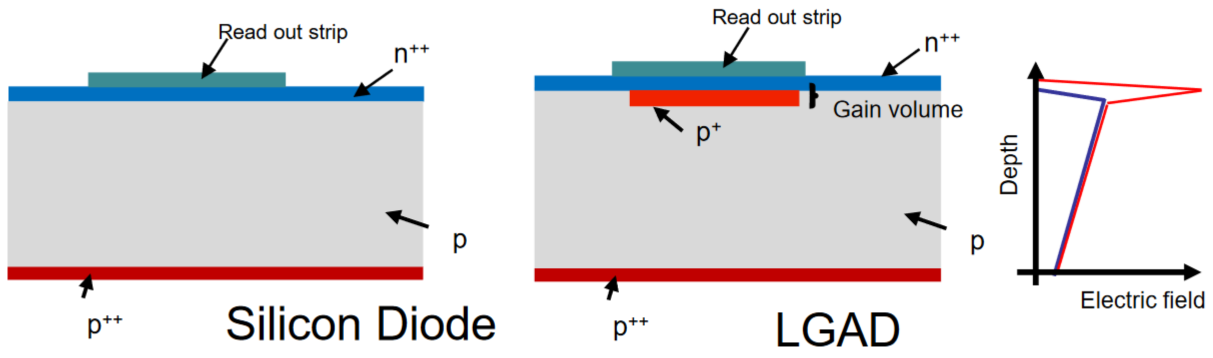

Ultra Fast Silicon Detector (UFSD)
Technology considered
for HL-LHC upgrades

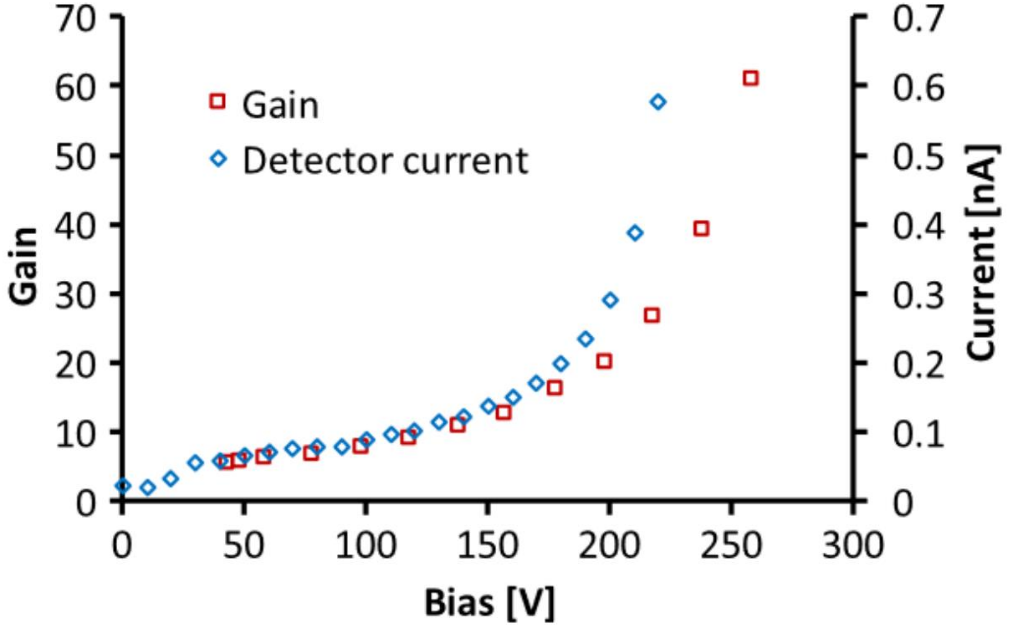

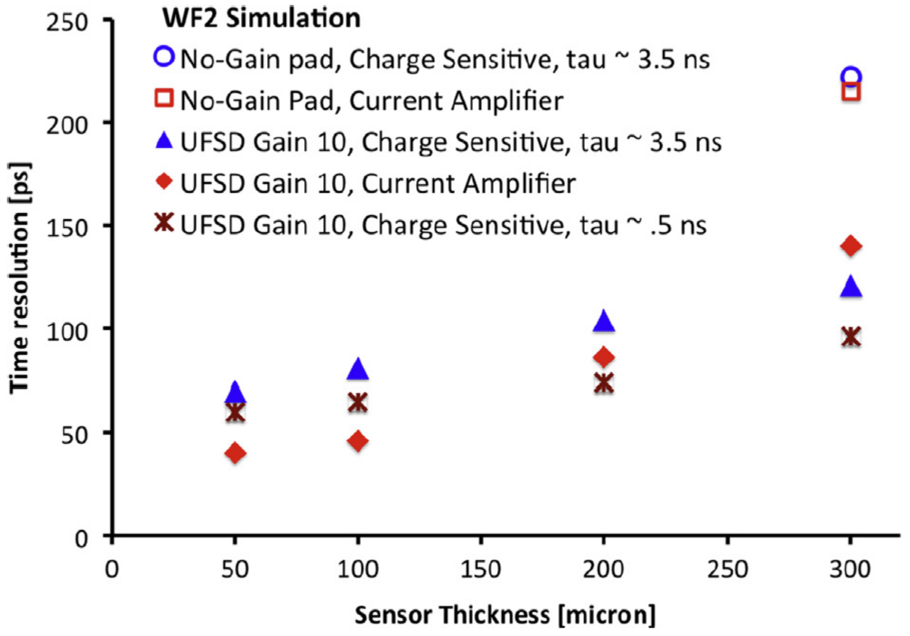

Fig. 16. Simulated time resolutions for a sequence of prototypes read-out using discrete components electronics.

LGAD: current status (2022)

HADES, https://arxiv.org/pdf/2005.12965.pdf

- Good timing precision with σ_{T_0} <60 ps for particle identification via time-of-flight.
- Operation for particle fluxes of $J > 10^7$ p/(cm^{2}s).
- Detection efficiency for MIPs close to 100%.
- Low material budget, below 0.5 mm Si equivalent.
- Position determination capabilities of δx<0.5 mm.
- Vacuum operation capability.
- Active area of up to 8 cm^2.

Current fill factors of LGAD sensors: ~ 55-60%
gain: ~ 20
bias voltage: ~ 300V

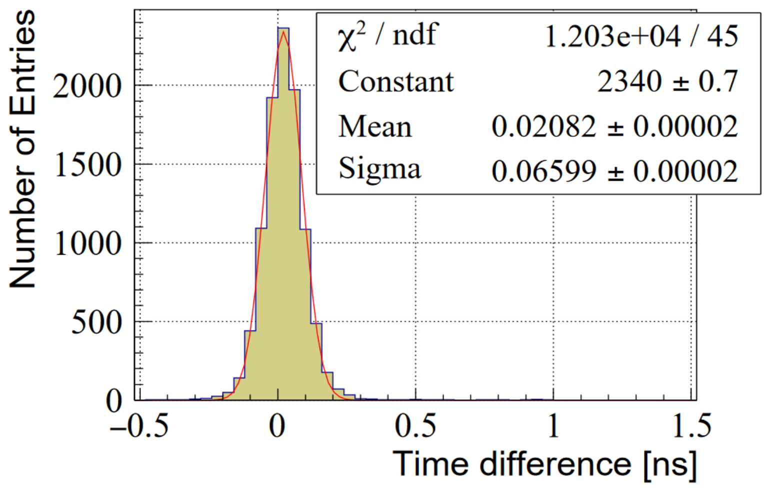

Fig. 15 Result of the time precision procedure based on a fit to the data presented in Fig. 14. As explained in the text, the lowest ToT values, which were outside of the range of interest, were excluded from the fit. The obtained time precision for this two-channel combination was 66 ps $/\sqrt{2} = 47$ ps.

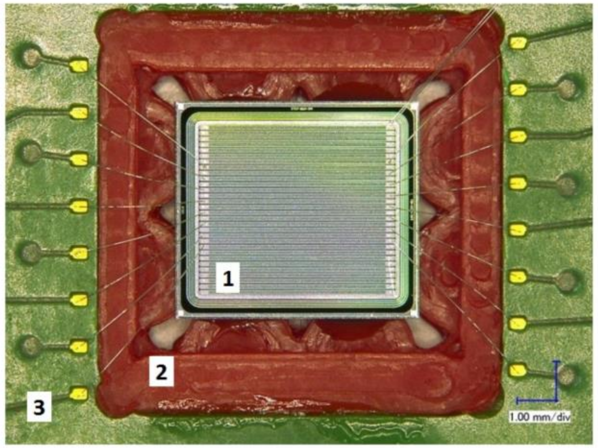

Fig. 1 Photograph of the LGAD sensor (1) with size of 5.0 mm x 4.3 mm mounted on a PCB plate (3) with the help of an adapter (2) to ensure the correct sensor positioning. 16 of 30 readout strips were bonded to the PCB traces.